Università degli Studi di Trieste

Graduate School in MOLECULAR BIOMEDICINE

PhD Thesis

Metabolic control of YAP and TAZ by the mevalonate pathway

Giovanni Sorrentino

XXVI ciclo – Anno Accademico 2012/2013

UNIVERSITÀ DEGLI STUDI DI TRIESTE

XXVI CICLO DEL DOTTORATO DI RICERCA IN

BIOMEDICINA MOLECOLARE

Metabolic control of YAP/TAZ
by the Mevalonate Pathway

Settore scientifico-disciplinare BIO/13

DOTTORANDO
Giovanni Sorrentino

COORDINATORE DEL CORSO DI DOTTORATO
Prof. Guidalberto Manfioletti

SUPERVISORE DELLA TESI e RELATORE
Prof. **Giannino Del Sal**

ANNO ACCADEMICO 2012/2013

"*Grandi cose, per verità, in questo breve trattato propongo all'osservazione e alla contemplazione di quanti studiano la natura. Grandi, dico, e per l'eccellenza della material stessa, e per la novità non mai udita nei secoli, e infine per lo strumento mediante il quale queste cose stesse si sono palesate al nostro senso. Grande cosa è certamente alla immensa moltitudine delle stelle fisse che fino a oggi si potevano scorgere con la facoltà naturale, aggiungerne e far manifeste all'occhio umano alter innumeri, prima non mai vedute e che il numero delle antiche e note superano più di dieci volte. Bellissima cosa e mirabilmente piacevole, vedere il corpo della Luna, lontano da noi quasi sessanta raggi terrestri, così da vicino come distasse solo due di queste dimensioni; così che si mostrano il diametro stesso della Luna quasi trenta volte, la sua superficie quasi novecento, il volume quasi ventisettemila volte maggiori che quando si guardano a occhio nudo: e quindi con la certezza della sensata esperienza chiunque può comprendere che la Luna non è ricoperta da una superficie liscia e levigata, ma scabra e ineguale, e, proprio come la faccia della Terra, piena di grandi sporgenze, profonde cavità e anfratti. Inoltre non mi pare si debba stimar cosa da poco l'aver rimosso le controversie intorno alla Galassia, o Via Lattea, e aver manifestato al senso oltre che all'intelletto l'essenza sua; e inoltre il mostrare a dito che la sostanza degli astri fino a oggi chiamati dagli astronomi nebulose è di gran lunga diversa da quel che si è fin qui creduto, sarà cosa grata e assai bella. Ma quel che di gran lunga supera ogni meraviglia, e principalmente ci spinse a renderne avvertiti tutti gli astronomi e filosofi, è l'aver scoperto quattro astri erranti, da nessuno, prima di noi, conosciuti né osservati, che, a somiglianza di Venere e Mercurio intorno al Sole, hanno le loro rivoluzioni attorno a un certo astro cospicuo tra i conosciuti, ed ora lo precedono ora lo seguono, non mai allontanandosene oltre determinati limiti. E tutte queste cose furono scoperte e osservate pochi giorni or sono con l'aiuto d'un occhiale che io inventai dopo aver ricevuto l'illuminazione della grazia divina. Altre cose più mirabili forse da me e da altri si scopriranno in futuro con l'aiuto di questo strumento, della cui forma e struttura e dell'occasione d'inventarlo dirò prima brevemente, poi narrerò la storia delle osservazioni da me fatte*"

Galileo Galilei
(***Sidereus Nuncius**, **Padova, 12 Marzo 1610**)

This thesis is dedicated to my parents who always supported me unconditionally. Thank you.

INDEX

Table of Contents

ABSTRACT

The YAP and TAZ mediators of the Hippo pathway promote tissue proliferation and organ growth. However, how their biological properties intersect with cellular metabolism remains unexplained. In this thesis, I show that YAP/TAZ activity is controlled by the SREBP/mevalonate pathway. Inhibition of the rate-limiting enzyme of this pathway (HMG-CoA-reductase) by statins opposes YAP/TAZ nuclear localization and transcriptional responses. Mechanistically, the geranylgeranyl pyrophosphate produced by the mevalonate cascade is required for activation of Rho-GTPases that, in turn, activate YAP/TAZ by inhibiting their phosphorylation and promoting their nuclear accumulation. The mevalonate-YAP/TAZ axis is required for proliferation and self-renewal of breast cancer cells. In *Drosophila,* inhibition of mevalonate biosynthesis and geranylgeranylation blunts the eye overgrowth induced by Yorkie, the YAP/TAZ ortholog. In tumor cells YAP/TAZ activation is promoted by increased levels of mevalonic acid produced by SREBP transcriptional activity, which is induced by its oncogenic cofactor mutant-p53. These findings reveal an additional layer of YAP/TAZ regulation by metabolic cues.

INTRODUCTION

Breast cancer and TP53 mutations

Tumor progression is a complex series of cellular and molecular events that take place gradually during the cancer development. Breast cancer is the most frequent invasive tumor diagnosed in women, causing hundreds of thousands deaths yearly worldwide. Like other tumors, it is a disease with a complex, heterogeneous genetic and biochemical background (Walerych et al., 2012). Despite therapeutic advances, about 20% of patients will experince metastases and die. During the initial diagnosis, it is possible to estimate the overall prognosis by evaluating clinicopathologial features including tumor size, histopathological grade, lymph node involvement and tumor expression of the estrogen receptor (ER), progesterone receptor (PR) and human epidermal growth factor receptor 2 (HER2). However, breast cancer is a heterogeneous disease characterized by different molecular drivers. Based on this, it is possible to classify breast cancers into al least five intrinsic subtypes: luminal A, luminal B, basal-like, HER2-enriched and normal-like. This classification reflects groups with different survival and chemotherapy response (Perou et al., 2000).

Triple negative breast cancers (TNBC) are defined by lack of expression of estrogen (ER), progesterone (PR), and HER2 receptors, and represent approximately 15% of all breast cancer, although they account for a much higher proportion of breast cancer related mortality (Oakman et al., 2010). The majority of TNBC are of basal-like molecular subtype, characterized by high proliferation rates, poor differentiation, basal marker (cytokeratin5/6) expression, and aggressive clinical course, with early relapse and decreased survival. In addition to aggressive biological characteristics, poor outcomes in TNBC relate to a distinct lack of therapeutic options, with treatment of either TNBC or basal-like breast cancer (BLBC) limited to conventional chemotherapy. Thus, there is an urgent need to find effective targeted agents in this disease (Turner et al., 2013).

Despite no single genetic or metabolic state could be considered as critical for its formation and progression, in TNBC the presence of mutated TP53 gene is one of the most important genetic trait of this subtype of tumor. TP53 mutations are usually uncommon in well-differentiated and hormone receptor positive subtypes, while are significantly pervasive in HER2 and basal-like tumors. Moreover, according to the

current release of the International Agency for Research on Cancer (IARC) TP53 database (http://www-p53.iarc.fr/), included in COSMIC, ~70% of the breast cancer alterations in TP53 are missense mutations (Walerych et al., 2012).

The p53 tumour suppressor pathway is considered one of the most important signalling pathways against tumour formation and progression. p53 can be envisioned at the centre of a highly interconnected network that conveys and transduces signals, which can represent stress conditions. Indeed, these signals can originate from external factors (such as γ-rays, UV light, DNA damaging agents…) or internal ones (like oncogene activation, high levels of reactive oxygen species (ROS), ribonucleotide depletion…) and may compromise genomic stability and promote neoplastic transformation. In response to these stresses p53 becomes stabilized and activated, events that are regulated by a refined combination of post-translational modifications and interacting protein partners. Once activated, p53 acts essentially as a transcription factor able to promote the coordinated expression of an array of target genes that are the executors of p53-induced cellular responses, such as cell cycle arrest, senescence or apoptosis (Kruse and Gu, 2009) (Fig. 1). The relevance of the p53 pathway in tumour suppression is underscored by the observation that germline mutations in the p53 gene (*TP53*) are causative of the Li-Fraumeni syndrome, whose patients are characterized by 25-fold increase in the chance of developing early onset cancers, compared with the general population (Malkin et al., 1990).

The phenotypic effects of *TP53* mutations can be classified into three non-mutually exclusive groups (Fig. 2). First, most mutations observed in human tumours abrogate the tumour suppressor functions of the affected allele. This "loss of function" is due to reduction of p53 binding to its consensus DNA sequence and, consequently, hampered transcriptional activation of p53 target genes (Kato et al., 2003).

Second, most missense mutations also produce a full-length mutant p53 capable of inhibiting, to varying degrees, the function of the wild-type protein encoded by the second allele. This "dominant-negative" effect is achieved by oligomerization of mutant and wild-type proteins, forming a heterotetramer defective in sequence specific DNA binding (Dittmer et al., 1993; Milner and Medcalf, 1991).

Finally, several mutations were shown to confer mutant p53 with new functions that are independent of wild-type p53. Such activities, commonly described as mutant p53 "gain

of function" (GOF) can actively contribute to various aspects of tumour progression. The molecular mechanisms of mutant p53-induced oncogenesis in breast cancer can be summarized as follow (Fig.3):

- Cell transformation: in 1993 it was shown that p53 mutants of both human and mouse origin, but not their wild-type counterparts, can transform p53-null cells (Dittmer et al., 1993). Accordingly, experiments performed knocking down mutant p53 in several human cancer cell lines, demonstrated that down-regulation of endogenous mutant p53 rendered those cells less tumorigenic (Bossi et al., 2006; Bossi et al., 2008). Mutant p53 was shown to cooperate with activated oncogenic Ras in transformation of primary mouse embryo fibroblasts (MEFs)(Lang et al., 2004). This property is due to the ability of different p53 mutants to bind and inactivate p53 family members, p63 and p73 (Gaiddon et al., 2001; Strano et al., 2001): indeed, in cells without mutant p53, both p63 and p73 prevent Ras-induced cell transformation by triggering senescence (Fang et al., 1999; Guo et al., 2009).

- Drug resistence: one distinctive feature of many p53 mutants is the ability to confer an elevated resistance to cells towards a variety of pro-apoptotic signals (Blandino et al., 1999).

- Genomic instability: a connection between mutant p53 and increased genomic instability was demonstrated by showing that human p53 mutants could disrupt normal spindle checkpoint control, leading to accumulation of cells with polyploid genomes (Gualberto et al., 1998).

- Cell migration and invasion: although p53 knockout mice are highly tumour prone, these lesions do not metastasize frequently nor generally display invasive pathology (Attardi and Jacks, 1999). On the contrary, presence of mutant p53 leads to a marked increase in the incidence of highly metastatic carcinomas in various mouse models (Doyle et al., 2010; Lang et al., 2004; Morton et al., 2010; Olive et al., 2004). Indeed, another aspect of mutant p53 gain of function that has recently emerged is its ability to drive cell migration and invasion (Adorno et al., 2009). This is achieved by two non-mutually exclusive mechanisms of inhibition of p63 anti-metastatic functions.

- Alteration of gene expression: although two thirds of missense mutations in the DBD, including all "hotspot" mutations, abrogate the ability to recognize wild-type p53 response elements (Kato et al., 2003), modulation of gene transcription by mutant p53 is

well documented and the list of mutant p53 target genes is constantly growing (Girardini et al., 2011). For some mutant p53 target genes, it became clear that mutant p53 interacts with sequence-specific transcription factors, resulting in either augmentation or attenuation of their activity. Recently a genome-wide expression analysis identified the mevalonate pathway as significantly up-regulated by mutant p53. Here, mutant p53 has been found to associate with sterol gene promoters, acting as transcriptional coactivators for SREBP transcription factors (Freed-Pastor et al., 2012) to enhance the expression of many mevalonate pathway genes (e.g. HMGCR and HMGCS1). Enhanced mevalonate metabolism in breast cancer cells with missense mutations on TP53 resulted in aberrant protein prenylation and contributed to the maintenance of malignancy. Importantly, the inhibition of mutant p53 by siRNA could efficiently reverse these metabolic dysregulations (Freed-Pastor et al., 2012) making thus the mevalonate pathway an important executor of mutant p53 gain-of-function in cancer cells.

Cancer metabolism and the mevalonate pathway

Cancer cell need to reprogram their metabolism to supply their high energetic requirement. This phenomenon was first described by Otto Warburg and was called "Warburg effect". Warburg found that cancer cells prefer glycolysis to generate energy even in normal aerobic conditions (Kroemer and Pouyssegur, 2008).
Cancer cells metabolism is also characterized by the increased export of acetyl-CoA from the mitochondria to the cytosol, where it serves as a precursor for several lipids. In this manner the acetyl-CoA can be employed for fatty acids and mevalonate metabolism (Gruenbacher and Thurnher, 2014; Zadra et al., 2013) (Fig. 4) . Through the mevalonate pathway, cells synthesize fundamental biomolecules such as cholesterol, isoprenoids, Heme A, ubiquinon, dolichols…(Fig. 5). In the first enzymatic step of this metabolic pathway, the enzyme HMGCR (3-hydroxy-3-metylglutaryl-CoA reductase) converts the HMG-CoA (produced from acetyl-CoA) into mevalonate (mevalonic acid). By three enzymatic reactions, mevalonate is converted in isopentenyl pyrophosphate (IPP), which represents the isoprenoid precursor molecule. IPP is in fact essential for the synthesis of farnesyl pyrophosphate (FPP) and geranylgeranyl pyrophosphate (GGPP)

used by the cell as activated isoprenoid substrates in post-translational modification, which is referred to as protein prenylation (Konstantinopoulos et al., 2007). The enzymatic transfer of farnesyl- or geranylgeranyl moieties to proteins enables them to attach to cell membranes and to carry out their biological functions. Many members of the Ras and Rho superfamilies of GTPases depend on prenylation for appropriate membrane targeting and subcellular localization (Casey and Seabra, 1996). It is well established that Rho GTPases affect cellular activities like migration, invasion, proliferation and survival (Sahai and Marshall, 2002). For this reason, the positive role of the mevalonate pathway on Rho GTPases represents a main mechanism by which lipid metabolism dysregulation can contribute to tumorigenesis (Freed-Pastor et al., 2012).

Squalene synthase can convert FPP in squalene, which in turn is converted in lanosterol then in cholesterol. Feedback inhibition by cholesterol and isoprenoid intermediates of the mevalonate pathway controls HMG-CoA reductase levels (Goldstein and Brown, 1990) (Fig. 5). Beside of being essential for membranes building, cholesterol results essential also in regulating signal-transduction pathways involved in cancer. An example of this is the Hedgehog (Hh) pathway. This is a signal-transduction pathway, regulated by a group of secreted molecules that are essential for proliferation and differentiation. Hedgehog molecules undergo to several post-translational modifications such as the addition of cholesterol molecules that lead to the membrane tethering and consequent secretion of mature Hh ligands (Jeong and McMahon, 2002).

The mevalonate pathway enzymes are under transcriptional control of a family of endoplasmic reticulum membrane-bound transcription factors designed as Sterol Regulatory Element-Binding Proteins (SREBPs) (Brown and Goldstein, 1997). SREBPs directly activate the expression of more than 30 genes dedicated to the synthesis of cholesterol, isoprenoids, fatty acids, triglycerides and phospholipids. These transcription factors belong to the basic helix-loop-leucine zipper (bHLH-Zip) family and are synthesized as inactive precursor bound to the endoplasmic reticulum (ER). Each precursor is composed by three domains: a) an NH_2-terminal domain of about 480 amino acids that contains the region for DNA binding; b) two hydrophobic transmemebrane-spanning segments interrupted by a short loop of about 30 amino acids that projects into the lumen of the ER; and c) a regulatory COOH-terminal domain of

about 590 amino acids. To localize into the nucleus and act as transcription factor, the NH_2-terminal domain must be released from the membrane proteolytically. Essential for this maturation process are three proteins. One is an escort protein designed SREBP cleavege-activating protein (SCAP). The other two are proteases, designed Site-1 protease (S1P) and Site-2 protease (S2P). SCAP is a sensor of sterols: when cells become depleted in cholesterol, SCAP escorts the SREBP from the ER to the Golgi apparatus, where the two proteases reside. S1P cleaves SREBP and the NH_2-terminal domain is then released from the membrane via a second cleavage mediated by S2P. The NH_2-terminal domain (nSREBP) translocates to the nucleus, where it binds sterol response elements (SREs) in the promoters of multiple genes of the mevalonate pathway (Edwards et al., 2000; Horton et al., 2002) (Fig. 6 and 7).

In mammals there are three SREBP isoforms: SREBP-1a, SREBP-1c and SREBP-2. SREBP-1a is a potent activator of all the genes involved in the synthesis of cholesterol, fatty acids and tryglicerides. SREBP-1c preferentially enhances transcription of genes required for fatty acid synthesis, while SREBP-2 preferentially activates genes essential for cholesterol synthesis (Horton et al., 2002).

Several studies suggest a role for SREBPs in determination of cell and organ growth both in mice and in flies. Indeed, nSREBP transgenic mice develop a strongly enlarged fatty liver while SREBP knock-out in drosophila caused reduction in organ size (Brown and Goldstein, 1997; Horton et al., 2003; Knebel et al., 2012; Porstmann et al., 2008) (Fig. 8).

Several common oncogenic events can regulate SREBP activity and the mevalonate pathway. Transcriptional activity of SREBP in human mammary cancer is boosted by mutant-p53 that acts as a transcription co-activator (Freed-Pastor et al., 2012). PI3K/Akt/mTOR pathway, often found activated in a variery of cancers, sustains SREBPs transcriptional activity, which is required for Akt-induced lipogenesis and cell growth (Porstmann et al., 2008). Decreased adenosine monophosphate-activated protein kinase (AMPK) promotes tumorigenesis and pharmacological activation of AMPK has anticancer potential. The mevalonate pathway is also regulated by the activity of AMPK, which phosphorylates HMGCR (Motoshima et al., 2006) and SREBPs (Li et al., 2011) to inhibit their activity. It is then possible that anticancer effect of AMPK activation and tumor suppressor activity of its upstream kinases (e.g. liver kinase B1,

LKB1), are at least in part due to inhibition of mevalonate pathway.

The nuclear form of SREBP trancription factors are also regulated by ubiquitin-mediated proteasomal degradation. Due to the presence of a phosphodegron, SREBPs are recognized by the oncosuppressor SCF(Fbw7) ubiquitin ligase, which target them for proteasomal degradation thus regulating the synthesis of cholesterol and fatty acids (Sundqvist et al., 2005).

Glycolisis and metabolic reprogramming of cancer cells are often supported by the activation of the hypoxia-inducible-factor 1 (HIF-1). The activation of many oncogenes can result in stabilization of HIF-1. HMGCR mRNA levels are regulated by HIF-1 transcriptional activity (Pallottini et al., 2008) thus linking the mevalonate pathway to several upstream oncogenic signals.

A direct role for the mevalonate pathway in oncogenesis has been shown by Clendening and colleagues. They demonstrated that dysregulation of the mevalonate pathway can make a casual contribution to transformation and that HMGCR increased anchorage-independent growth in soft agar as well as in xenograft. Moreover HMGCR cooperated with RAS to promote the transformation of primary mouse embryonic fibroblasts. High mRNA levels of HMGCR and other mevalonate pathway genes correlated with poor prognosis in meta-analysis of breast cancer, making the mevalonate pathway an important metabolic driver of oncogenesis in human cancers and a new candidate for anticancer drug development (Clendening et al., 2010; Freed-Pastor et al., 2012).

Thus, reprogramming of metabolism by cancer cells can lead to aberrant activation of the mevalonate pathway and, as consequence, to the increase of key cellular metabolites such us farnesyl pyrophosphate, geranylgeranyl pyrophosphate and cholesterol that, by different ways, can sustain tumorigenesis.

Tumor metabolism as target of anticancer drug development

The first-generation of chemotherapeutics were identified either through accidental observations or on the basis of their similarity to essential cofactors in haematopoiesis. As an example, the evidence that survivors of mustard gas exposure resulting from warfare suffered from leukopaenia led to the use of the mustard gas derivative nitrogen mustard in lymphoma treatment (Goodman et al., 1946). Soon did it become clear that

such chemotherapeutics act by interfering with the integrity of DNA or the cytoskeleton. These early anticancer drugs — for example, platinum derivatives, topoisomerase inhibitors, nucleoside analogues, vinca alkaloids and taxanes — still represent the most clinically-used chemotherapeutics today (Dobbelstein and Moll, 2014). Importantly, these treatments are often not effective for several cancers and also can cause strong toxicity by affecting normal cells as well as cancer cells.

The discovery that some cellular targets are genetically altered in cancer and are essential for cancer growth ("oncogene addiction") led to the development of the second-generation cancer therapeutics. These drugs, by selectively targeting these aberrant genes, are specific for cancer cells and for this reason are so-called "smart drugs". One of the pioneering example is imatinib (Gleevec; Novartis), a small molecule inhibitor of BCR-ABL kinase for the treatment of chronic myeloid leukemia (CML)(Capdeville et al., 2002). Other examples of key oncogenic pathways targeted by small molecules are: RAS-RAF-MEK; Hedgehog; JAK-STAT; HER2. As expected, the side effects of drugs that target these signaling pathways are relatively milder than those that target DNA or cytoskeleton, however acquisition of drug resistance often leads to tumor relapses (Dobbelstein and Moll, 2014).

In the past 10 years, it has turned out that, similar to DNA replication, several other cellular "machinaries" are required for tumor cell proliferation and survival with strong selectivity (Dobbelstein and Moll, 2014). This phenomenon is explained by the existence of chronic "stress" conditions in tumors and the ensuing "non-oncogene addiction" of cancer cells. These abnormal cellular conditions have been recognized as novel hallmarks of cancer (Hanahan and Weinberg, 2011) and represent the targets for third-generation of anticancer drugs. Among these hallmarks, particularly interesting for drug discovery is the "cancer metabolism".

Proliferating cancer cells exhibit significantly different metabolic requirements than most normal differentiated cells. For example, in order to support their high rates of proliferation, cancer cells consume additional nutrients and divert those nutrients into synthesis of macromolecules such as lipids and nucleic acids (Vander Heiden et al., 2009). Given that all cancer cells rely on metabolic perturbation to support their growth and survival, targeting metabolism has the potential to impact cancers arising from many different tissues (Luo et al., 2009).

Altered expression of metabolic enzymes or changes in metabolic pathway regulation are downstream of many oncogenic signals or tumor suppressor genes, and cancers with specific genetic lesions are addicted to these metabolic changes (DeBerardinis et al., 2008). As an example, HMGCR and isocitrate dehydrogenases (IDH1/2) are often deregulated or mutated in cancers (Clendening et al., 2010; McCarthy, 2012). Thus targeting tumor metabolism as a downstream consequence of driver mutations is an attractive therapeutic strategy because it is central to the growth and survival of cancer cells (Vander Heiden, 2011). Moreover, many metabolic enzymes can be already efficiently targeted with small molecule (e.g. statins, metformin, rapamycin…).

An example of anticancer activity exerted by inhibitors of metabolic enzymes is represented by statins. This family of inhibitors, originally developed as cholesterol-lowering drugs that target the HMGCR enzyme, are among the most therapeutically effective and financially successful pharmaceuticals created. Cellular cholesterol is obtained in two ways. It can be obtained both by receptor-mediated uptake of LDL-cholesterol from blood plasma, or by endogenous synthesis from acetyl-coenzime A (CoA) by the activity of HMGCR and the mevalonate pathway. Inhibition of this enzyme triggers a robust homeostatic feedback response in cells attempting to up-regulate and restore the cholesterol levels through activation of SREBPs transcription factors. SREBPs activate transcription of several enzyme of the mevalonate pathway, including the LDL-receptor gene, which at cell surface internalize LDL-cholesterol particles, thus lowering circulating cholesterol levels (Brown and Goldstein, 1997). While the liver is obviously the favourite site of action of statins, the same feedback response happens in other normal tissues and cancer.

The antiproliferative activity of statins was shown several years ago (Jakobisiak et al., 1991). Subsequent research on several transformed cells in culture has shown that the anti-ploriferative effect of statins is largely tumor-selective both *in vitro* and *in vivo,* including both liquid and solid tumors (e.g. leukemia, myeloma, breast, prostate, colorectal, lung, pancreas, ovarian, head and neck cancers) (Clendening and Penn, 2012). Since statins have been prenscribed to lower the cholesterol levels of millions of patients for many years, there is a wealth of data that can be mined for evidence of whether statins use is associated with cancer incidence, recurrence and grade. Some results of epidemiological data report that statins users have reduction of cancer

incidence, grade and recurrence (Ahern et al., 2011; Cauley et al., 2006; Kumar et al., 2008). Recently, Nielsen and co-workers, by assessing mortality among patients from the entire Danish population who had received a diagnosis of cancer, found that statin use in patients with cancer was associated with reduced cancer-related mortality (Nielsen et al., 2013).

By contrast other studies found no association between statin use and cancer risk (Bonovas et al., 2005). Importantly, several prospective clinical trials addressing whether statins decrease cancer incidence are now underway.

The Hippo pathway

The Hippo pathway is a tumor-suppressor cascade that links signals from the plasma membrane into the nucleus, where it controls the transcription of several target genes that regulates cellular processes such as proliferation, organ growth, tissue regeneration, embryonic development, survival and differentiation (Halder and Johnson, 2011; Pan, 2010; Yu and Guan, 2013). The Hippo signal acts similarly to other well known signal transduction pathways such as: EGF (epidermal growth factor), TGFβ (transforming growth factor-β) and WNT signalling pathways with the difference that Hippo does not have specific extracellular molecules and receptors (Yu and Guan, 2013).

The core of the Hippo pathway is composed by highly conserved protein kinases with similar functions in mammalian and *D.melanogaster*. These kinases are the serine/threonine kinases MST1, MST2, LATS1 and LATS2 (Harvey et al., 2003; Wu et al., 2003). They act in concert with scaffolding protein Salvador homolog 1 (SAV1; which interacts with MST1/2) and MOB kinase activator 1 (MOB1; which interacts with LATS1/2). Downstream to this cassette, operate the nuclear factors YAP (Yes-associated protein) and TAZ (transcriptional co-activator with PDZ-binding motif, or WWTR1) (Huang et al., 2005) and the TEA domain-containing sequence-specific transcription factors TEAD1-4 (Wu et al., 2008). TAZ is homologous to YAP with 46% amino acid sequence identity and displaying similar domain organization. YAP and TAZ are transcriptional co-activators unable to bind the DNA themselves but form complexes with TEADs to regulate gene expression. YAP and TAZ are also able to bind and regulate other transcription factors such as SMADs (Alarcon et al., 2009), T-

14

box transcription factor 5 (TBX5)(Murakami et al., 2005), RUNT-related transcription factor (RUNX) 1 and 2 (Yagi et al., 1999) as well as p73 (Strano et al., 2001).

When MST kinases are activated, they phosphorylate and activate LATS, which in turn, phosphorylate their downstream targets YAP and TAZ. This event results in their cytoplasmic retention and β-TRCP (β-transducin repeat-containing E3 ubiquitin ligase)-dependent degradation by proteasome (Yu and Guan, 2013). Thus, when the Hippo pathway is activated, YAP and TAZ nuclear activities are inhibited (Fig. 9).

Both YAP and TAZ are essential for embryonic development: only a fraction of TAZ knockout (KO) mice is viable and deletion of YAP results in embryonic lethality at embryonic day 8.5. The double knockout of YAP and TAZ has an even more dramatic phenotype: embryos die before the morula stage at embryonic day 2 (Makita et al., 2008; Morin-Kensicki et al., 2006).

Regulation of Hippo pathway

The number of signals and mechanisms regulating the Hippo pathway is increasing progressively. In mammals, three main upstream mechanisms have been connected to Hippo regulation (Yu and Guan, 2013): regulators of the Hippo core cassette MST/LATS; the actin cytoskeleton; and regulators of cell polarity and cell-cell junction (Fig. 10).

MSTs are regulated by a number of proteins including: TAO (thousand and one aminoacid protein)(Poon et al., 2011) and MARK1 (MAP/microtubule affinity regulating kinase 1)(Mohseni et al., 2014) directly phosphorilates and activates MSTs. KIBRA (kidney and brain protein) (Genevet et al., 2010) and Expanded are instead adaptor proteins for MSTs activity.

LATSs kinases are regulated by NF2, the tumor suppressor protein Merlin, which promotes LATSs activation by inducing their plasma membrane localization (Hamaratoglu et al., 2006).

The Crumbs homolog complex (CRB) localizes to apical junction and regulates cell polarity. Together with AMOT (angiomotin adaptor proteins) CRB inhibits YAP by promoting its cytoplasmic retention. Another regulator of cell polarity is Scribble. It is required for the recruitment of MST and/or LATS to TAZ in breast cancer cells and

links cell polarity to YAP/TAZ inactivation (Cordenonsi et al., 2011).

E-cadherin localization at adherens junctions suppresses the nuclear localization and activity of YAP by regulating MST kinase activity (Kim et al., 2011). Moreover, the E-cadherin-associated protein α-catenin regulates YAP by sequestering YAP-14-3-3 protein complex in the cytoplasm (Schlegelmilch et al., 2011).

A still poorly understood mechanism able to regulate the Hippo pathway is represented by actin cytoskeleton. Infact, the mechanical properties of extracellular environment regulate the localization and activity of YAP and TAZ through a mechanism that requires F-actin and that is conserved also in *D.melanogaster* (Dupont et al., 2011; Sansores-Garcia et al., 2011). As consequences, transduction of signals impinging in actin citoskeleton are able to indirectly regulate YAP and TAZ activity. G protein-coupled receptors (GPCRs) regulators such as lysophosphatidic acid and sphingosine-1-phosphate regulate RHO GTPases activity that, in turn, causes actin cytoskeleton rearrangements and consequent YAP/TAZ activation (Yu et al., 2012). The mechanism by which this layer of regulation occurs is still generally unknown and may involve both Hippo-dependent and –independent regulation of YAP/TAZ (Dupont et al., 2011; Yu et al., 2012).

In addition to these four major upstream regulators, there are several other proteins that modulate the activity of YAP/TAZ. Among them, Homeodomain-interacting protein kinase 2 (HIPK2), which promotes YAP abundance; 14-3-3 proteins, which mediate cytoplasmic YAP/TAZ retention after Hippo pathway activation; casein kinase 1 and β-TRCP, which mediate YAP/TAZ protein degradation; and finally protein tyrosine phosphatase non-receptor type 14 (PTPN14), which promotes the nucleus-to-cytoplasm translocation of YAP during contact inhibition (Johnson and Halder, 2014).

The Hippo pathway in growth control and cancer

Inhibition of the Hippo kinase or overexpression of Yorkie (the *D.melanogaster* homolog of YAP and TAZ), during fly developlment, lead to strong overgrowth of imaginal discs and the corresponding adult organs (Harvey et al., 2003) (Fig. 11). These phenotypic effects are due to both increase in cell proliferation (cells continue to proliferate after tissues have reached their proper size) and resistance to apoptotic

stimuli.

YAP-mediated control of organ size is maintained also in mice. Infact, YAP overexpression or MST/LATS loss increases liver and heart size by increasing tissue cell number (Dong et al., 2007; von Gise et al., 2012) (Fig. 11). However, in tissues such as intestine and skin, YAP activation leads to enlargement of stem cell compartment without increase in organ size. To date, it is not well understood how YAP and TAZ drive cell proliferation; this is likely to involve the expression of many target genes of YAP/TAZ-TEADs transcription factors, many of which directly affect growth and survival.

Disregulation of Hippo pathway is associated with cancer. Elevated protein levels and nuclear localization of YAP and TAZ have been reported in several solid tumors (liver, skin, lung, breast, colon) (Harvey et al., 2013) (Fig. 12). In line, inhibition of Hippo pathway or YAP overexpression in mice liver causes tumor formation (Dong et al., 2007; Zhou et al., 2009) (Fig. 11).

The mechanisms involved in YAP/TAZ-induced cell transformation involve enhanced cell proliferation, apoptosis resistance, inhibition of senescence and epithelial to mesenchymal transition (EMT). TAZ, which is overexpressed in about 85% of grade-3 breast cancer, has been shown to be a inducer of cancer stem cells traits, metastasis and chemoresistance and its levels correlates with poor clinical outcome (Bartucci et al., 2014; Cordenonsi et al., 2011) (Fig. 12). YAP is amplified in several human cancers through mechanisms that remain still unknown (Harvey et al., 2013).

The germline or somatic mutations in components of the Hippo pathway are rare (Harvey et al., 2013) with the exception to the NF2 gene. The oncosuppressor NF2 (Merlin) is frequently mutated in neurofibromatosis, a genetic disorder of nervous system associated with tumorigenesis (Asthagiri et al., 2009). NF2 inhibits YAP/TAZ pathway by activating LATS in the plasma membrane. Moreover, activating mutations in YAP and TAZ have not been reported in human cancers. The fact that the core components of the Hippo pathway are largely unaffected by mutations, suggests other mechanisms of aberrant activation of YAP and TAZ in cancer.

A divergent role for YAP and TAZ in response of cancer cells to apoptosis has been shown. In fact, YAP is able to bind the C-terminal region of the member of the p53 family of transcription factors, p73. After DNA damage the binding of YAP to p73

causes the increase of transactivation functions of p73 thus favouring apoptosis in this cellular context (Strano et al., 2005; Strano et al., 2001). In contrast, TAZ has been proposed to confer chemoresistance to breast cancer stem cells (Bartucci et al., 2014; Cordenonsi et al., 2011; Lau et al., 2014).

The Hippo pathway as target for cancer therapy

The hyperactivation of YAP and TAZ in a variety of human tumors opens the possibility that direct or indirect inhibition of these nuclear transducers could be used as a new strategy for therapeutic intervention for many cancers. Several preclinical experimental evidences support this idea. Experiments performed with human cancer cell lines have demonstrated the efficacy of reducing YAP and TAZ levels (by short interference RNA) in reducing cell proliferation in vitro and in vivo in xenograft assays (Bartucci et al., 2014; Diep et al., 2012; Lamar et al., 2012). However, due to the lack of catalytic activity, direct pharmacological inhibition of YAP/TAZ is considered challenging.

NF2 deletion in liver mice leads to tumorigenesis. Importantly, simultaneous reduction of YAP levels totally rescued the NF2 loss-induced tumorigenesis (Zhang et al., 2010). The same rescue was obtained by expression of a dominant negative version of TEAD2 (that binds YAP but not the DNA)(Liu-Chittenden et al., 2012). Thus, disruption of YAP-TEADs interaction is considered an attractive strategy to inhibit the YAP/TAZ activity in cancer. In this context, a promising strategy to identify small-molecules inhibitors of this protein-protein interaction is through high-throughput screening. A library of FDA-approved drugs was screened for identify inhibitors of YAP transcriptional activity. One of the best hits was the compound verteporfin which was showed to act as an inhibitor of YAP-TEADs interaction. Verteporfin was effective also *in vivo* delaying tumor progression in NF2-depleted mouse model of liver cancer (Liu-Chittenden et al., 2012).

Another strategy for identification of YAP inhibitors by high-throughput screening is by monitoring the localization of YAP and TAZ within the cells. Through this strategy, dobutamine, an β-adrenergic receptor agonist, was found to inhibit YAP by forcing its cytoplasmic localization in HEK293 cells (Bao et al., 2011).

Upstream regulators of the Hippo pathway are instead, in principle, undruggable. The Hippo kinases MST1/2 and LATS1/2, in fact, negatively regulate YAP and TAZ causing their cytoplasmic sequestration and degradation. In this direction, small-molecules agonists would be most desirable.

The recent identification of some agonists/antagonists of GPCRs as YAP/TAZ regulators, opens new unexplored routes for therapeutic intervention (Yu et al., 2012). Agonists of Gα_s-coupled receptors-such as adrenaline, glucagone and dopamine- results in strong YAP phosphorylation and inhibition *in vitro* and *in vivo* indicating that YAP activity could be modulated by molecules belonging to the FDA-approved class of drugs. Recently, inhibitors of the EGFR-PI3K-PDK1 pathway have been shown to inhibit YAP activity in a LATS-dependent fashion (Fan et al., 2013).

The discovery that F-actin represents a critical biological input for YAP and TAZ activation, in response to mechanical stress, unveiled other potential strategies for blunting YAP/TAZ activation. Indeed the F-actin inhibitors cytochalasin D, latrunculin B; the myosin inhibitor blebbistatin; the Rho inhibitors C3 and the Rho kinase inhibitor Y27632 all cause inactivation of YAP/TAZ by controlling its cytoplamsic sequestration /degradation (Dupont et al., 2011). Unfortunately, the use of these drugs in vivo is challenging due to the high toxicity of these drugs that target cytoskeleton, which is essential for many basic cellular functions.

An important concern in targeting YAP/TAZ is the lack of a clear understanding of the long-term consequences of YAP and TAZ inhibition *in vivo*. For example, YAP depletion in mouse intestine causes WNT hypersensitivity with subsequent enhanced stem cell expansion and hyperplasia. Thus, YAP inhibition may also have the unexpected effect to promote colon cancer growth (Barry et al., 2013).

In sum, although studies aimed at targeting the YAP/TAZ nuclear activity for anticancer therapy are still in the early phase, very promising preclinical data have been already published and open the possibility to use, soon, the Hippo cascade as target in the prevention and treatment of human malignancies (Johnson and Halder, 2014).

Drug repositioning for cancer drug discovery

Despite the huge amount of money being invested in cancer treatment, cancer remains one of the leading causes of mortality worldwide. Research expenditure by the US National Institute of Health has increased by more than two-fold, and pharmaceutical

industries have doubled their R&D spending. Only 5% of oncology drugs entering Phase I clinical trials are ultimately approved (Gupta et al., 2013). Drug development requires an average of 13 years of research and an investment of US$1.8 billion to bring a single drug from the bench to a patient's bedside, with often and often only a marginal therapeutic success (disease-free survival often increased only of few months). In general, if the drug is found efficacious in Phase III trials, it receives the FDA (or EMA in U.E.) approval. Most drugs, however, fail to receive FDA approval, often because they did not effectively target the disease for which they were discovered (Gupta et al., 2013).

Pharma companies have adopted several strategies to reduce the cost and time involved in cancer drug development. One of such strategy is to evaluate, as anticancer agents, already used non-cancer drugs that have already been approved for noncancerous disease, whose targets have already been discovered. This approach is called "drug repositioning" and its major advantage is that the pharmacokinetic, pharmacodynamic, and toxicity profiles of drugs are well known because of the preclinical and Phase I studies. Therfore , these drugs could be rapidly tested in Phase II and III clinical studies with a significant reduction of the associated cost.

The idea beyond the repositioning starts from the observation that almost all drugs possess more then one target and thus produce off-target effects. Yet, many different disease share common molecular pathways and target in the cell. Thus, it is likely that the same drug can be therapeutic for more than one disease (Gupta et al., 2013). Some examples of non-cancer drugs, now under investigation for cancer treatments are: Aspirin (original indication: analgesic); Valproic Acid (original indication: antiepileptic); Metformin (original indication: diabetes mellitus); Statins (original indication: myocardial infraction); Bisphosphonates (original indication: anti-bone resorption). The use of FDA-approved drug libraries (and collection of compounds that have failed the drug discovery process for reasons other than toxicity) in cell-based high throughput screening could represent the starting point for the identification of new uses for old drugs.

AIM OF THE THESIS

In multicellular organisms the regulation of organ size is a crucial developmental process finely controlled by multiple signals that converge in the control of cell proliferation, apoptosis and stemness. Deregulation of these signals can lead to aberrant tissue growth and cancer. The Hippo tumor-suppressor pathway has emerged as a fundamental limiting factor for organ size, acting as inhibitor of the YAP and TAZ proto-oncogenes. These highly related transcriptional coactivators promote tissue growth through the simultaneous induction of cell proliferation, stem cell amplification, and inhibition of cell differentiation and apoptosis. In tumors, YAP/TAZ endow cells with cancer stem cells properties and metastatic potential. In line, aberrant YAP/TAZ stabilization and activity is frequent in a variety of human cancers, altogether making YAP/TAZ ideal therapeutic targets for cancer. However, efforts in this direction are frustrated by the fact that the Hippo cascade is largely undruggable: the Hippo kinases MST1/2 and LATS1/2 in fact negatively regulate YAP/TAZ, causing their cytoplasmic sequestration and degradation. That said, it recently emerged how YAP/TAZ regulation goes well beyond the core Hippo kinases, opening unexplored routes for therapeutic intervention. The work presented in this thesis aimed to identify small molecules able to inhibit the oncogenic properties of YAP and TAZ in breast cancer by means of FDA-approved "drug repositioning" strategy. Since the mechanisms of action of FDA-approved compounds are well known, we reasoned that the identification of new YAP/TAZ inhibitors could also unveil new layers of Hippo pathway regulation. Importantly, the identified lead-compound could be immediately tested in clinical trial for breast cancer patients with high levels of YAP/TAZ.

RESULTS

The Mevalonate pathway promotes YAP/TAZ nuclear localization and activity

Aiming at identifying small-molecule inhibitors of YAP/TAZ function, we performed a high-content, fluorescence microscopy-based, high-throughput screening using a library of FDA-approved drugs composed by a collection of 640 clinically-used compounds with known and well-characterized bioactivity, safety and bioavailability. Cytoplasmic YAP/TAZ localization has been largely used as highly reliable read-out of their inhibition in living cells (Zhao et al., 2007). We thus monitored the effect on YAP/TAZ subcellular localization of each compound of the library added at two different concentrations (1 and 10μM) to the culture medium of the breast cancer cell line MDA-MB-231 (Fig. 13a). YAP/TAZ localization was detected by immunofluorescence and analysis of their subcellular localization was quantified through automated image analysis. When cultured at low density, cells displayed a robust YAP/TAZ nuclear localization, unaffected by the vast majority of compounds. However, we could identify about 30 drugs that significantly induced cytoplasmic relocalization of YAP/TAZ. The majority of these hits were adrenergic agonists, a finding consistent with the recent identification of some GPCR agonists as YAP/TAZ inhibitors (Yu et al., 2012). Strikingly, the compounds with the strongest YAP/TAZ inhibitory effect were all the five statins present in the library (Fig. 13a and Fig. 20, b and c). Cerivastatin was the strongest hit showing high activity at both 1 and 10 μM and was selected, together with Simvastatin, for further analysis.

Statins are a class of drugs largely used to lower the cellular cholesterol levels in patients with hypercholesterolemia by inhibiting the enzyme HMG-CoA-reductase (HMGCR)(Clendening and Penn, 2012; Demierre et al., 2005; Larsson, 1996). This enzyme catalyzes the production of mevalonic acid (MVA), which represents the rate-limiting step of cholesterol biosynthesis (the mevalonate pathway) (Fig. 13b). To test if the mevalonate pathway is a general regulator of YAP/TAZ in different cellular contexts, we analyzed the effect of Cerivastatin on the subcellular localization of YAP/TAZ in multiple cell lines, derived from six different tumor types. Inhibition of the mevalonate pathway caused a dramatic accumulation of YAP/TAZ in the cytoplasm of all the cell lines tested (Fig. 13, c and d and Fig. 20e). Similar results were obtained by treating cells with Simvastatin (Fig. 20d). Importantly, nuclear YAP/TAZ

23

localization was completely rescued by addition of mevalonic acid to the culture medium, thus bypassing statin-mediated HMGCR inhibition. Taken together, these results suggested an unsuspected relevance of the mevalonate pathway in sustaining YAP/TAZ activity, as well as a role for statins as YAP/TAZ inhibitors. To support this notion, we next tested if inhibition of the mevalonate pathway was sufficient to block nuclear YAP/TAZ activity. To this end, we first used a synthetic YAP/TAZ responsive luciferase reporter (8XGTII-lux) as read-out of their transcriptional function (Dupont et al., 2011). As showed in Figure 13e, statins inhibited YAP/TAZ activity in all the cell lines tested (MDA-MB-231, H1299 and HCT-116 cells), in a mevalonic acid-dependent manner. YAP/TAZ inhibition was obtained also upon *Hmgcr* depletion by RNAi (Fig. 21a) supporting the notion that an active mevalonate pathway is required for YAP/TAZ function. We also monitored the effect of Cerivastatin on well-established YAP/TAZ endogenous target genes (*Birc5, Ankrd1, Cyr61, Ctgf*); as shown in Figure 13f, the results demonstrated that the mevalonate pathway is required to sustain the YAP/TAZ gene expression program.

Geranylgeranyl pyrophosphate mediates mevalonate-dependent YAP/TAZ nuclear localization and activity

The mevalonate pathway is crucial for the biosynthesis of cholesterol but also of other crucial metabolites (see Fig. 13b)(Goldstein and Brown, 1990). To gain insights into the molecular mechanisms controlling YAP/TAZ cytoplasmic localization after HMGCR inhibition, we dissected the mevalonate pathway by inhibiting distinct enzymes in order to identify the specific metabolic intermediate involved in YAP/TAZ regulation (Fig. 13b). Interestingly, only the farnesyl diphosphate synthase inhibitor (bisphosphonate) Zoledronic Acid (ZA) and the geranylgeranyl transferase inhibitor GGTI-298 were able to reproduce the effect of statins on YAP/TAZ localization, while the inhibition of squalene synthase (with YM-53601) or of farnesyl-transferase (with FTI-227) had no effect (Fig. 14a and Fig. 21, b and c). Adding back mevalonic acid could not rescue the inhibitory effect of ZA and GGTI-298, consistent with these inhibitors acting downstream to the HMGCR enzyme (Fig. 14a). In contrast, re-exposure to geranylgeranyl pyrophosphate (GGPP), but not to farnesyl phyrophosphate (FPP) or

squalene, rescued statin and bisphosphonate-dependent inhibition of YAP/TAZ, both in terms of localization and transcriptional activity (Fig. 14b-d and Fig. 21d-g). These findings indicated that protein geranylgeranylation was responsible for the positive effect of the mevalonate pathway on YAP/TAZ activity.

Activation of YAP/TAZ by geranylgeranyl pyrophosphate is mediated by Rho-GTPases

Asking what geranylgeranylated factors may foster YAP/TAZ activity, we focused on the Rho family of GTPases, recently identified as one of the key upstream inputs that, by modulating actin cytoskeleton, positively control YAP/TAZ activity (Dupont et al., 2011; Sansores-Garcia et al., 2011; Wada et al., 2011; Yu et al., 2012). The enzymatic activity of Rho-GTPases relies on their ability to properly localize at the plasma membrane, a process promoted by the transfer of a geranylgeranyl moiety to a C-terminal Cysteine residue. We thus aimed to determine whether the GGPP produced by the mevalonate pathway regulated YAP/TAZ activity through activation of Rho-GTPases. We used the activity of RhoA as proof-of-principle, and assayed if statins were able to affect the activity of transfected RhoA by reducing its geranylgeranylation and membrane localization. For these experiments we compared cells expressing GFP and GFP-RhoA fusion protein; as shown in Fig. 15a, GFP alone accumulated in the nucleus, while GFP-RhoA localized in Golgi, ER vesicles and plasma membranes (as previously reported) (Casey and Seabra, 1996; Keller et al., 2005). After statin treatment, GFP-RhoA was no longer localized at cellular membranes, resulting indistinguishable from GFP alone (Fig. 15a and Fig. 22, a and d)(Keller et al., 2005). At the endogenous level, Cerivastatin increased the cytoplasmic pool of RhoA, with consequent reduction of GTP-bound, active RhoA as revealed by a rhotekin assay (Fig. 22, b and e). Adding back GGPP to Cerivastatin-treated cultures rescued RhoA membrane-bound localization and activity (Fig. 15a and Fig. 22, a, b and e). This result, together with the effects of statins on YAP/TAZ activity shown above, is consistent with the notion that statins inhibit YAP/TAZ by depleting cells of GGPP and, as such, of active Rho-GTPases.

To test whether geranylgeranylation sustains YAP/TAZ through Rho-GTPases, we decided to experimentally bypass the requirement of geranylgeranylation for Rho membrane attachment, and verify if the activity of YAP/TAZ becomes resistant to geranylgeranyl transferase inhibition. For this, we generated a mutant GFP-RhoA bearing a C-terminal consensus for farnesylation (GFP-RhoA-F), instead of its natural geranylgeranylation motif (Fig. 15b). Indeed, farnesylation is known to serve as alternative route for membrane localization of small GTPases (e.g., Ras)(Casey and Seabra, 1996). As shown in Figure 15c, GFP-RhoA-F efficiently localized on membranes and sustained YAP/TAZ nuclear localization and transcriptional activity in a manner independent of geranylgeranyl transferase but still dependent on HMGCR (Fig. 15c-f and Fig. 22f and 23a-e). Together, these findings suggest that the mevalonate pathway promotes YAP/TAZ activity by providing the geranylgeranyl pyrophosphate essential for Rho-GTPases membrane localization and activation.

The Mevalonate pathway regulates YAP/TAZ phosphorylation and activity independently of LATS kinases

At the protein level, inhibition of Rho GTPases using the established C3 inhibitor leads to YAP phosphorylation and TAZ degradation thus inhibiting their activity (Dupont et al., 2011; Yu et al., 2012). In keeping with the idea that the mevalonate pathway regulates YAP/TAZ through Rho, treatment with Cerivastatin or ZA also caused YAP phosphorylation in S127 and TAZ instability (Fig. 16a and Fig. 21g). To test the functional relevance of YAP phosphorylation upon of Rho inhibition, we carried out luciferase assays in cells depleted of endogenous YAP/TAZ and reconstituted with either wild-type YAP or a version of YAP bearing S to A substitutions in the main YAP phosphorylation sites (5SA-YAP) including the LATS targeted sites S127 and S381(Zhao et al., 2010). As shown in Figure 16c, wild-type, but not phosphomutant YAP, is inhibited by coexpression of C3. Thus, YAP/TAZ phosphorylation is instrumental for their regulation downstream of Rho.

LATS1/2 are the main kinases responsible for YAP phosphorylation and inactivation. However, loss of LATS1/2 by independent siRNAs was unable to rescue the inhibitory effect of C3 (Fig. 16d and Fig. 21h). Similarly, LATS1/2 inactivation was

ineffective at inhibiting YAP phosphorylation and at rescuing the YAP nuclear localization in Cerivastatin-treated cells (Fig. 16, b and e). By comparison, the same LATS1/2 knockdowns were sufficient to quantitatively rescue a similar degree of inhibition caused by overexpression of the LATS1/2 inducer NF2 (Fig. 16, c and d)(Aragona et al., 2013). These results demonstrate that Rho signaling controls YAP phosphorylation by inhibiting a yet unknown protein kinase.

The control of YAP/TAZ activity by Rho has been so far equated to the effects of Rho over the F-actin cytoskeleton, a fundamental input for YAP/TAZ activity. However, the requirements of F-actin and Rho appear different. As shown in Figure 16 f and g, lowering mechanical signals by inhibiting F-actin polymerization by treatment with latrunculin A - or plating cells on a soft extracellular matrix - inhibits YAP/TAZ activity in a manner that is not only independent on the LATS1/2 activity but also independent from YAP/TAZ phosphorylation, as previously reported (Aragona et al., 2013; Dupont et al., 2011). As such, we conclude that Rho-activity defines a pathway for YAP/TAZ regulation distinct from YAP/TAZ activation by the cytoskeleton. Indeed, statin doses unable to affect F-actin polymerization (Fig. 22c) or cell spreading are still sufficient to blunt Rho function and YAP/TAZ activity (Fig. 13c and 15a). Conversely, higher doses of statin that do affect cell morphology and phalloidin staining cannot be overtly rescued by phosphomutant-YAP (see below, Fig. 17a).

The Mevalonate pathway is required for YAP/TAZ biological activities

Substantial evidences in mouse tumor models indicate that mevalonate pathway inhibitors display tumor suppressive effects, a conclusion remarkably supported by recent epidemiological data in humans (Freed-Pastor et al., 2012; Nielsen et al., 2013). YAP and TAZ have been linked to cancer cell proliferation, migration and cancer stem cells self renewal (Cordenonsi et al., 2011; Lei et al., 2008). We thus tested the effect of statins on these biological activities. As shown in Figure 17a, Cerivastatin showed antiproliferative and apoptotic effects in a mevalonate-dependent manner. Importantly, sustaining YAP/TAZ activity through overexpression of constitutively active YAP-5SA (that upon statin treatment remains nuclear, Fig. 21i) was sufficient to counteract these

effects (Fig. 17a and Fig. 23f-h). Treatments with higher doses of Cerivastatin are instead only partially rescued by YAP-5SA.

We next tested if geranylgeranylation inhibition was able to counteract cell motility induced by YAP-overexpression. Both overexpression of YAP-WT and 5SA resulted in a marked increase in cell migration as evaluated by a wound-healing assay. GGTI-treatment blunted the effects of YAP-WT but was less effective in YAP-5SA expressing cells (Fig. 24, a and b). Moreover, treatment with statins strongly reduced the self-renewal capability of cancer stem cells as monitored by the capacity to generate mammospheres from individual cells (Fig. 17b). Remarkably, mammospheres formation in cells treated with titrated doses of Cerivastatin was rescued by overexpression of TAZ-S89A (Fig. 17c), suggesting that statins oppose self-renewal of cancer stem cells subpopulations by inhibiting nuclear TAZ activity (Cordenonsi et al., 2011).

To demonstrate that mevalonate pathway could regulate YAP/TAZ activity *in-vivo*, we used Drosophila as an established model system in which overexpression of the YAP/TAZ orthologue *Yki* causes organ overgrowth (Zhao et al., 2007) (Fig. 17, d and e). Specifically, we used the GAL4/UAS system for targeted *Yki* gene overexpression in the fly eyes (Ren et al., 2010). Strikingly, statins (delivered through the food of developing flies) efficiently rescued eye overgrowth induced by Yki (Fig. 17, d and e). Similar results were obtained after silencing of the endogenous geranylgeranyl transferase (*ggt-I*) (Fig. 17, d and e). Accordingly, the expression of the two well-established Yki target genes, *Diap-1* and *Expanded*, was strongly inhibited by both statins treatment and *ggt-I* silencing (Fig. 17f). These results indicate that the mevalonate pathway is essential for Yki activity *in-vivo*.

Consistently, the protein levels of both TAZ and its target gene CTGF were reduced in tumors arising from MDA-MB-231 cells (that rely on YAP/TAZ for proliferation; Fig. 23i) orthotopically injected in the flank of immunocompromized mice and treated with zoledronic acid. This was also accompanied by a significative reduction of tumor growth (Fig. 17, g and h and Fig. 23j).

The Mevalonate pathway master regulators SREBPs and mutant-p53 regulate YAP/TAZ activity in cancer cells

Having identified the mevalonate pathway as regulator of YAP/TAZ function, we next aimed to investigate the upstream regulators of this metabolic control. The enzymes of the mevalonate pathway are under transcriptional control of sterol regulatory element-binding proteins SREBPs (Horton et al., 2002). SREBP1 and SREBP2 exist as latent membrane-bound precursors: when cells need sterols - for example after reduction of lipoprotein concentration in plasma - SREBPs are unleashed from membranes by proteolytic cleavage, and enter in the nucleus to transcribe the enzymes of the mevalonate pathway and thus maintain cellular lipids homeostasis (Brown and Goldstein, 1997).We reasoned that SREBPs may regulate YAP/TAZ functions by modulating the mevalonate pathway. To test this, we activated endogenous SREBPs by maintaining cells in medium with serum containing low levels of lipoproteins (2% Ultroser), forcing cells to rely upon their own *de-novo* synthesis for cholesterol and isoprenoids(Parsons et al., 2006) (Fig. 25, a and g). Activation of mevalonate pathway under these conditions was able to increase the activity of YAP/TAZ both in MDA-MB-231 and in confluent-plated MCF10A MII cells (Fig. 25b-e). Strikingly, simultaneous inhibition of SREBP1 and SREBP2 by siRNA transfection caused a marked reduction of YAP/TAZ target genes expression due to mevalonate-dependent reduction of YAP/TAZ nuclear localization (Fig. 18, a and b). Similar results were obtained by pharmacological inhibition of SREBPs cleavage by Fatostatin (Kamisuki et al., 2009) (Fig. 18c and Fig. 25, f and g). Similarly to mevalonate inhibition, loss of SREBPs activity limits cell proliferation and overexpression of YAP-5SA efficiently rescued this effect (Fig. 18d).

These results indicate that the SREBPs-mevalonate axis is a relevant input for YAP/TAZ activity and implicate that aberrant SREBPs function could lead to unscheduled activation of YAP/TAZ. In breast cancer cells, oncogenic mutant-p53 acts as a positive transcriptional cofactor for SREBPs, leading to elevated expression of mevalonate enzymes (Freed-Pastor et al., 2012) (Fig. 26a). Notably, depletion of mutant-p53 in MDA-MB-231 cells inhibits YAP/TAZ activity as judged by the reduction in nuclear localization of YAP/TAZ and reduced transcriptional activity (Fig.

18e-h and Fig. 26, b and c). Conversely overexpression of mutant-p53 in p53-null H1299 cells activated YAP/TAZ, but only when the mevalonate pathway was concomitantly active (Fig. 18i), a finding consistent with mutant-p53 intercepting YAP/TAZ through the SREBP/mevalonate axis.

The metabolic link between mutant-p53 and YAP/TAZ was further demonstrated through analyzing levels of YAP/TAZ gene signatures, together with that of mevalonate pathway genes in a TGCA dataset of human breast cancer samples (Cerami et al., 2012). After patient stratification based on the p53 mutational status, we found that samples expressing missense mutant-p53 displayed higher activation of mevalonate (Freed-Pastor et al., 2012) and YAP/TAZ (Zhang et al., 2009) pathways as compared to wild-type p53 expressing patients (Fig. 18j and Table 1). Similar results were obtained by first stratifying tumors with mutant-p53 transcriptional signature (Girardini et al., 2011) (Fig. 26d and Table 1). These evidences suggest that YAP/TAZ could be a relevant executor of the pro-oncogenic functions of mutant-p53.

DISCUSSION

Tissue growth necessarily requires a tight coordination between metabolism and pathways controlling cell proliferation. The mechanisms of this interplay are only starting to be elucidated. Here we reveal that the mevalonate pathway has profound impact on the function of YAP and TAZ, master transcriptional regulators of normal organ growth and tumor growth. Inhibition of the mevalonate pathway impairs YAP/TAZ-dependent transcriptional responses in a variety of cell types and biological assays, impacting on cell proliferation, organ growth, and self-renewal of cancer stem cell populations. SREBPs factors are upstream transcriptional regulators for many of the enzymes of the mevalonate cascade, and, consistently, SREBPs are essential for full YAP/TAZ activity. Mechanistically, we linked the mevalonate pathway to activation of Rho small GTPases by geranylgeranylation, reduction of YAP/TAZ inhibitory phosphorylation and sustained YAP/TAZ nuclear accumulation (Fig. 19).

Intriguingly, the Rho-dependent YAP/TAZ regulatory pathway here identified can be experimentally uncoupled from two of the main inputs affecting YAP/TAZ activation, namely, the mechanical/cytoskeletal pathway and the NF2/Hippo cascade. Indeed, a phosphorylation mutant form of YAP (YAP 5SA) is resistant to Rho inhibition or NF2/Hippo activation, but is still inhibited by low mechanical stresses (i.e., soft ECM, F-actin disruption). This indicates that mechanotransduction operates with a modality of YAP/TAZ regulation that is primarily independent of phosphorylation, while the Rho-YAP/TAZ pathway acts by inhibiting YAP/TAZ phosphorylation. The identity of the relevant kinase remains an open issue. It has been recently reported that LATS1/2 purified from cells with inhibited Rho activity display enhanced in vitro kinase activity on recombinant YAP; however, the functional requirement of LATS1/2 downstream of Rho-GTPases was not investigated (Yu et al., 2012). Our results, and those of a recent related study by Wang et al.(Wang et al., 2014), do not support a role for LATS1/2 as the kinase downstream of Rho GTPases.

These results imply that Rho-GTPases inhibit a yet unknown kinase that targets YAP/TAZ in the same serines targeted by LATS1/2.

Rho GTPases are well known organizers of the F-actin cytoskeleton. Indeed, the relevance of Rho signaling for YAP/TAZ function was originally discovered in cells

31

treated with the C3 toxin inhibitor in the context of studies centered on YAP/TAZ regulation by mechanical forces and cytoskeletal tension (Dupont et al., 2011). In light of these associations, it has been recently implied that the mevalonate pathway regulates YAP/TAZ through F-actin. After functional evaluations, our results do not fully support these conclusions, as statins can inhibit YAP/TAZ at concentrations barely effective on cytoskeletal integrity. Collectively, the data support the view that Rho GTPases are only one segment, required but not sufficient, of a complex network by which the cytoskeleton impinges on YAP/TAZ activity through distinct mechanisms. That said, cytoskeletal tension is essential for YAP/TAZ function, to the extent that loss of this input – as in cells treated with the F-actin inhibitor latrunculinA or cultured in soft ECMs - opposes YAP/TAZ function in a dominant manner. As such cytoskeleton disruption overcome any known modality of YAP/TAZ activation, whether cell mechanics, Rho activation, loss of Hippo signaling, or Wnt growth factors (Aragona et al., 2013; Dupont et al., 2011).

The SREBP/mevalonate pathway is deeply connected to a number of aspects of cell biology including lipid metabolism, cell structure, nutrient levels and cell signalling (Brown and Goldstein, 1997). As such, the SREBP/mevalonate pathway may act as an hub for other metabolic and non-metabolic signals, in order to finely adjust the levels of YAP/TAZ activation to the cell needs (Fig. 19). This has implication in cancer, where metabolic control is corrupted by oncogenes and YAP/TAZ are aberrantly active. As a paradigm, we have shown that missense mutant-p53 conspires with SREBP to trigger unscheduled activation of YAP/TAZ in both cancer cells and human primary tumors; as such, YAP/TAZ may represent critical effector of the pro-oncogenic function of mutant p53 (Fig. 19). In line, statins have been recently reported to inhibit YAP-dependent transcription of the pro-metastatic gene RHAMM in MDA-MB-231 breast cancer cells, expressing mutant-p53 (Girardini et al., 2011; Wang et al., 2014).

It is important to emphasize that, based on our results, other cellular signalling known to regulate SREBP activity and, in general, the mevalonate pathway could, in principle, have profound impact on YAP/TAZ biological activities. In this regard, oncogenic factors such as PI3K, mTOR and HIF1 may take advantage of mevalonate-YAP/TAZ axis to exert their pro-survival activities. On the contrary, oncosuppressor proteins such as AMPK, LKB1 and Fbw7, by restraining SREBP activation, could indirectly blunt YAP/TAZ nuclear activities. In line, the use of drugs known to regulate all the above-mentioned factors (e.g. Rapamycin, Wortmannin, Metformin, AICAR…) could be

another route to pharmacologically counteract the aberrant YAP/TAZ activation in cancer cells.

Clendening et al., recently put forward the provocative idea that dysregulation of the mevalonate pathway, and expression of HMGCR itself, may have sufficient oncogenic potential to drive malignant progression and anchorage-independent growth, in line with the correlation of high HMGCR mRNA levels with poor patient prognosis and reduced survival (Clendening et al., 2010). Our results suggest that aberrant YAP/TAZ may be the most likely candidate mediators of these responses, as we show that statins, bisphosphonates and GGT-inhibitors work through YAP/TAZ regulation, and that these drugs have potential to target YAP/TAZ malignant effects in cancer cells.

In sum, the discovery that YAP/TAZ is controlled by mevalonate and Rho-GTPases reveals unexpected connections between metabolism, proliferation and stemness (Piccolo et al., 2013).

EXPERIMENTAL PROCEDURES

Reagents and plasmids:

The library of FDA-approved drugs (Screen-Well FDA-Approved Drug Library, 640 chemical compounds dissolved at 10mM in DMSO) was obtained from Enzo Life Sciences (Enzo Life Sciences Inc.,Plymouth Meeting, PA, USA).

The following compounds were purchased from Sigma Aldrich: Cerivastatin (SML0005), Simvastatin (S6196), FTI-277 (F9803), GGTI-298 (G5169), DL-Mevalonic Acid 5-Phosphate (79849), Geranylgeranyl Pyrophosphate (#G6025), Farnesyl pyrophosphate (F6892), Squalene (S3626), Zoledronic Acid (SML0223), Fatostatin (F8932). YM-53601 (18113) was purchased from Cayman. LatrunculinA was previously described[13].

pEGFP-RhoA^{V14} was a kind gift from C. Schneider. The retroviral constructs (pLPC) coding for GFP-RhoA^{V14} (CLVL) and GFP-RhoA^{V14}-F (CVLS) were generated by PCR mutagenesis from pEGFP-RhoA^{V14}.

The sequences of primers used are reported in Table 2.

All constructs were confirmed by sequencing and used to generate stable clones of MDA-MB-231 and H1299 cells (Fig. 15e and f and Fig. 16, d and e).

8xGTII-Lux and the retroviral constructs coding for siRNA-resistant Flag-YAP-WT and Flag-YAP-5SA were previously described. NF2 is Addgene #19701. pcDNA3-p53R280K was previously described[26]. pRK5-C3 is a kind gift from A.Hall.

Cell Lines

MDA-MB-231, HCT116, MDA-MB-468, SKOV-3, HEK293A and PANC-1 were cultured in DMEM supplemented with 10% FBS (*Fetal bovine serum*), and antibiotics. MCF10A MII cells were previously described[4] and were cultured in DMEM/F12 (LONZA) with 5% HS (horse serum), glutamine and antibiotics, freshly supplemented with insulin, EGF, hydrocortisone, and cholera toxin. H1299 cells were cultured in RPMI 1640 with 10% FBS and antibiotics. Cells have been authenticated by STR profiling and are free from mycoplasma contamination. Treatment with inhibitors: Zoledronic Acid (ZA) (50μM), FTI-277 (1μM), YM-53601 (1μM), GGTI-298 (1μM) alone or with mevalonic acid (0.5 mM), GGPP, FPP, Squalene (20μM). Experiments in Fig. 18 and Fig. 25 and 26 were performed by maintaining cells in DMEM supplemented with 2% Ultroser G (Pall BioSpera) for 48h in order to ensure that cells

rely on *de novo* lipid synthesis induced by SREBPs proteins.

High Content Screening

For the screening experiments, MDA-MB-231 cells (3.0×10^3 per well) were seeded on black clear-bottom 384-well plates (PerkinElmer). Twenty-four hours later, the FDA-approved drugs were transferred robotically from library stock plates (0.1mM and 1mM in DMSO) to the plates containing the cells; controls were added to columns 1, 2, 23 and 24 of each plate. Cells were fixed at 48 h after plating, i.e. 24h after addition of drugs, and processed immediately for immunofluorescence. Briefly, cells were fixed with 4% paraformaldehyde for 15 min, permeabilized with 0.5% Triton X-100 in phosphate buffered saline (PBS) solution for 10 min, followed by 30 min blocking in 3% FBS. Cells were then incubated with a mouse antibody against YAP/TAZ (Santa Cruz Biotechnology) diluted in blocking solution for 1 h. Cells were further washed with PBS and incubated for 1h with a secondary antibody conjugated to Alexa Fluor-594 (Life Technologies), and stained with Hoechst 33342 (Life Technologies).

Image acquisition was performed using an ImageXpress Micro automated high-content screening fluorescence microscope (Molecular Devices) at a 10x magnification; a total of 16 images were acquired per wavelength, well and replicate, corresponding to ca. 4,500 cells analyzed per experimental condition and replicate. Image analysis to identify cells presenting predominantly nuclear YAP/TAZ localization was performed using the 'Multi-Wavelength Translocation' application module implemented in MetaXpress software (Molecular Devices).

Screening was performed in duplicate, at two drug concentrations (1μM and 10μM); final concentration of DMSO in the culture medium was 1% (v/v) for all experimental conditions. The screening was performed at the ICGEB High-Throughput Screening Facility (http://www.icgeb.org/high-throughput-screening.html).

Transfections

siRNA transfections were performed with Lipofectamine RNAi-MAX (Life technologies) in antibiotics-free medium according to manufacturer instructions. Sequences of siRNAs are reported in Table 2.

YAP/TAZ siRNA, LATS1-2 siRNA and oligo sequences for qRT-PCR were previously described.

Negative control siRNA was: AllStars negative control siRNA Qiagen 1027281.

DNA transfections were done with Lipofectamine® LTX & Plus Reagent (Invitrogen) or Lipofectamine 2000 (for H1299 cells) (Life Technologies) according to manufacture instructions. Lentiviral particles were prepared by transiently transfecting HEK293T cells with lentiviral vectors together with packaging vectors (pMD2-VSVG and psPAX2) using the standard calcium-phosphate method. Retroviral packaging was made by calcium phosphate transfection of 293-GP packaging cells with the appropriate plasmids in combination with pMD2ENV coding for envelope proteins, and collected 48 hours later. Infected cells were selected with Puromycin 2 mg/ml.

Luciferase Assay

Luciferase assays were performed in MDA-MB-231 cells, in HCT-116 cells and in H1299 cells with the established YAP/TAZ-responsive reporter 8xGTII-Lux. Cell lysates were analysed using Dual-Luciferase Reporter Assay System (Promega, cod. E1910). Luciferase reporters (300 ng/cm^2) were transfected together with CMV-Renilla (100 ng/cm^2) to normalize for transfection efficiency. pcDNA3 and pcDNA3-p53R280K plasmids were co-transfected at 100 ng/cm^2. For luciferase assays in siRNA transfected cells, siRNA transfection was achieved first and, after 48h, transfection of plasmid DNA was performed. Cells were harvested 24h after DNA transfection.

YAP/TAZ nuclear localization

For the quantification of the number of cells with nuclear YAP/TAZ at least 300 cells from different fields were counted.

Viability assay

Cells (10^4 per well) were plated in 96-well plates and treated as indicated. Cell viability was assayed with ATPlite (Perkin Elmer) or WST-1 (Promega) according to manufacturer instructions using *EnSpire* Multilabel Reader (Perkin Elmer).

Wound-healing assay

1,5 million of cells were plated in 3cm well plates and the monolayer of cells were wounded with a sterile plastic tip. Cell migration was observed 12h later by microscopy.

Mammosphere Assay

Mammosphere assays were performed as previously described (Cordenonsi et al., 2011).

Antibodies

The antibodies used for Western blot and immunofluorescence are: Anti-YAP/TAZ (1:1,000 for western blot, 1:100 for immunofluorescence) is sc101199 (Santa Cruz Biotechnology), anti-p53 (1:1,000) is DO-1 (Santa Cruz Biotechnology), anti-actin (1:2,000) is C11 (Sigma), anti-BIRC-5 (1:1,000) is sc-10811 (Santa Cruz Biotechnology), anti-Cyr61 (1:1,000) is sc-13100 (Santa Cruz Biotechnology), anti SREBP-2 (1:1,000) is 10007663 (Cayman) and Anti-ANKRD1 (1:1,000) is 11427-1-AP (Proteintech (DBA), anti-pYAP (1:1,000) (Ser127) is 4911S (Cell Signaling), anti-TAZ (1:1,000) is HPA007415 (Sigma). Anti-PARP-85 (1:1,000) is TB273 (Promega), anti-FLAG (1:1,000) is F3165 (Sigma), anti-H3 (1:10,000) is ab1791 (Abcam), anti-Dlg5 (1:1,000) is AO8971 (Sigma), anti-vinculin (1:5,000) is V4505 (Sigma) and anti-Tubulin (1:5,000) is T5168.

Quantitative Real-Time PCR

Cells were harvested in Qiazol lysis reagent (Qiagen) for total RNA extraction, and contaminant DNA was removed by DNase treatment. Retrotranscription was performed with Quantitect reverse transcription kit (Qiagen). The obtained cDNA was properly diluted and used in qRT-PCR reactions performed with SsoAdvanced SYBR Green Supermix (Biorad) using CFX96 Touch Real-Time PCR Detection System and analyzed with Biorad CFX Manager software. Each experiment was performed at least three times. Expression levels are always given relative to histone H3. PCR oligo sequences for human samples are reported in Table 2.

Immunofluorescence and Western Blot

Immunofluorescence staining was performed as previously described. Briefly, cells were fixed in 4% paraformaldehyde for 10 min, whashed in PBS, permeabilized with Triton 0.1% for 10 min and blocked in PBS FBS 3% for 30 min. Antigen recognition was done by incubating primary antibody for 1h at 37°C and with Goat anti-mouse Alexa Fluor 568 (Life Technologies) as secondary antibody for 30 min a 37°C. Nuclei were counterstained with Hoechst 33342 (Life Technologies).

Western blot (WB) analysis was performed as previously described[31].

Isolation of GTP-loaded RhoA GTPase

The GTP-loaded form of RhoA were pulled down with GST-RHOTEKIN beads (Cytoskeleton, Denver, CO, USA), according to the manufacturer's instructions.

Subcellular fractionation

Cells were lysed on 10cm plates using 500uL of buffer (250mM Surcose, 20mM HEPES, 10mM KCl, 1,5mM $MgCl_2$, 1mM EDTA, 1mM EGTA) and kept in ice for 20min. Nuclear pellet was obtained after centrifugation at 720G for 5min and washed and lysed with standard lysis buffer RIPA. The supernatant (cytoplasmic fraction) was collected and sample buffer was added. Histone H3 was used as nuclear marker while tubulin as cytoplasmic marker.

Biostatistical analysis

Gene expression data, TP53 mutation status and clinical annotation for Breast Cancer samples (TCGA dataset) were obtained from the Memorial Sloan Kettering Cancer Genomics Portal (http://www. cbioportal.org/public-portal; last accessed July 6, 2013). Starting from the Breast Invasive Carcinoma dataset (TCGA, Provisional, n=928) we selected the patients with only known TP53 status and in particular only the patients with TP53 wild type or with TP53 missense mutation, obtaining a subset of 657 samples. Each patient was classified having high or low levels of Mevalonate Pathway signature of YAP/TAZ signature and of ten genes signature as already described. The genes composing each signature are described in Table 1. Statististical independences between the different molecular conditions ware calculated by Pearson's chi-squared contingency table tests in R/Bioconductor environment (R Core Team (2013)). R: A

language and environment for statistical computing. R Foundation for Statistical Computing, Vienna, Austria. URL http://www.R-project.org/).

Gene expression and mutation data

For the gene expression data and mutation status we used the dataset "Breast Cancer project. 1002 cases" available at The Cancer Genome Atlas (TCGA, Nature in Press). Sequence files are in CGHub (https://cghub.ucsc.edu/). All other molecular, clinical and pathological data are available through the TCGA Data Portal (https://tcga-data.nci.nih.gov/tcga/). The data can be explored/analyzed easily through the cBio Cancer Genomics Portal (http://cbioportal.org)

Drosophila stocks and treatments

All the stocks were raised at 25°C on standard food. *UAS-ykiV5* (stock n. 28819), *GMR GAL4* (stock n. 9146), *beta ggt-I* RNAi (stock n. 34687), *y,w; T(2;3)B3, CyO: TM6B, Tb/Pin88K* (stock n. 2506), *w^{1118}/Dp(1;Y)y^{+}; CyO/nub^{1} b^{1} sna^{Sco}lt^{1} stw^{3}; MKRS/TM6B, Tb* (stock n. 3703) were supplied by Bloomington Stock Center. We used the balancer *CyO, TM6B (Tb)* to rebalance the *GMR GAL4* strain and to discriminate the *GMR GAL4 /+; UAS Yki V5/+* larvae. We used the strains n. 3703 and n. 2506 in the crosses to obtain the genotype *GMR GAL4/+; beta ggt-I RNAi/ UAS-ykiV5*.

The parental crosses were maintained for egg deposition on the food added with Simvastatin (Sigma) 2,5 mM. The progeny that over-expresses Yorkie performed the entire development on the same medium.

Preparation of adult Drosophila for Scanning Electron Microscopy

The adult flies were anesthetized with ether and twenty flies were fixed with 1% glutaraldehyde in PBS 1X for 30 min, washed with PBS 1X for three times and dehydrated through 2 X 30%, 2 X 50%, 2 X 70%, 2 X 90% and 2 x 100% ethanol. We performed the critical point drying and, after the drying run, the flies were metallized before being inserted into the SEM for observation and imaging.

E y e   m e a s u r e m e n t s

The eye areas were measured for 30 individuals of each genotype by means of an image analysis system (Leica QWIN 3) using a stereomicroscope (Leica MZ12, 4X magnification). We calculated the mean value of individual measurements, the error bars represent standard deviation. P values were calculated using an unpaired t test.

Drosophila total RNA extraction and qRT–PCR

Total RNA was extracted from 30 fly heads for each genotype using the RNAqueos-4 PCR Kit (AMBION) reagent following the manufacturer's protocol. To remove any DNA from the preparation, the samples were incubated with DNase I RNase free (AMBION) (1Umg^{-1} RNA) at 37°C for 30 minutes, in a total volume of 100µl. After this treatment, the enzyme was inactivated with the DNase inactivation reagent (AMBION). DNase-treated RNA was precipitated at -80°C overnight, and after centrifugation it was dissolved in 50µl of nuclease-free water.

For the first-strand cDNA synthesis, 5µg of total RNA were used as a template for oligonucleotide dT primed reverse transcription using SuperScript III RNaseH-reverse transcriptase (Invitrogen), according to manufacturer's instructions. Real-time RT–PCR was performed in the SmartCycler Real-time PCR (Cepheid) using SYBR green (Celbio) according to the manufacturer's protocol.

PCR oligo sequences are reported in Figure 21.

Mouse strain and animal care

For *in vivo* studies, one million of MDA-MB-231 cells were resuspended in 100 µl of DMEM, injected into the mammary fat of previously anesthetized 7 weeks old SCID female mice (1-3% isoflurane, Merial Italia S.p.A, Italy) as previously described. At day 12 after cell injection, mice were subjected to intravenous injection of zoledronic acid ([1-hydroxy-2- (1H-imidazoledronic acid-1-yl) ethylidene] (200µg/Kg body weight), every 4 days until the end of the experiment (day 40). The mice were used and housed in a specific pathogen-free (SPF) animal facility. Procedures involving animals and their care were performed in conformity with institutional guidelines (D.L. 116/92 and subsequent complementing circulars) and all experimental protocols were approved by the ethical Committee of the University of Padua (CEASA). Tumor growth at the

injection site was monitored by repeated caliper measurements. Tumor volume was calculated using the formula: tumor volume (mm3) = D × d2/2, where D and d are the longest and the shortest diameters, respectively. At day 40 the animals were sacrificed and the primary tumors were extracted and directly frozen in liquid nitrogen to perform molecular analyses.

Statistical analyses

No statistical method was used to predetermine sample size. The experiments were not randomized. For biochemical experiments we performed the experiments at least three independent times. Experiments for which we showed representative images were performed successfully at least 3 independent times. No samples or animal were excluded from the analysis. The investigators were not blinded to allocation during experiments and outcome assessment. All p values were two-tailed t-test and statistical significance was set at p=0.05. The variance was similar between groups that we compared.

REFERENCES

Adorno, M., Cordenonsi, M., Montagner, M., Dupont, S., Wong, C., Hann, B., Solari, A., Bobisse, S., Rondina, M. B., Guzzardo, V*., et al.* (2009). A Mutant-p53/Smad complex opposes p63 to empower TGFbeta-induced metastasis. Cell *137*, 87-98.

Ahern, T. P., Pedersen, L., Tarp, M., Cronin-Fenton, D. P., Garne, J. P., Silliman, R. A., Sorensen, H. T., and Lash, T. L. (2011). Statin prescriptions and breast cancer recurrence risk: a Danish nationwide prospective cohort study. J Natl Cancer Inst *103*, 1461-1468.

Alarcon, C., Zaromytidou, A. I., Xi, Q., Gao, S., Yu, J., Fujisawa, S., Barlas, A., Miller, A. N., Manova-Todorova, K., Macias, M. J*., et al.* (2009). Nuclear CDKs drive Smad transcriptional activation and turnover in BMP and TGF-beta pathways. Cell *139*, 757-769.

Aragona, M., Panciera, T., Manfrin, A., Giulitti, S., Michielin, F., Elvassore, N., Dupont, S., and Piccolo, S. (2013). A mechanical checkpoint controls multicellular growth through YAP/TAZ regulation by actin-processing factors. Cell *154*, 1047-1059.

Asthagiri, A. R., Parry, D. M., Butman, J. A., Kim, H. J., Tsilou, E. T., Zhuang, Z., and Lonser, R. R. (2009). Neurofibromatosis type 2. Lancet *373*, 1974-1986.

Attardi, L. D., and Jacks, T. (1999). The role of p53 in tumour suppression: lessons from mouse models. Cell Mol Life Sci *55*, 48-63.

Bao, Y., Nakagawa, K., Yang, Z., Ikeda, M., Withanage, K., Ishigami-Yuasa, M., Okuno, Y., Hata, S., Nishina, H., and Hata, Y. (2011). A cell-based assay to screen stimulators of the Hippo pathway reveals the inhibitory effect of dobutamine on the YAP-dependent gene transcription. J Biochem *150*, 199-208.

Barry, E. R., Morikawa, T., Butler, B. L., Shrestha, K., de la Rosa, R., Yan, K. S., Fuchs, C. S., Magness, S. T., Smits, R., Ogino, S.*, et al.* (2013). Restriction of intestinal stem cell expansion and the regenerative response by YAP. Nature *493*, 106-110.

Bartucci, M., Dattilo, R., Moriconi, C., Pagliuca, A., Mottolese, M., Federici, G., Benedetto, A. D., Todaro, M., Stassi, G., Sperati, F.*, et al.* (2014). TAZ is required for metastatic activity and chemoresistance of breast cancer stem cells. Oncogene.

Blandino, G., Levine, A. J., and Oren, M. (1999). Mutant p53 gain of function: differential effects of different p53 mutants on resistance of cultured cells to chemotherapy. Oncogene *18*, 477-485.

Bonovas, S., Filioussi, K., Tsavaris, N., and Sitaras, N. M. (2005). Use of statins and breast cancer: a meta-analysis of seven randomized clinical trials and nine observational studies. J Clin Oncol *23*, 8606-8612.

Bossi, G., Lapi, E., Strano, S., Rinaldo, C., Blandino, G., and Sacchi, A. (2006). Mutant p53 gain of function: reduction of tumor malignancy of human cancer cell lines through abrogation of mutant p53 expression. Oncogene *25*, 304-309.

Bossi, G., Marampon, F., Maor-Aloni, R., Zani, B., Rotter, V., Oren, M., Strano, S., Blandino, G., and Sacchi, A. (2008). Conditional RNA interference in vivo to study mutant p53 oncogenic gain of function on tumor malignancy. Cell Cycle *7*, 1870-1879.

Brown, M. S., and Goldstein, J. L. (1997). The SREBP pathway: regulation of cholesterol metabolism by proteolysis of a membrane-bound transcription factor. Cell *89*, 331-340.

Capdeville, R., Buchdunger, E., Zimmermann, J., and Matter, A. (2002). Glivec (STI571, imatinib), a rationally developed, targeted anticancer drug. Nat Rev Drug Discov *1*, 493-502.

Casey, P. J., and Seabra, M. C. (1996). Protein prenyltransferases. J Biol Chem *271*, 5289-5292.

Cauley, J. A., McTiernan, A., Rodabough, R. J., LaCroix, A., Bauer, D. C., Margolis, K. L., Paskett, E. D., Vitolins, M. Z., Furberg, C. D., and Chlebowski, R. T. (2006). Statin use and breast cancer: prospective results from the Women's Health Initiative. J Natl Cancer Inst *98*, 700-707.

Cerami, E., Gao, J., Dogrusoz, U., Gross, B. E., Sumer, S. O., Aksoy, B. A., Jacobsen, A., Byrne, C. J., Heuer, M. L., Larsson, E.*, et al.* (2012). The cBio cancer genomics portal: an open platform for exploring multidimensional cancer genomics data. Cancer Discov *2*, 401-404.

Clendening, J. W., Pandyra, A., Boutros, P. C., El Ghamrasni, S., Khosravi, F., Trentin, G. A., Martirosyan, A., Hakem, A., Hakem, R., Jurisica, I., and Penn, L. Z. (2010). Dysregulation of the mevalonate pathway promotes transformation. Proc Natl Acad Sci U S A *107*, 15051-15056.

Clendening, J. W., and Penn, L. Z. (2012). Targeting tumor cell metabolism with statins. Oncogene *31*, 4967-4978.

Cordenonsi, M., Zanconato, F., Azzolin, L., Forcato, M., Rosato, A., Frasson, C., Inui, M., Montagner, M., Parenti, A. R., Poletti, A.*, et al.* (2011). The Hippo transducer TAZ confers cancer stem cell-related traits on breast cancer cells. Cell *147*, 759-772.

DeBerardinis, R. J., Lum, J. J., Hatzivassiliou, G., and Thompson, C. B. (2008). The biology of cancer: metabolic reprogramming fuels cell growth and proliferation. Cell Metab *7*, 11-20.

Demierre, M. F., Higgins, P. D., Gruber, S. B., Hawk, E., and Lippman, S. M. (2005). Statins and cancer prevention. Nat Rev Cancer *5*, 930-942.

Diep, C. H., Zucker, K. M., Hostetter, G., Watanabe, A., Hu, C., Munoz, R. M., Von Hoff, D. D., and Han, H. (2012). Down-regulation of Yes Associated Protein 1 expression reduces cell proliferation and clonogenicity of pancreatic cancer cells. PLoS One *7*, e32783.

Dittmer, D., Pati, S., Zambetti, G., Chu, S., Teresky, A. K., Moore, M., Finlay, C., and Levine, A. J. (1993). Gain of function mutations in p53. Nat Genet *4*, 42-46.

Dobbelstein, M., and Moll, U. (2014). Targeting tumour-supportive cellular machineries in anticancer drug development. Nat Rev Drug Discov *13*, 179-196.

Dong, J., Feldmann, G., Huang, J., Wu, S., Zhang, N., Comerford, S. A., Gayyed, M. F., Anders, R. A., Maitra, A., and Pan, D. (2007). Elucidation of a universal size-control mechanism in Drosophila and mammals. Cell *130*, 1120-1133.

Doyle, B., Morton, J. P., Delaney, D. W., Ridgway, R. A., Wilkins, J. A., and Sansom, O. J. (2010). p53 mutation and loss have different effects on tumourigenesis in a novel mouse model of pleomorphic rhabdomyosarcoma. J Pathol *222*, 129-137.

Dupont, S., Morsut, L., Aragona, M., Enzo, E., Giulitti, S., Cordenonsi, M., Zanconato, F., Le Digabel, J., Forcato, M., Bicciato, S., *et al.* (2011). Role of YAP/TAZ in mechanotransduction. Nature *474*, 179-183.

Edwards, P. A., Tabor, D., Kast, H. R., and Venkateswaran, A. (2000). Regulation of gene expression by SREBP and SCAP. Biochim Biophys Acta *1529*, 103-113.

Fan, R., Kim, N. G., and Gumbiner, B. M. (2013). Regulation of Hippo pathway by mitogenic growth factors via phosphoinositide 3-kinase and phosphoinositide-dependent kinase-1. Proc Natl Acad Sci U S A *110*, 2569-2574.

Fang, L., Lee, S. W., and Aaronson, S. A. (1999). Comparative analysis of p73 and p53 regulation and effector functions. J Cell Biol *147*, 823-830.

Freed-Pastor, W. A., Mizuno, H., Zhao, X., Langerod, A., Moon, S. H., Rodriguez-Barrueco, R., Barsotti, A., Chicas, A., Li, W., Polotskaia, A.*, et al.* (2012). Mutant p53 disrupts mammary tissue architecture via the mevalonate pathway. Cell *148*, 244-258.

Gaiddon, C., Lokshin, M., Ahn, J., Zhang, T., and Prives, C. (2001). A subset of tumor-derived mutant forms of p53 down-regulate p63 and p73 through a direct interaction with the p53 core domain. Mol Cell Biol *21*, 1874-1887.

Genevet, A., Wehr, M. C., Brain, R., Thompson, B. J., and Tapon, N. (2010). Kibra is a regulator of the Salvador/Warts/Hippo signaling network. Dev Cell *18*, 300-308.

Girardini, J. E., Napoli, M., Piazza, S., Rustighi, A., Marotta, C., Radaelli, E., Capaci, V., Jordan, L., Quinlan, P., Thompson, A.*, et al.* (2011). A Pin1/mutant p53 axis promotes aggressiveness in breast cancer. Cancer Cell *20*, 79-91.

Goldstein, J. L., and Brown, M. S. (1990). Regulation of the mevalonate pathway. Nature *343*, 425-430.

Goodman, L. S., Wintrobe, M. M., and et al. (1946). Nitrogen mustard therapy; use of methyl-bis (beta-chloroethyl) amine hydrochloride and tris (beta-chloroethyl) amine hydrochloride for Hodgkin's disease, lymphosarcoma, leukemia and certain allied and miscellaneous disorders. J Am Med Assoc *132*, 126-132.

Gruenbacher, G., and Thurnher, M. (2014). Mevalonate metabolism in cancer. Cancer Lett.

Gualberto, A., Aldape, K., Kozakiewicz, K., and Tlsty, T. D. (1998). An oncogenic form of p53 confers a dominant, gain-of-function phenotype that disrupts spindle checkpoint control. Proc Natl Acad Sci U S A *95*, 5166-5171.

Guo, X., Keyes, W. M., Papazoglu, C., Zuber, J., Li, W., Lowe, S. W., Vogel, H., and Mills, A. A. (2009). TAp63 induces senescence and suppresses tumorigenesis in vivo. Nat Cell Biol *11*, 1451-1457.

Gupta, S. C., Sung, B., Prasad, S., Webb, L. J., and Aggarwal, B. B. (2013). Cancer drug discovery by repurposing: teaching new tricks to old dogs. Trends Pharmacol Sci *34*, 508-517.

Halder, G., and Johnson, R. L. (2011). Hippo signaling: growth control and beyond. Development *138*, 9-22.

Hamaratoglu, F., Willecke, M., Kango-Singh, M., Nolo, R., Hyun, E., Tao, C., Jafar-Nejad, H., and Halder, G. (2006). The tumour-suppressor genes NF2/Merlin and Expanded act through Hippo signalling to regulate cell proliferation and apoptosis. Nat Cell Biol *8*, 27-36.

Hanahan, D., and Weinberg, R. A. (2011). Hallmarks of cancer: the next generation. Cell *144*, 646-674.

Harvey, K. F., Pfleger, C. M., and Hariharan, I. K. (2003). The Drosophila Mst ortholog, hippo, restricts growth and cell proliferation and promotes apoptosis. Cell *114*, 457-467.

Harvey, K. F., Zhang, X., and Thomas, D. M. (2013). The Hippo pathway and human cancer. Nat Rev Cancer *13*, 246-257.

Horton, J. D., Goldstein, J. L., and Brown, M. S. (2002). SREBPs: activators of the complete program of cholesterol and fatty acid synthesis in the liver. J Clin Invest *109*, 1125-1131.

Horton, J. D., Shimomura, I., Ikemoto, S., Bashmakov, Y., and Hammer, R. E. (2003). Overexpression of sterol regulatory element-binding protein-1a in mouse adipose tissue produces adipocyte hypertrophy, increased fatty acid secretion, and fatty liver. J Biol Chem *278*, 36652-36660.

Huang, J., Wu, S., Barrera, J., Matthews, K., and Pan, D. (2005). The Hippo signaling pathway coordinately regulates cell proliferation and apoptosis by inactivating Yorkie, the Drosophila Homolog of YAP. Cell *122*, 421-434.

Jakobisiak, M., Bruno, S., Skierski, J. S., and Darzynkiewicz, Z. (1991). Cell cycle-specific effects of lovastatin. Proc Natl Acad Sci U S A *88*, 3628-3632.

Jeong, J., and McMahon, A. P. (2002). Cholesterol modification of Hedgehog family proteins. J Clin Invest *110*, 591-596.

Johnson, R., and Halder, G. (2014). The two faces of Hippo: targeting the Hippo pathway for regenerative medicine and cancer treatment. Nat Rev Drug Discov *13*, 63-79.

Kamisuki, S., Mao, Q., Abu-Elheiga, L., Gu, Z., Kugimiya, A., Kwon, Y., Shinohara, T., Kawazoe, Y., Sato, S., Asakura, K.*, et al.* (2009). A small molecule that blocks fat synthesis by inhibiting the activation of SREBP. Chem Biol *16*, 882-892.

Kato, S., Han, S. Y., Liu, W., Otsuka, K., Shibata, H., Kanamaru, R., and Ishioka, C. (2003). Understanding the function-structure and function-mutation relationships of p53 tumor suppressor protein by high-resolution missense mutation analysis. Proc Natl Acad Sci U S A *100*, 8424-8429.

Keller, P. J., Fiordalisi, J. J., Berzat, A. C., and Cox, A. D. (2005). Visual monitoring of post-translational lipid modifications using EGFP-GTPase probes in live cells. Methods *37*, 131-137.

Kim, N. G., Koh, E., Chen, X., and Gumbiner, B. M. (2011). E-cadherin mediates contact inhibition of proliferation through Hippo signaling-pathway components. Proc Natl Acad Sci U S A *108*, 11930-11935.

Knebel, B., Haas, J., Hartwig, S., Jacob, S., Kollmer, C., Nitzgen, U., Muller-Wieland, D., and Kotzka, J. (2012). Liver-specific expression of transcriptionally active SREBP-1c is associated with fatty liver and increased visceral fat mass. PLoS One *7*, e31812.

Konstantinopoulos, P. A., Karamouzis, M. V., and Papavassiliou, A. G. (2007). Post-translational modifications and regulation of the RAS superfamily of GTPases as anticancer targets. Nat Rev Drug Discov *6*, 541-555.

Kroemer, G., and Pouyssegur, J. (2008). Tumor cell metabolism: cancer's Achilles' heel. Cancer Cell *13*, 472-482.

Kruse, J. P., and Gu, W. (2009). Modes of p53 regulation. Cell *137*, 609-622.

Kumar, A. S., Benz, C. C., Shim, V., Minami, C. A., Moore, D. H., and Esserman, L. J. (2008). Estrogen receptor-negative breast cancer is less likely to arise among lipophilic statin users. Cancer Epidemiol Biomarkers Prev *17*, 1028-1033.

Lamar, J. M., Stern, P., Liu, H., Schindler, J. W., Jiang, Z. G., and Hynes, R. O. (2012). The Hippo pathway target, YAP, promotes metastasis through its TEAD-interaction domain. Proc Natl Acad Sci U S A *109*, E2441-2450.

Lang, G. A., Iwakuma, T., Suh, Y. A., Liu, G., Rao, V. A., Parant, J. M., Valentin-Vega, Y. A., Terzian, T., Caldwell, L. C., Strong, L. C.*, et al.* (2004). Gain of function

of a p53 hot spot mutation in a mouse model of Li-Fraumeni syndrome. Cell *119*, 861-872.

Larsson, O. (1996). HMG-CoA reductase inhibitors: role in normal and malignant cells. Crit Rev Oncol Hematol *22*, 197-212.

Lau, A. N., Curtis, S. J., Fillmore, C. M., Rowbotham, S. P., Mohseni, M., Wagner, D. E., Beede, A. M., Montoro, D. T., Sinkevicius, K. W., Walton, Z. E.*, et al.* (2014). Tumor-propagating cells and Yap/Taz activity contribute to lung tumor progression and metastasis. EMBO J *33*, 468-481.

Lei, Q. Y., Zhang, H., Zhao, B., Zha, Z. Y., Bai, F., Pei, X. H., Zhao, S., Xiong, Y., and Guan, K. L. (2008). TAZ promotes cell proliferation and epithelial-mesenchymal transition and is inhibited by the hippo pathway. Mol Cell Biol *28*, 2426-2436.

Li, Y., Xu, S., Mihaylova, M. M., Zheng, B., Hou, X., Jiang, B., Park, O., Luo, Z., Lefai, E., Shyy, J. Y.*, et al.* (2011). AMPK phosphorylates and inhibits SREBP activity to attenuate hepatic steatosis and atherosclerosis in diet-induced insulin-resistant mice. Cell Metab *13*, 376-388.

Liu-Chittenden, Y., Huang, B., Shim, J. S., Chen, Q., Lee, S. J., Anders, R. A., Liu, J. O., and Pan, D. (2012). Genetic and pharmacological disruption of the TEAD-YAP complex suppresses the oncogenic activity of YAP. Genes Dev *26*, 1300-1305.

Luo, J., Solimini, N. L., and Elledge, S. J. (2009). Principles of cancer therapy: oncogene and non-oncogene addiction. Cell *136*, 823-837.

Makita, R., Uchijima, Y., Nishiyama, K., Amano, T., Chen, Q., Takeuchi, T., Mitani, A., Nagase, T., Yatomi, Y., Aburatani, H.*, et al.* (2008). Multiple renal cysts, urinary concentration defects, and pulmonary emphysematous changes in mice lacking TAZ. Am J Physiol Renal Physiol *294*, F542-553.

Malkin, D., Li, F. P., Strong, L. C., Fraumeni, J. F., Jr., Nelson, C. E., Kim, D. H., Kassel, J., Gryka, M. A., Bischoff, F. Z., Tainsky, M. A., and et al. (1990). Germ line p53 mutations in a familial syndrome of breast cancer, sarcomas, and other neoplasms. Science *250*, 1233-1238.

McCarthy, N. (2012). Metabolism: unmasking an oncometabolite. Nat Rev Cancer *12*, 229.

Milner, J., and Medcalf, E. A. (1991). Cotranslation of activated mutant p53 with wild type drives the wild-type p53 protein into the mutant conformation. Cell *65*, 765-774.

Mohseni, M., Sun, J., Lau, A., Curtis, S., Goldsmith, J., Fox, V. L., Wei, C., Frazier, M., Samson, O., Wong, K. K.*, et al.* (2014). A genetic screen identifies an LKB1-MARK signalling axis controlling the Hippo-YAP pathway. Nat Cell Biol *16*, 108-117.

Morin-Kensicki, E. M., Boone, B. N., Howell, M., Stonebraker, J. R., Teed, J., Alb, J. G., Magnuson, T. R., O'Neal, W., and Milgram, S. L. (2006). Defects in yolk sac vasculogenesis, chorioallantoic fusion, and embryonic axis elongation in mice with targeted disruption of Yap65. Mol Cell Biol *26*, 77-87.

Morton, J. P., Timpson, P., Karim, S. A., Ridgway, R. A., Athineos, D., Doyle, B., Jamieson, N. B., Oien, K. A., Lowy, A. M., Brunton, V. G.*, et al.* (2010). Mutant p53 drives metastasis and overcomes growth arrest/senescence in pancreatic cancer. Proc Natl Acad Sci U S A *107*, 246-251.

Motoshima, H., Goldstein, B. J., Igata, M., and Araki, E. (2006). AMPK and cell proliferation--AMPK as a therapeutic target for atherosclerosis and cancer. J Physiol *574*, 63-71.

Murakami, M., Nakagawa, M., Olson, E. N., and Nakagawa, O. (2005). A WW domain protein TAZ is a critical coactivator for TBX5, a transcription factor implicated in Holt-Oram syndrome. Proc Natl Acad Sci U S A *102*, 18034-18039.

Nielsen, S. F., Nordestgaard, B. G., and Bojesen, S. E. (2013). Statin use and reduced cancer-related mortality. N Engl J Med *368*, 576-577.

Oakman, C., Viale, G., and Di Leo, A. (2010). Management of triple negative breast cancer. Breast *19*, 312-321.

Olive, K. P., Tuveson, D. A., Ruhe, Z. C., Yin, B., Willis, N. A., Bronson, R. T., Crowley, D., and Jacks, T. (2004). Mutant p53 gain of function in two mouse models of Li-Fraumeni syndrome. Cell *119*, 847-860.

Pallottini, V., Guantario, B., Martini, C., Totta, P., Filippi, I., Carraro, F., and Trentalance, A. (2008). Regulation of HMG-CoA reductase expression by hypoxia. J Cell Biochem *104*, 701-709.

Pan, D. (2010). The hippo signaling pathway in development and cancer. Dev Cell *19*, 491-505.

Parsons, R. B., Price, G. C., Farrant, J. K., Subramaniam, D., Adeagbo-Sheikh, J., and Austen, B. M. (2006). Statins inhibit the dimerization of beta-secretase via both isoprenoid- and cholesterol-mediated mechanisms. Biochem J *399*, 205-214.

Perou, C. M., Sorlie, T., Eisen, M. B., van de Rijn, M., Jeffrey, S. S., Rees, C. A., Pollack, J. R., Ross, D. T., Johnsen, H., Akslen, L. A.*, et al.* (2000). Molecular portraits of human breast tumours. Nature *406*, 747-752.

Piccolo, S., Cordenonsi, M., and Dupont, S. (2013). Molecular pathways: YAP and TAZ take center stage in organ growth and tumorigenesis. Clin Cancer Res *19*, 4925-4930.

Poon, C. L., Lin, J. I., Zhang, X., and Harvey, K. F. (2011). The sterile 20-like kinase Tao-1 controls tissue growth by regulating the Salvador-Warts-Hippo pathway. Dev Cell *21*, 896-906.

Porstmann, T., Santos, C. R., Griffiths, B., Cully, M., Wu, M., Leevers, S., Griffiths, J. R., Chung, Y. L., and Schulze, A. (2008). SREBP activity is regulated by mTORC1 and contributes to Akt-dependent cell growth. Cell Metab *8*, 224-236.

Ren, F., Zhang, L., and Jiang, J. (2010). Hippo signaling regulates Yorkie nuclear localization and activity through 14-3-3 dependent and independent mechanisms. Dev Biol *337*, 303-312.

Sahai, E., and Marshall, C. J. (2002). RHO-GTPases and cancer. Nat Rev Cancer *2*, 133-142.

Sansores-Garcia, L., Bossuyt, W., Wada, K., Yonemura, S., Tao, C., Sasaki, H., and Halder, G. (2011). Modulating F-actin organization induces organ growth by affecting the Hippo pathway. EMBO J *30*, 2325-2335.

Schlegelmilch, K., Mohseni, M., Kirak, O., Pruszak, J., Rodriguez, J. R., Zhou, D., Kreger, B. T., Vasioukhin, V., Avruch, J., Brummelkamp, T. R., and Camargo, F. D. (2011). Yap1 acts downstream of alpha-catenin to control epidermal proliferation. Cell *144*, 782-795.

Strano, S., Monti, O., Pediconi, N., Baccarini, A., Fontemaggi, G., Lapi, E., Mantovani, F., Damalas, A., Citro, G., Sacchi, A.*, et al.* (2005). The transcriptional coactivator Yes-

associated protein drives p73 gene-target specificity in response to DNA Damage. Mol Cell *18*, 447-459.

Strano, S., Munarriz, E., Rossi, M., Castagnoli, L., Shaul, Y., Sacchi, A., Oren, M., Sudol, M., Cesareni, G., and Blandino, G. (2001). Physical interaction with Yes-associated protein enhances p73 transcriptional activity. J Biol Chem *276*, 15164-15173.

Sundqvist, A., Bengoechea-Alonso, M. T., Ye, X., Lukiyanchuk, V., Jin, J., Harper, J. W., and Ericsson, J. (2005). Control of lipid metabolism by phosphorylation-dependent degradation of the SREBP family of transcription factors by SCF(Fbw7). Cell Metab *1*, 379-391.

Turner, N., Moretti, E., Siclari, O., Migliaccio, I., Santarpia, L., D'Incalci, M., Piccolo, S., Veronesi, A., Zambelli, A., Del Sal, G., and Di Leo, A. (2013). Targeting triple negative breast cancer: is p53 the answer? Cancer Treat Rev *39*, 541-550.

Vander Heiden, M. G. (2011). Targeting cancer metabolism: a therapeutic window opens. Nat Rev Drug Discov *10*, 671-684.

Vander Heiden, M. G., Cantley, L. C., and Thompson, C. B. (2009). Understanding the Warburg effect: the metabolic requirements of cell proliferation. Science *324*, 1029-1033.

von Gise, A., Lin, Z., Schlegelmilch, K., Honor, L. B., Pan, G. M., Buck, J. N., Ma, Q., Ishiwata, T., Zhou, B., Camargo, F. D., and Pu, W. T. (2012). YAP1, the nuclear target of Hippo signaling, stimulates heart growth through cardiomyocyte proliferation but not hypertrophy. Proc Natl Acad Sci U S A *109*, 2394-2399.

Wada, K., Itoga, K., Okano, T., Yonemura, S., and Sasaki, H. (2011). Hippo pathway regulation by cell morphology and stress fibers. Development *138*, 3907-3914.

Walerych, D., Napoli, M., Collavin, L., and Del Sal, G. (2012). The rebel angel: mutant p53 as the driving oncogene in breast cancer. Carcinogenesis *33*, 2007-2017.

Wang, Z., Wu, Y., Wang, H., Zhang, Y., Mei, L., Fang, X., Zhang, X., Zhang, F., Chen, H., Liu, Y.*, et al.* (2014). Interplay of mevalonate and Hippo pathways regulates RHAMM transcription via YAP to modulate breast cancer cell motility. Proc Natl Acad Sci U S A *111*, E89-98.

Wu, S., Huang, J., Dong, J., and Pan, D. (2003). hippo encodes a Ste-20 family protein kinase that restricts cell proliferation and promotes apoptosis in conjunction with salvador and warts. Cell *114*, 445-456.

Wu, S., Liu, Y., Zheng, Y., Dong, J., and Pan, D. (2008). The TEAD/TEF family protein Scalloped mediates transcriptional output of the Hippo growth-regulatory pathway. Dev Cell *14*, 388-398.

Yagi, R., Chen, L. F., Shigesada, K., Murakami, Y., and Ito, Y. (1999). A WW domain-containing yes-associated protein (YAP) is a novel transcriptional co-activator. EMBO J *18*, 2551-2562.

Yu, F. X., and Guan, K. L. (2013). The Hippo pathway: regulators and regulations. Genes Dev *27*, 355-371.

Yu, F. X., Zhao, B., Panupinthu, N., Jewell, J. L., Lian, I., Wang, L. H., Zhao, J., Yuan, H., Tumaneng, K., Li, H.*, et al.* (2012). Regulation of the Hippo-YAP pathway by G-protein-coupled receptor signaling. Cell *150*, 780-791.

Zadra, G., Photopoulos, C., and Loda, M. (2013). The fat side of prostate cancer. Biochim Biophys Acta *1831*, 1518-1532.

Zhang, H., Liu, C. Y., Zha, Z. Y., Zhao, B., Yao, J., Zhao, S., Xiong, Y., Lei, Q. Y., and Guan, K. L. (2009). TEAD transcription factors mediate the function of TAZ in cell growth and epithelial-mesenchymal transition. J Biol Chem *284*, 13355-13362.

Zhang, N., Bai, H., David, K. K., Dong, J., Zheng, Y., Cai, J., Giovannini, M., Liu, P., Anders, R. A., and Pan, D. (2010). The Merlin/NF2 tumor suppressor functions through the YAP oncoprotein to regulate tissue homeostasis in mammals. Dev Cell *19*, 27-38.

Zhao, B., Li, L., Lei, Q., and Guan, K. L. (2010). The Hippo-YAP pathway in organ size control and tumorigenesis: an updated version. Genes Dev *24*, 862-874.

Zhao, B., Wei, X., Li, W., Udan, R. S., Yang, Q., Kim, J., Xie, J., Ikenoue, T., Yu, J., Li, L*., et al.* (2007). Inactivation of YAP oncoprotein by the Hippo pathway is involved in cell contact inhibition and tissue growth control. Genes Dev *21*, 2747-2761.

Zhou, D., Conrad, C., Xia, F., Park, J. S., Payer, B., Yin, Y., Lauwers, G. Y., Thasler, W., Lee, J. T., Avruch, J., and Bardeesy, N. (2009). Mst1 and Mst2 maintain hepatocyte quiescence and suppress hepatocellular carcinoma development through inactivation of the Yap1 oncogene. Cancer Cell *16*, 425-438.

FIGURES

FIGURE 1
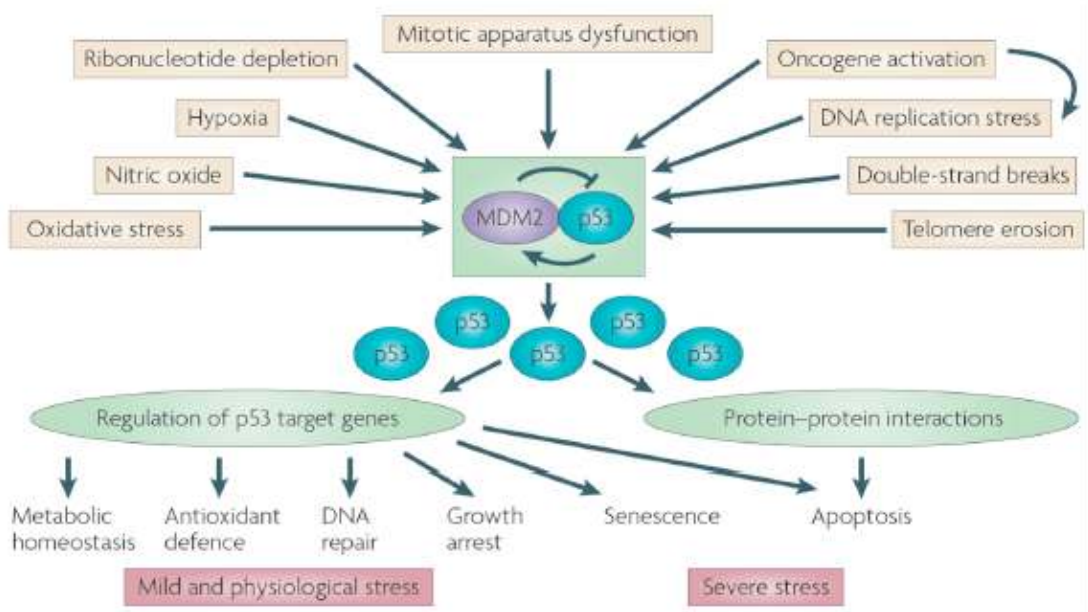
Figure 1. Simplified scheme of the p53 pathway. The p53–MDM2 feedback loop is the "heart" of the p53 pathway. Under normal conditions, it maintains constantly low steady-state p53 levels and activity. Various stress signals, related in many ways to carcinogenesis, impinge on this central loop to release p53 from MDM2-mediated inhibition. This increases p53 protein levels and activity, inducing various phenotypic changes. The nature of the phenotypic response to p53 activation is, at least partially, proportionate to the amplitude, duration and nature of the activating signal. Recent evidence indicates that p53 has an important role also in enabling the cell to adjust its metabolism in response to mild normal physiological fluctuations, including those in glucose and other nutrient levels, oxygen availability and reactive oxygen species levels. From Levine and Oren, 2009.
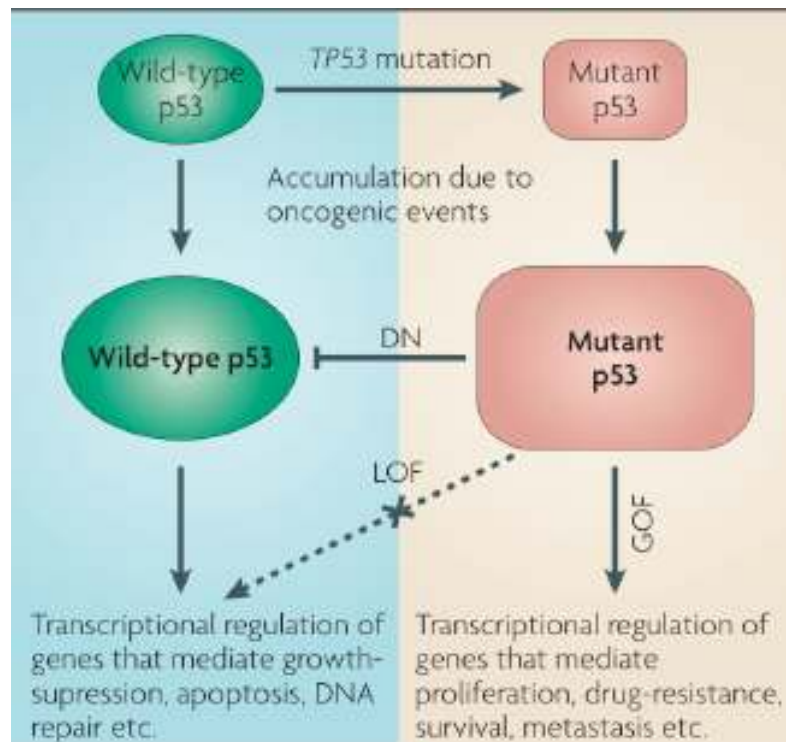
Figure 2. Schematic representation of the functional impacts of *TP53* mutations. LOF (loss-of-function); DN (dominant-negative effects); GOF (gain-of-function). From Brosh and Rotter, 2009.

FIGURE 3
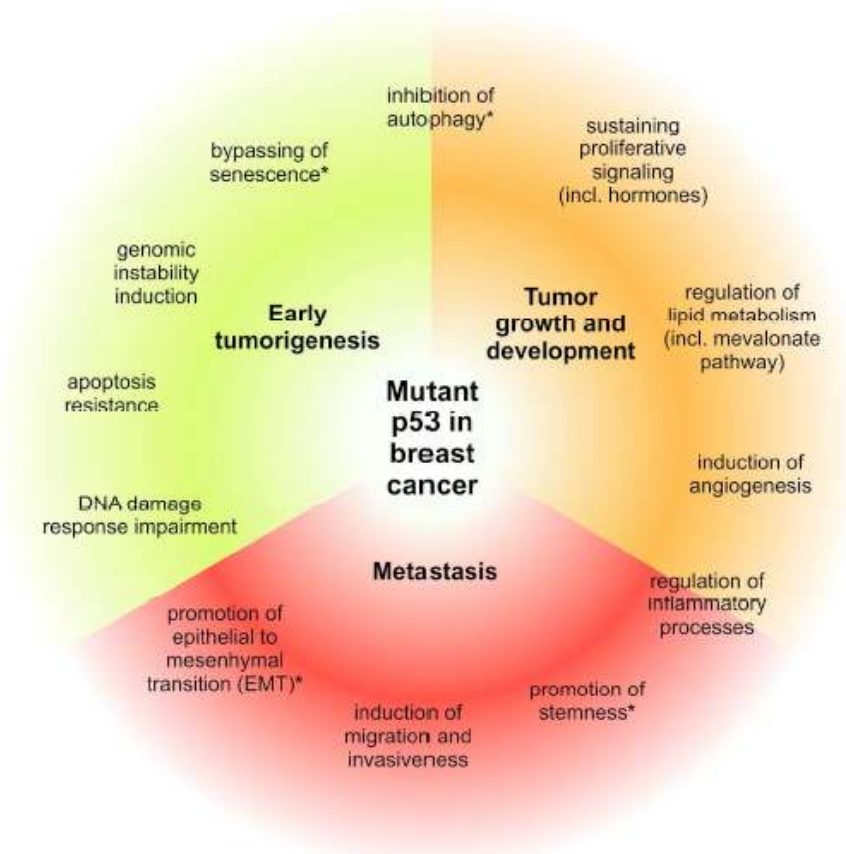
Figure 3. Mutant p53 involvement in processes associated with breast cancer development. Mutant p53 is known to affect multiple oncogenic processes. Although different oncogenic mechanisms overlap during tumorigenesis, here they are arbitrarily divided into mechanisms indispensable for early tumorigenesis at the level of single cell biochemistry (green), mechanisms supporting multicellular tumor mass growth (orange), and features necessary for metastasis to secondary sites (red). The asterisks (*) indicate oncogenic mechanisms known to be important for breast cancer, linked to p53 gain-of-function (GOF) in other tumors, but not yet directly tested for mutant p53 dependence in mammary carcinoma cells or mouse models. See text for detailed information and references. From Walerych et al., 2012.

FIGURE 4
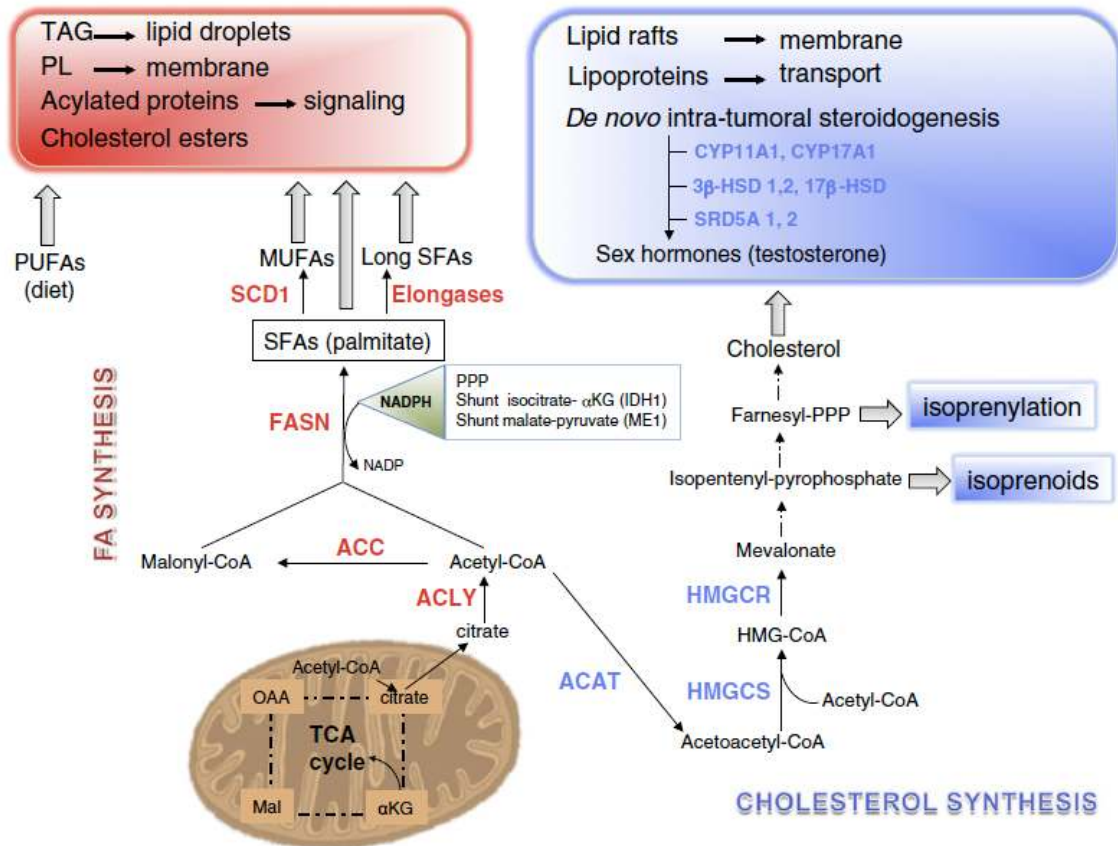
Figure 4. Lipids metabolism in cancer. Citrate generated in TCA cycle is exported to the cytosol to fuel the mevalonate and fatty acid (FA) synthesis pathways by conversion to acetyl-CoA by ATP citrate lyase (ACLY). Acetyl-CoA functions as a substrate for the synthesis of mevalonate by HMG-CoA synthase (HMGCS), followed by the reductase (HMGCR). Mevalonate is a precursor for cholesterol, and isoprenoids biosinthesis, Acetyl-CoA carboxylase 1 (ACC) initiates the first committed step to FA synthesis to produce malonyl-CoA. Seven malonyl-CoA molecules are added to acetyl-CoA by fatty acid synthase (FASN) to produce palmitic acid, a 16-carbon saturated FA (SFA). Palmitic acid can be further elongated to form long SFAs and/or desaturated by stearoyl-CoA desaturase 1 (SCD1) and by other desaturases to produce monounsaturated FA (MUFAs). From Zadra et al., 2013.

FIGURE 5
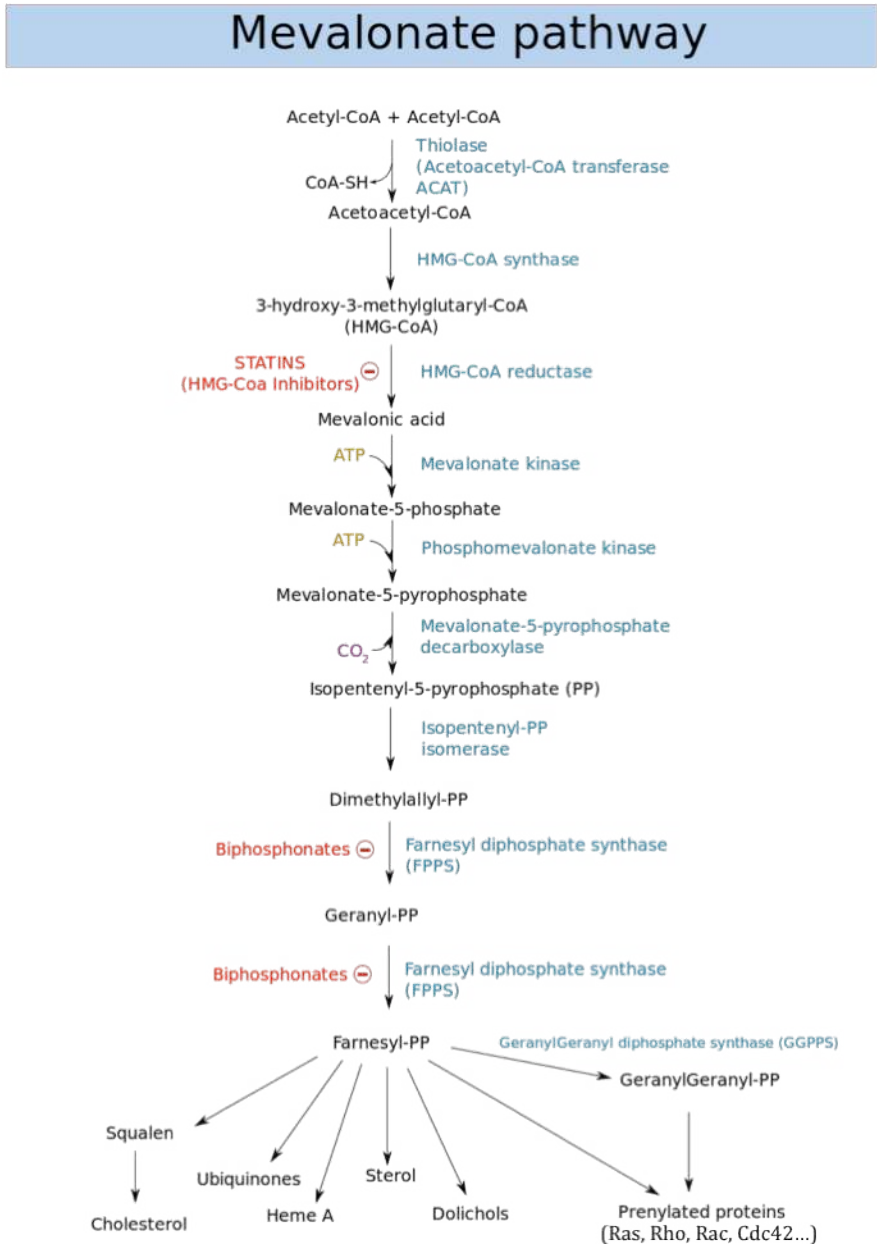
Figure 5. The mevalonate pathway. Mevalonate metabolism generates farnesyl pyrophosphate (FPP) and geranylgeranyl pyrophosphate (GGPP), which are required for protein prenylation (farnesylation and geranyl-geranylation). Statins and nitrogen-containing bisphosphonates (N-BPs) are two different classes of drugs that both inhibit mevalonate metabolism and thus also inhibit protein prenylation. FPP is also used by the cell as precursor for biosynthesis of cholesterol, ubiquinones, Hene A, Sterol and Dolichols.

FIGURE 6
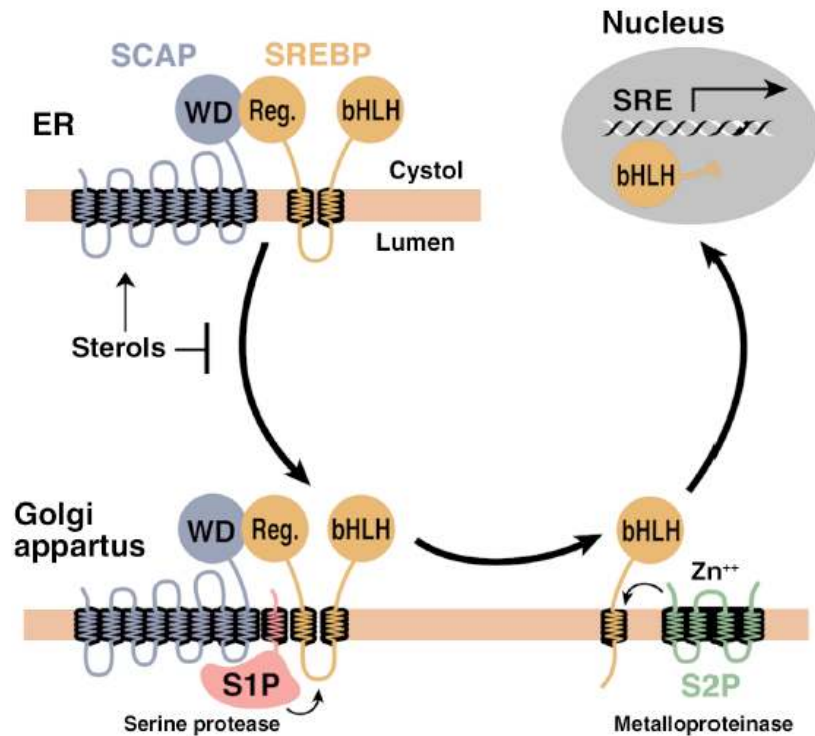
Figure 6. Model for the sterol-mediated proteolytic release of SREBPs from membranes. SCAP is a sensor of sterols and an escort of SREBPs. When cells are depleted of sterols, SCAP transports SREBPs from the ER to the Golgi apparatus, where two proteases, Site-1 protease (S1P) and Site-2 protease (S2P), act sequentially to release the NH2-terminal bHLH-Zip domain from the membrane. The bHLH-Zip domain enters the nucleus and binds to a sterol response element (SRE) in the enhancer/promoter region of target genes, activating their transcription. When cellular cholesterol rises, the SCAP/SREBP complex is no longer incorporated into ER transport vesicles, SREBPs no longer reach the Golgi apparatus, and the bHLH-Zip domain cannot be released from the membrane. As a result, transcription of all target genes declines. From Horton et al., 2002.

FIGURE 7
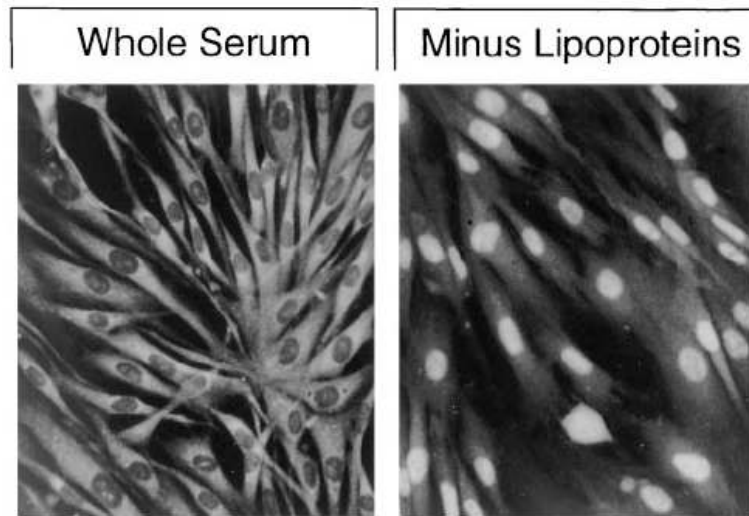
Figure 7. Immunofluorescence of SREBP-2 in Cultured Fibroblasts Grown in Whole Serum or Lipoprotein-Deficient Serum. From Brown and Goldstein, 1997.

FIGURE 8

Figure 8. SREBPs transgenic mice develop massively enlarged livers. The transgene encodes a truncated version of SREBP-1a (amino acids 1–460) driven by the phosphoenolpyruvate carboxykinase promoter. Both animals (wild type, left; transgenic, right) were fed a low carbohydrate/high protein diet for 2 weeks to induce expression of the transgene. From Brown and Goldstein, 1997.

FIGURE 9
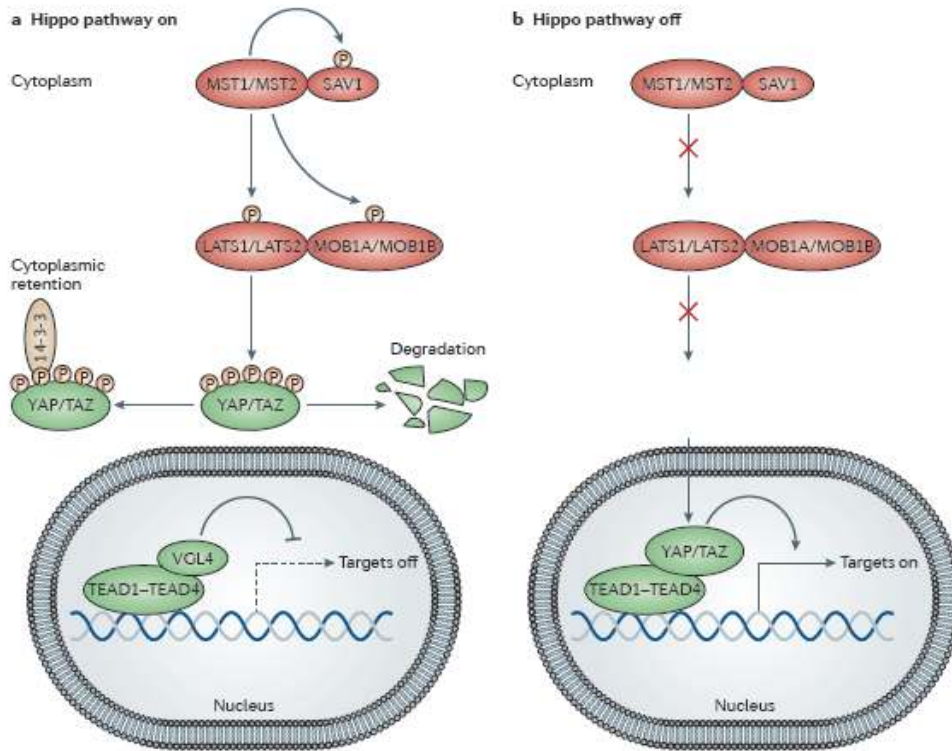
Figure 9. The core of the Hippo signalling pathway and its mode of action. Schematics of the core pathway components and how they interact are depicted. **a.** When the Hippo pathway is on, mammalian STE20-like protein kinase 1 (MST1) or MST2 phosphorylate Salvador homolog 1 (SAV1), and together they phosphorylate and activate MOB kinase activator 1A (MOB1A), MOB1B, large tumour suppressor homolog 1 (LATS1) kinase and LATS2 kinase, which then phosphorylate Yes-associated protein (YAP) and transcriptional co-activator with PDZ-binding motif (TAZ). Phosphorylated YAP and TAZ are sequestered in the cytoplasm by the 14-3-3 protein and shunted for proteasomal degradation. As a result, the TEA domain-containing sequence-specific transcription factors (TEADs) associate with the transcription cofactor vestigial-like protein 4 (VGL4) and suppress target gene expression. **b.** When the Hippo pathway is off, the kinases MST1, MST2, LATS1 and LATS2 are inactive, so YAP and TAZ are not phosphorylated and instead accumulate in the nucleus where they displace VGL4 and form a complex with TEADs, which promotes the expression of target genes. From Johnson et al., 2014.

FIGURE 10
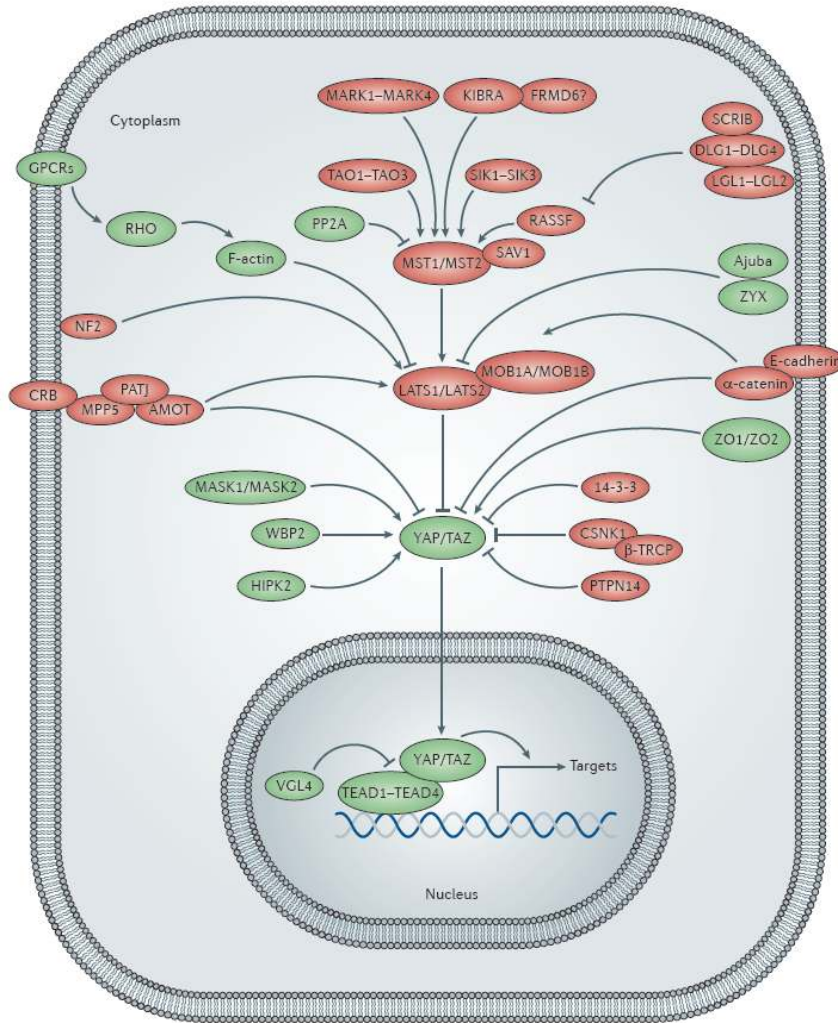
Figure 10. The Hippo pathway network. Mammalian Hippo pathway components that promote the activity of Yes-associated protein (YAP) and transcriptional co-activator with PDZ-binding motif (TAZ) are shown in green, whereas those that inhibit YAP and TAZ activity are shown in red. AMOT, angiomotin; β-TRCP, β-transducin repeat-containing E3 ubiquitin protein ligase; CSNK1, casein kinase 1; CRB, Crumbs homolog; DLG, discs large homolog; FRMD6, FERM domain-containing protein 6; GPCR, G protein-coupled receptor; HIPK, homeodomain-interacting protein kinase; KIBRA, kidney and brain protein; LATS, large tumour suppressor homolog; MARK, MAP/microtubule affinity-regulating kinase; MASK, multiple ankyrin repeats single KH domain-containing protein; MOB1A, MOB kinase activator 1A; MST, mammalian STE20-like protein kinase; NF2, neurofibromin 2 (also known as Merlin); PP2A, protein phosphatase 2A; PTPN14, protein tyrosine phosphatase, non-receptor type 14; RASSF, RAS association domain-containing family protein; SAV1, Salvador homolog 1; SCRIB, Scribble homolog; SIK, salt-inducible kinase; TAO, thousand and one amino acid protein kinase; TEAD, TEA domain-containing sequence-specific transcription factor; VGL4, vestigial-like protein 4; WBP2, WW domain-binding protein 2; ZO, zona occludens protein; ZYX, Zyxin protein. From Johnson et al., 2014.

FIGURE 11
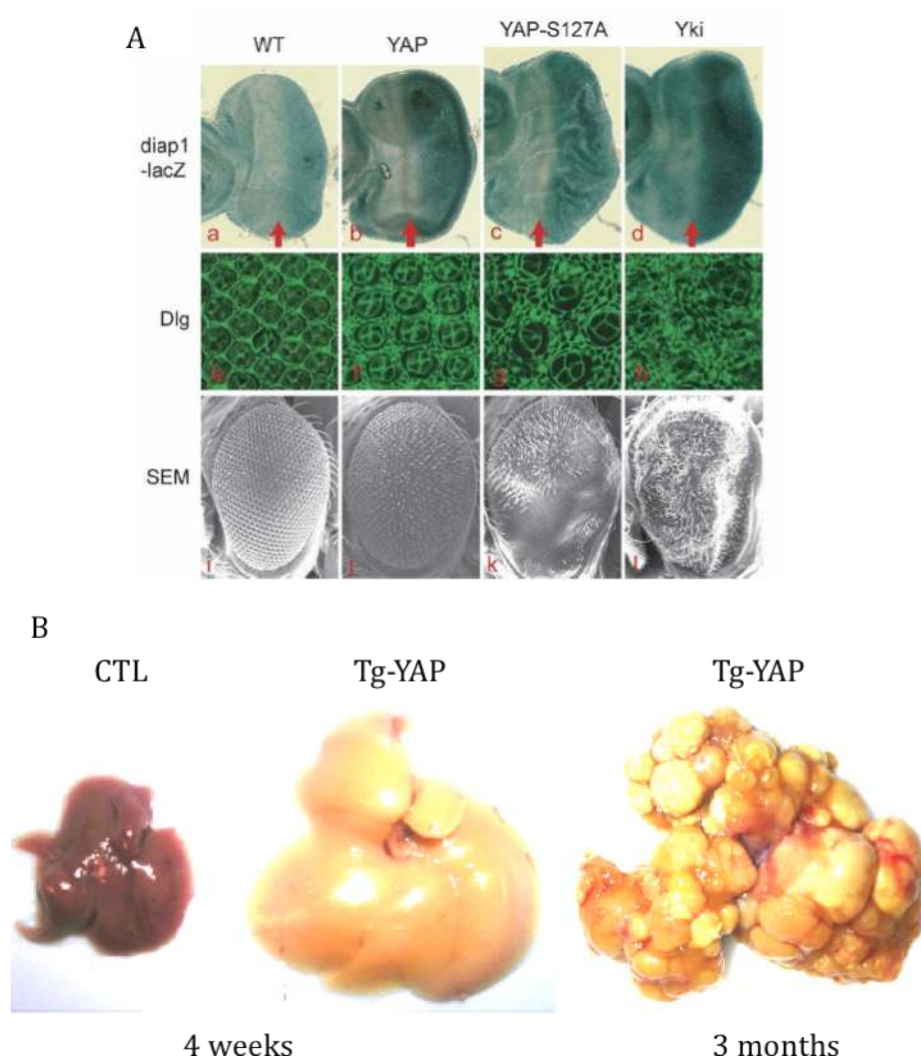
Figure 11. YAP/Yki induces organ growth in vivo. A) (Panels *a–d*) Third instar larval eye discs were analyzed for the transcriptional activities of *diap1-lacZ* reporter genes. Anterior is to the left. Red arrows indicate the morphogenetic furrow. (Panels *e–h*) Mid-pupal eye discs were stained with Discs large (Dlg) antibody to outline cells. SEM (scanning electron microscopy) images of fly adult eyes are presented in panels *i–l*. B) Liver from control (CTL) or transgenic YAP-overexpressing mice (Tg-YAP) raised on Dox for 4 weeks or 3 months, starting at birth. Note the increased in liver size (after 4 weeks) and the widespread development of HCC throughout the liver (after 3 month). From Zhao et al., 2007 and Dong et al., 2007.

FIGURE 12
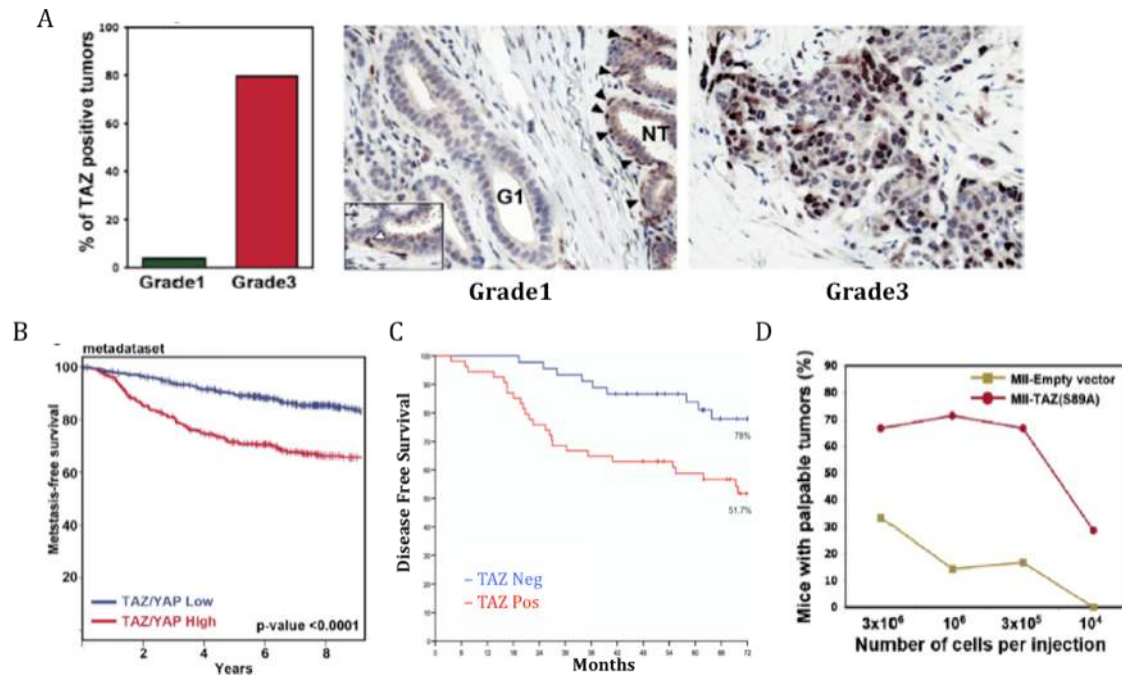
Figure 12. Taz is overexpressed in G3 Primary tumors and correlates with poor clinical outcome in breast cancer. A) Frequency of TAZ-positive G1 or G3 primary human breast cancers as judged by immunohistochemistry (IHC). Representative IHC pictures for TAZ expression in G1 (left) or G3 (right) invasive human breast cancer samples. B) Kaplan-Meier graphs representing the probability of cumulative metastasis-free survival in breast cancer patients from the metadataset stratified according to the TAZ/YAP signature. C) Kaplan–Meier curve representing DFS of patients with breast cancer stratified according to TAZ expression status. D) Tumor-seeding ability of empty vector and TAZ (S89A) overexpressing cells. From Cordenonsi et al., 2011 and Bartucci et al., 2014.

FIGURE 13
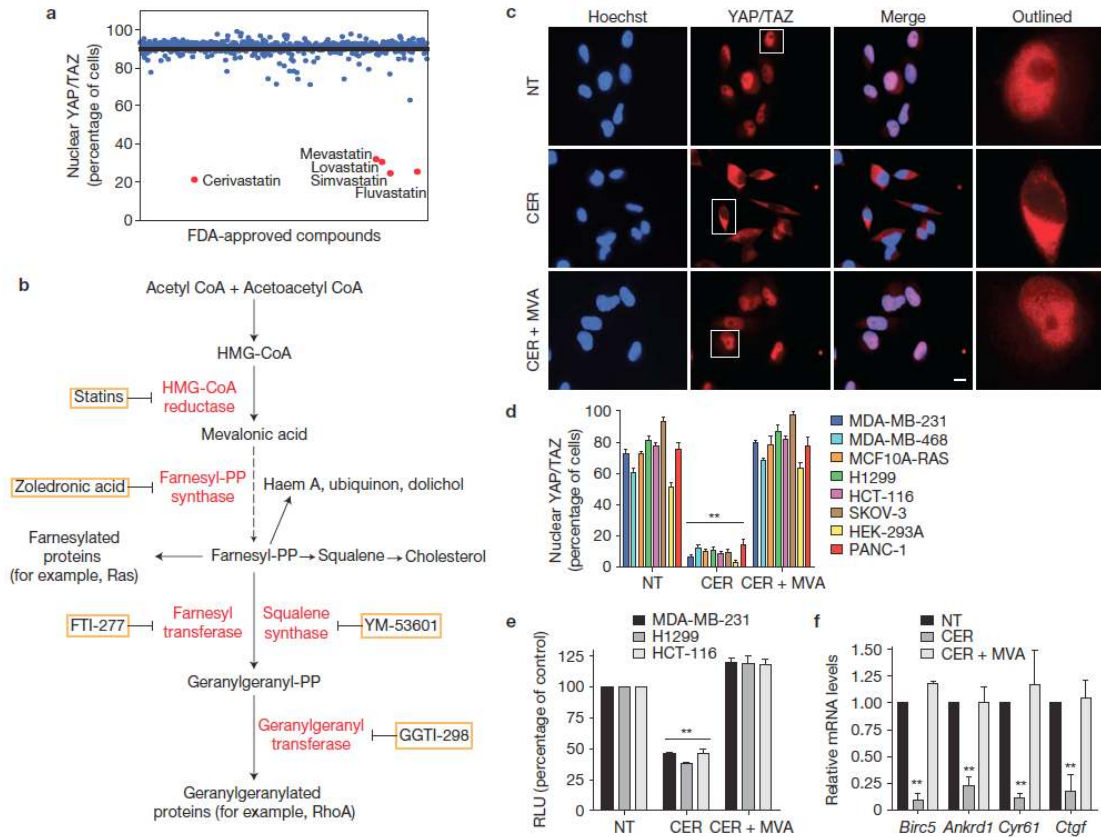
Figure 13. The Mevalonate pathway promotes YAP/TAZ nuclear localization and activity. (a) Results of high-content screening. **(b)** Schematic overview of the mevalonate pathway. Enzymes are shown in red and chemical inhibitors are boxed. **(c,d)** Cells were treated with DMSO (NT) or Cerivastatin (CER) 1μM alone or with mevalonic acid (MVA) 0.5 mM for 24h before fixation. (c) Representative images of immunofluorescence in MDA-MB-231 (d) Quantification of cells with nuclear YAP/TAZ in eight cancer cell lines. Data are derived from four independent experiments where at least 300 cells were scored. Error bars represent mean ± s.d., n=4. Scale bars, 15 μm. **(e)** Luciferase reporter assay (8XGTII-lux). Cells were treated as in c. Data are normalized to NT. Error bars represent mean ± s.d., from n=4 biological replicates. **(f)** qRT-PCR analysis in MDA-MB-231. Cells were treated with DMSO (NT) or Cerivastatin (CER) 1μM alone or with mevalonic acid 0.5 mM for 48h. Error bars represent mean ± s.d., from n=3 biological replicates. *P< 0.05, **P< 0.01; two-tailed Student's t-test is used throughout.
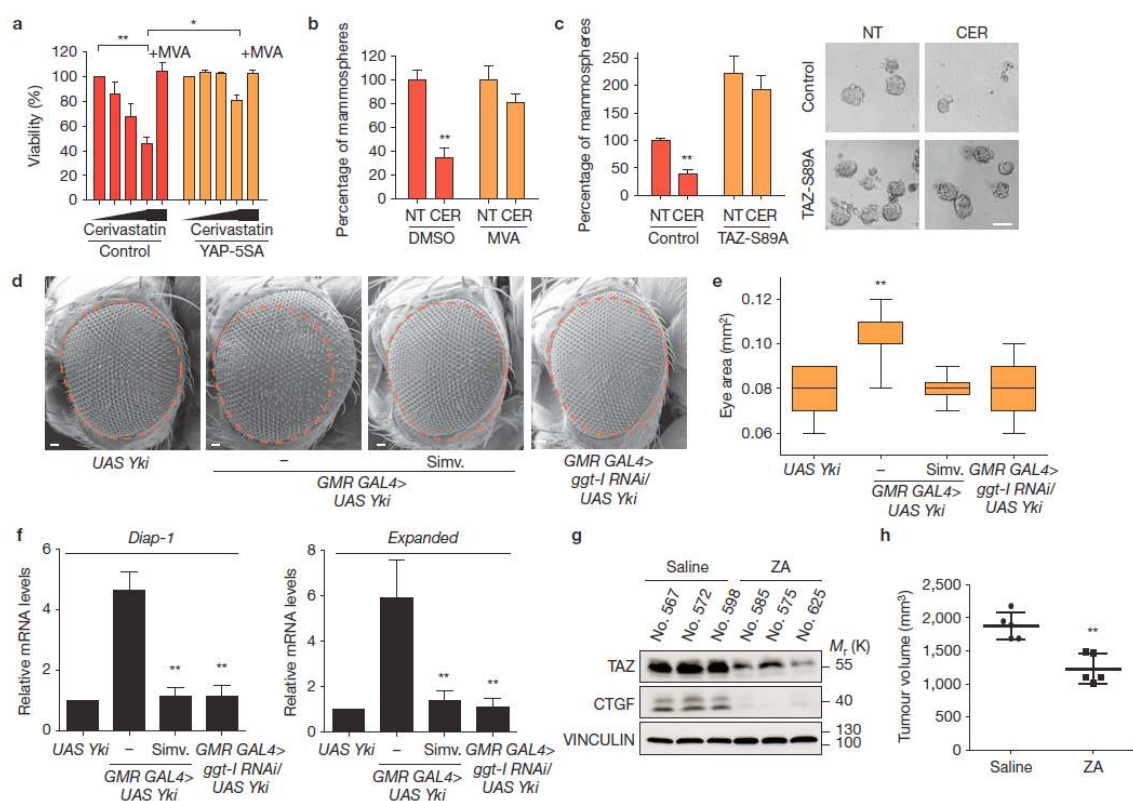
FIGURE 14
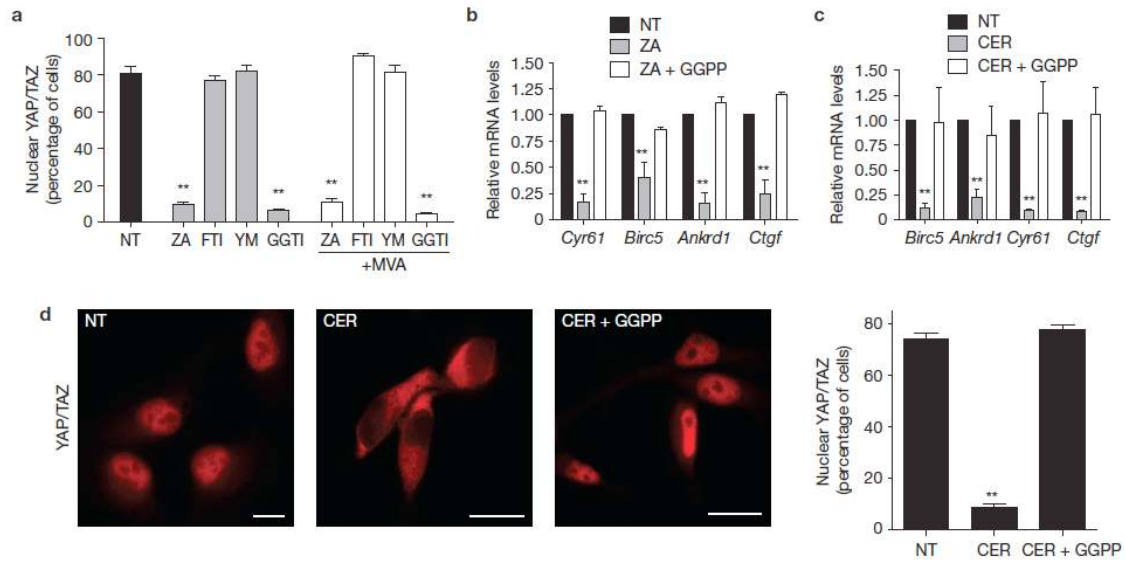
Figure 14. Geranylgeranyl pyrophosphate mediates mevalonate-dependent YAP/TAZ nuclear localization and activity. (a) Quantification of MDA-MB-231 cells with nuclear YAP/TAZ after treatment with the indicated inhibitors. Data are derived from three independent experiments where at least 300 cells were scored. Error bars represent mean ± s.d., n=3. **(b)** qRT-PCR analysis in MDA-MB-231. Cells were treated with DMSO (NT) or Zoledronic Acid (ZA) alone or with GGPP for 48h. Error bars represent mean ± s.d., from n=3 biological replicates. **(c)** qRT-PCR analysis in MDA-MB-231. Cells were treated with Cerivastatin 1μM alone or with geranylgeranyl pyrophosphate (GGPP) (20μM) for 48h. Error bars represent mean ± s.d., from n=3 biological replicates. **(d)** Immunofluorescence images of YAP/TAZ in MDA-MB-231 cells, after treatment with Cerivastatin 1μM alone or with geranylgeranyl pyrophosphate (GGPP) (20μM) for 24h. Representative images are shown. Experiment repeated four times. Data are derived from four independent experiments where at least 300 cells were scored. Error bars represent mean ± s.d.; n=4. Scale bars, 15 μm. *P< 0.05, **P< 0.01; two-tailed Student's t-test is used throughout.

FIGURE 15
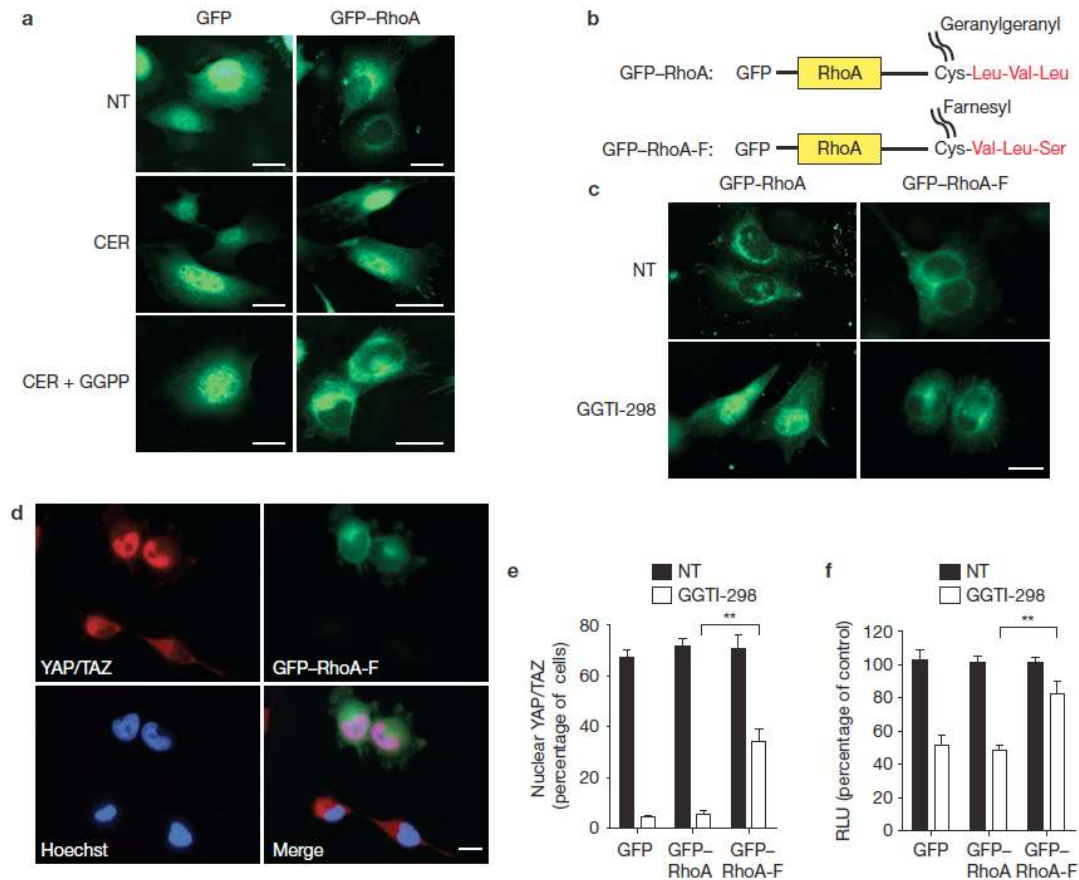
Figure 15. Activation of YAP/TAZ by geranylgeranyl pyrophosphate is mediated by Rho-GTPases. (a) H1299 cells transiently overexpressing GFP or GFP-RhoA were treated with Cerivastatin 1μM alone or with GGPP (20μM) for 24h. Representative images are shown. Experiment repeated three times. Scale bars, 15 μm. **(b)** Schematic representation of GFP-RhoA with geranylgeranylation consensus sequence (Cys-Leu-Val-Leu) and the mutant GFP-RhoA-F with farnesylation consensus sequence (Cys-Val-Leu-Ser). **(c)** Subcellular localization of transiently transfected GFP-RhoA and GFP-RhoA-F in H1299 cells after treatment with DMSO (NT) or GGTI-298 (1μM) for 24h. Representative images are shown. Experiment repeated three times. Scale bars, 15 μm. **(d)** Immunofluorescence showing YAP/TAZ subcellular localization in MDA-MB-231 cells transiently expressing or not the GFP-RhoA-F construct after treatment with GGTI-298 (1μM) for 24h. Representative images are shown. Experiment repeated three times. Scale bars, 15 μm. **(e)** Percentage of cells with nuclear YAP/TAZ in MDA-MB-231. Cells stably expressing the indicated constructs were treated with DMSO (NT) or GGTI-298 (1μM) for 24h. Data are derived from three independent experiments where at least 300 cells were scored. Error bars represent mean ± s.d., n=3. **(f)** Luciferase reporter assay (8XGTII-lux). Cells were treated as in e. Data are normalized to NT. Error bars represent mean ± s.d., from n=4 biological replicates. *P< 0.05, **P< 0.01; two-tailed Student's t-test is used throughout.

FIGURE 16
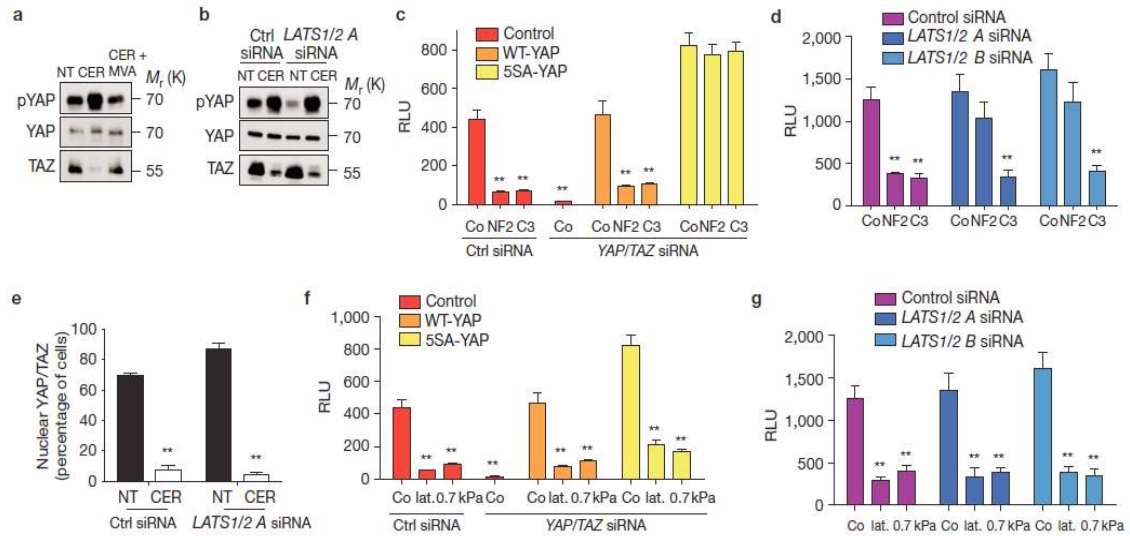
Figure 16. The Mevalonate pathway regulates YAP/TAZ phosphorylation and activity independently of LATS kinases. (a) MDA-MB-231 cells were treated with Cerivastatin 1μM alone or with mevalonic acid 0.5mM for 24h. Representative blots are shown. Experiment repeated three times. Also see uncropped figure scan in figures. **(b)** MDA-MB-231 were transfected with indicated siRNA for 48h and treated with Cerivastatin 1μM for 24h. siC is control siRNA. Representative blots are shown. Experiment repeated three times. Also see uncropped figure scan in figures. **(c)** Parental (control), siRNA-resistant WT-YAP and 5SA-YAP-overexpressing MDA-MB-231 cells were transfected with control siRNA (siC) or a combination of YAP/TAZ siRNA (*siYAP/TAZ*). The day after, cells were transfected with 8XGTII-lux reporter and with the indicated constructs and analyzed after 24h. Co is empty vector. Error bars represent mean ± s.d., from n=3 biological replicates. **(d)** MDA-MB-231 cells were transfected with control siRNA (siC) or two independent sets of siRNA targeting *Lats1* and *Lats2*. The day after, cells were transfected with 8XGTII-lux reporter and with the indicated constructs and analyzed after 24h. Co is empty vector. Error bars represent mean ± s.d., from n=3 biological replicates. **(e)** MDA-MB-231 cells were treated as in b then analyzed by immunofluorescence. Data are derived from three independent experiments where at least 300 cells were scored. Error bars represent mean ± s.d., n=3. **(f)** Parental (control), siRNA-resistant WT-YAP and 5SA-YAP-overexpressing MDA-MB-231 cells were transfected with control siRNA (siC) or a combination of YAP/TAZ siRNA (*siYAP/TAZ*). The day after, cells were transfected with 8XGTII-lux reporter and treated with Latrunculin A (lat.) for 24 hours or plated on hydrogels of 0.7KPa for 48h. Co is empty vector. Error bars represent mean ± s.d., from n=3 biological replicates. **(g)** Parental (control), siRNA-resistant WT-YAP and 5SA-YAP-overexpressing MDA-MB-231 cells were transfected with control siRNA (siC) or two independent sets of siRNA targeting *Lats1* and *Lats2*. The day after, cells were transfected with 8XGTII-lux reporter and treated with Latrunculin A (lat.) for 24 hours or plated on hydrogels of 0.7KPa for 48h. Co is empty vector.
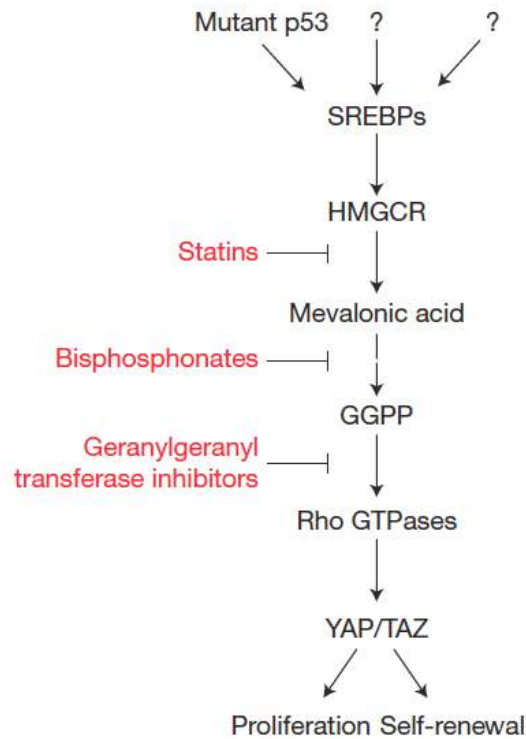
FIGURE 17

Figure 17. The Mevalonate pathway is required for YAP/TAZ biological activities.
(a) Viability assay of control and YAP-5SA stably expressing MCF10A MII cells after treatment with increasing amount of Cerivastatin (0, 0.1, 1, 10 μM and 10μM with mevalonic acid 0.5 mM) for 48h. Data are normalized to untreated. Error bars represent mean ± s.d., from n=3 biological replicates. **(b)** Quantification of primary mammospheres formed by MII cells treated with DMSO or Cerivastatin 1μM alone or with mevalonic acid 0.5 mM. Error bars represent mean ± s.d., from n=6 biological replicates. **(c)** Quantification (left) and representative images (right) of primary mammospheres formed by control or TAZ-S89A stably expressing MII cells. Error bars represent mean ± s.d., from n=6 biological replicates. Scale bars, 200 μm. **(d)** Adult eyes from flies with *UAS Yki:V5* (control), *GMR GAL4/+;UAS-YkiS168A/+*, *GMR GAL4/+;UAS-Yki:V5/+*, *GMR GAL4/+; UAS-Yki:V5/+* treated with Simvastatin 2,5 mM, *GMR GAL4/+; beta ggt-I RNAi/ UAS-ykiV5*. **(e)** Eye area measurement of indicated genotypes. n=30 flies per genotype. **(f)** qRT-PCR analysis of *Diap-1* (left) and *Expanded* (right) from drosophila heads of indicated genotypes. Error bars represent mean ± s.d., from n=3 biological replicates. **(g)** Lysates of tumors from control (saline) or zoledronic acid-treated mice were immunoblotted with the indicated antibodies. # are mice identificative numbers. n=3 mice per group. Also see uncropped figure scan in figures. **(h)** Tumor volumes 40 day after MDA-MB-231 cell injection. n=5 mice per group. *P< 0.05, **P< 0.01; two-tailed Student's t-test is used throughout.
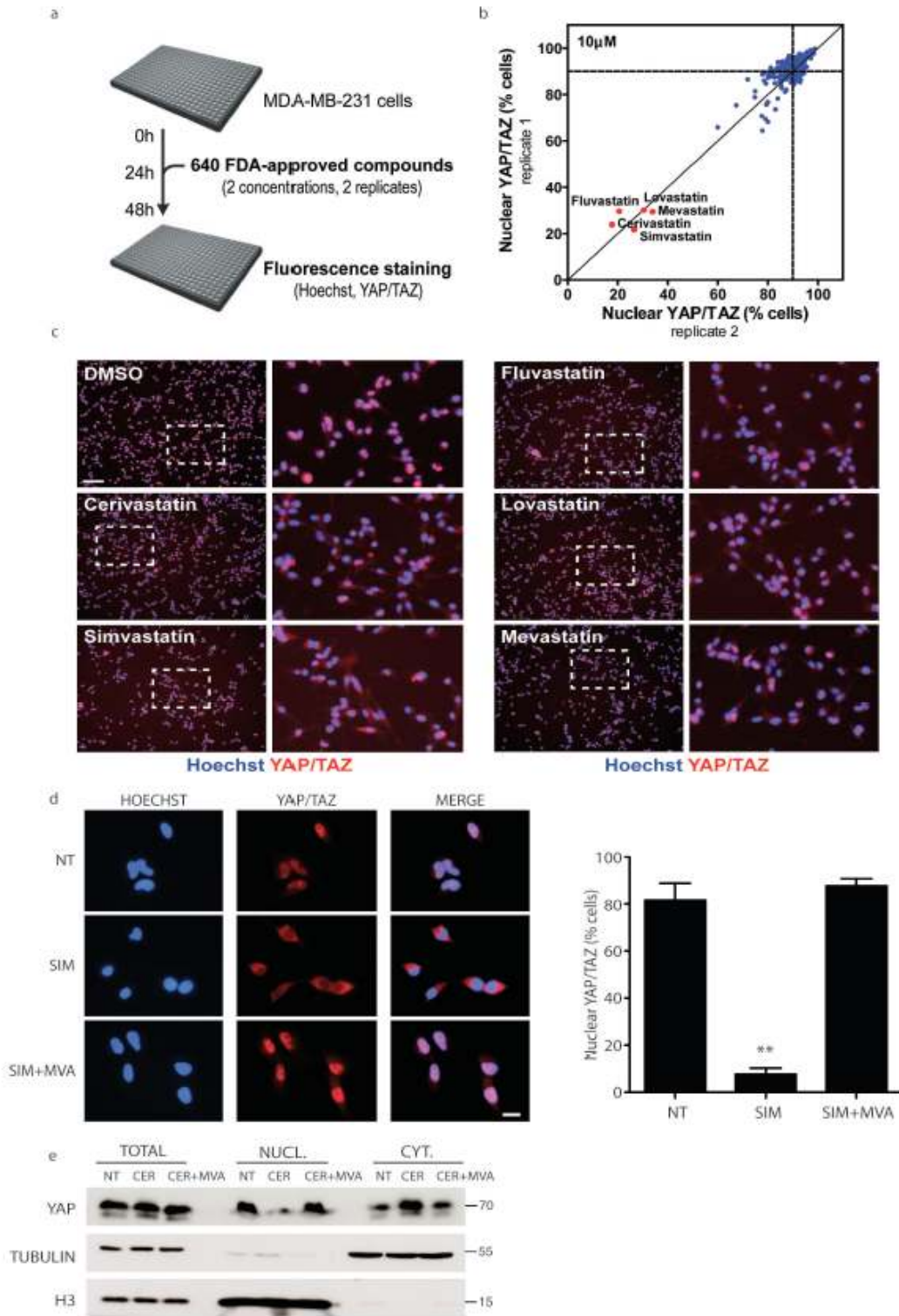
FIGURE 18
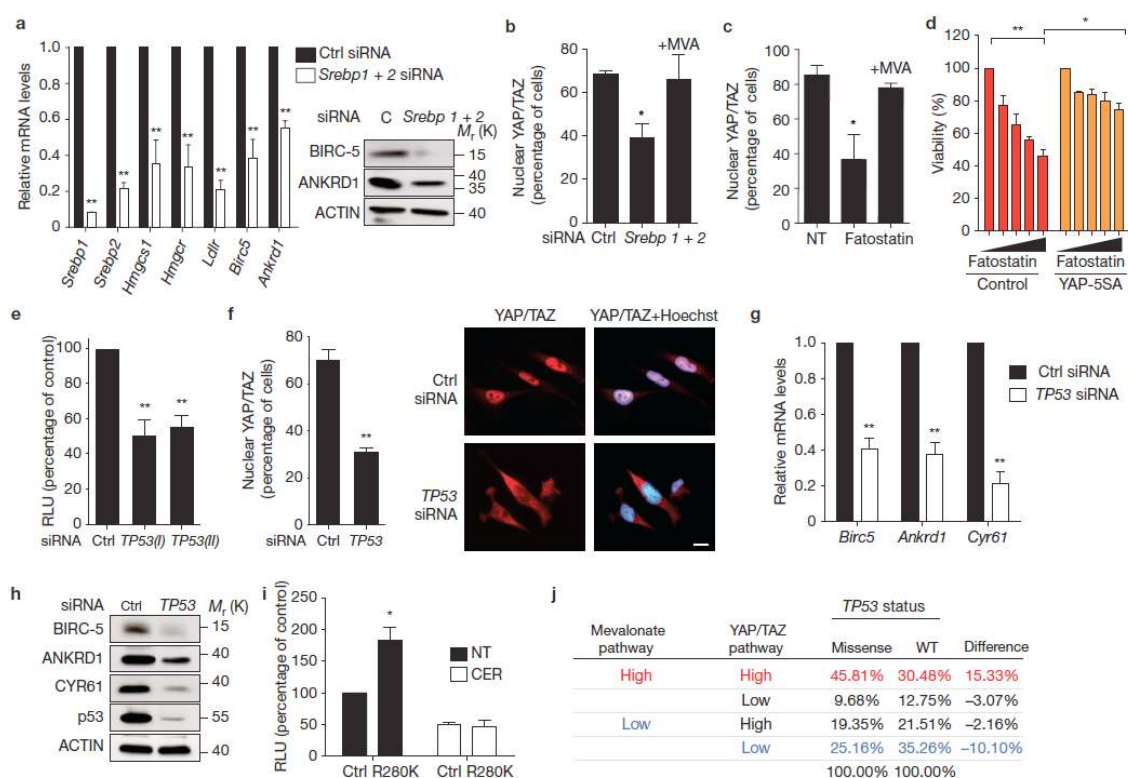
Figure 18. The Mevalonate pathway master regulators SREBPs and mutant-p53 regulate YAP/TAZ activity in cancer cells. (a) qRT-PCR (left) and Western Blot (right) analysis of SREBPs and YAP/TAZ target genes in MDA-MB-231 after *Srebp1* and *Srebp2* knockdown. siC is control siRNA. Representative blots are shown. Experiment repeated three times. Error bars represent mean ± s.d., from n=3 biological replicates. Also see uncropped figure scan in figures. (b,c) Nuclear YAP/TAZ localization in MDA-MB-231 cells after *Srebp1* and *Srebp2* knockdown (b) or treatment with Fatostatin 40µM for 48h (c) and mevalonic acid treatment (0,5 mM) for 24h. Data are derived from three independent experiments where at least 300 cells were scored. Error bars represent mean ± s.d., n=3. (d) Viability of control (CTL) or YAP-5SA stably expressing MII cells treated with increasing amount of Fatostatin (0, 5, 10, 20, 40 µM) for 48h. Data are normalized to untreated. Error bars represent mean ± s.d., from n=3 biological replicates. n=3. (e) Luciferase reporter assay (8XGTII-lux) in MDA-MB-231. Data are normalized to siRNA C (control siRNA). Error bars represent mean ± s.d., from n=4 biological replicates. (f,g,h) Nuclear YAP/TAZ localization (f), qRT-PCR (g) and Western Blot (h) in MDA-MB-231 cells after *TP53* knockdown. Representative images and blots are shown. Experiment repeated three times. Data are derived from three independent experiments where at least 300 cells were scored. Error bars represent mean ± s.d., scale bars, 15 µm. n=3. Also see uncropped figure scan in figures. (i) Luciferase reporter assay (8XGTII-lux) in H1299 cells transfected with pcDNA3 (CTL) or pcDNA3-p53K280R (K280R) and treated with DMSO (NT) or Cerivastatin (CER) 1µM. Data are normalized to untreated CTL. Error bars represent mean ± s.d., from n=3 biological replicates. (j) Contingency table frequencies of samples classified as having *TP53* wild type or *TP53* with missense mutation, high or low levels of Mevalonate Pathway signature, and of YAP/TAZ signature. The association among high/low levels of Mevalonate signature, YAP/TAZ, and TP53 resulted statistically significant (Pearson's Chi-squared Test, $p<10^{-10}$). n= 657 tumor samples. Scale bars, 15 µm. *P< 0.05, **P< 0.01; two-tailed Student's t-test is used throughout.

75

FIGURE 19

Figure 19. Model of mevalonate-dependent control of YAP/TAZ. By cooperating at increasing the levels of the HMGCR enzyme, mutant-p53 and SREBPs transcription factors activate the mevalonate pathway. Mevalonate is a precursor for geranylgeranyl pyrophosphate (GGPP) that, in turn, promotes Rho-GTPases membrane localization and activity thus leading to YAP/TAZ nuclear localization and activation. Inhibition of this pathway by means of statins, bisphosphonates or geranylgeranyl transferase inhibitors attenuates YAP/TAZ biological activities.

FIGURE 20

Figure 20. **Statins inhibit YAP/TAZ nuclear localizatio**n. **(a)** Schematic representation of the high-content screening. MDA-MB-231 cells were seeded in 384-well plates and 24h later the FDA-approved compounds were added to cells at 1 or 10 μM. 24h after treatment, cells were fixed and processed for immunofluorescence for YAP/TAZ and stained with Hoechst. Automated image acquisition and analysis was then performed to analyze the subcellular localization of YAP/TAZ. The screening was performed in duplicate; ca. 4,500 cells were analyzed per experimental condition and replicate. **(b)** Correlation between the two screening replicates at 10μM. Dashed lines represent the levels of cells treated with DMSO. n=2 biological replicates. **(c)** Representative images from the screening. MDA-MB-231 stained for Hoechst and YAP/TAZ after treatment with DMSO or the five statins present in the library are shown. Representative images are shown. Experiment repeated two times. Scale bars, 100 μm. **(d)** Cells were treated with DMSO (NT) or Simvastatin (SIM) 1μM alone or with mevalonic acid 0.5mM for 24h before fixation. Left: representative images of immunofluorescence in MDA-MB-231. Scale bars, 15 μm. Right: quantification of cells with nuclear YAP/TAZ. Representative images are shown. Experiment repeated four times. Data are derived from n=4 independent experiments where at least 300 cells were scored. Error bars represent mean ± s.d.. **(e)** Western blot showing nuclear-cytoplasmic fractionation of MDA-MB-231 cells after treatment with Cerivastatin 1μM alone or with mevalonic acid 0.5mM for 24h. Experiment repeated three times. Scale bars, 15 μm. *P< 0.05, **P< 0.01; Student's t-test is used throughout.
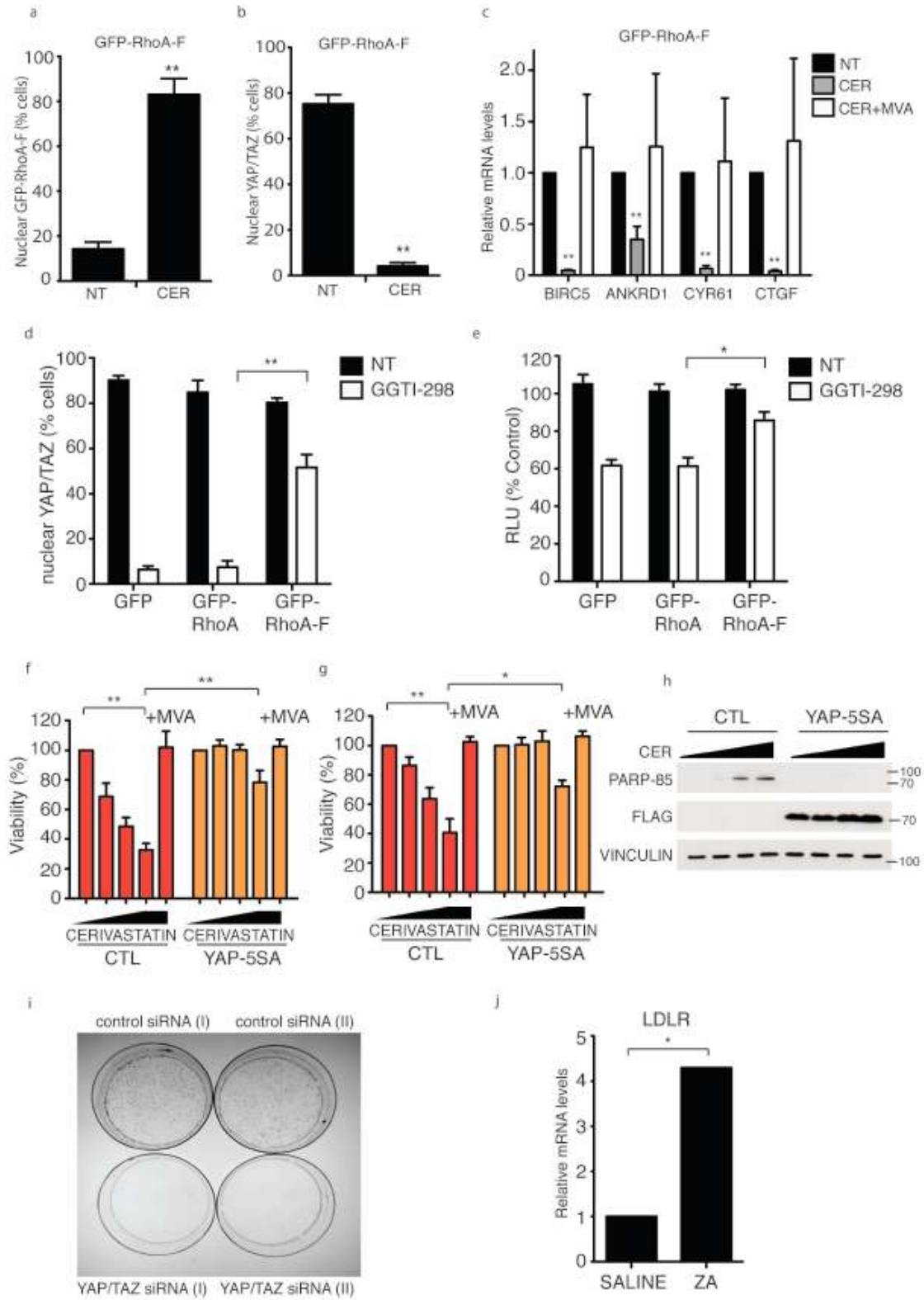
FIGURE 21
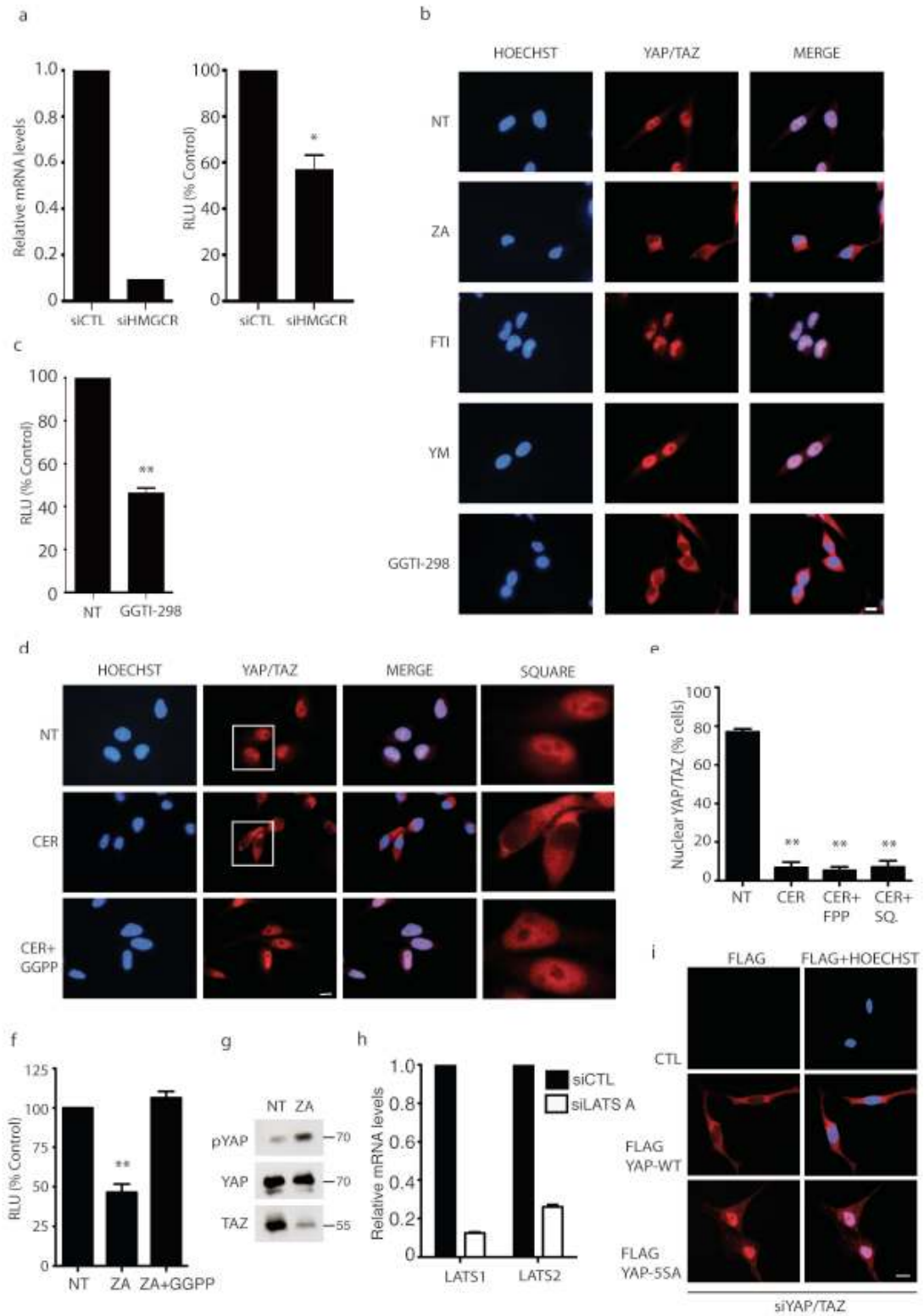
Figure 21. Bisphosphonates and geranylgeranyl transferase inhibitors block YAP/TAZ nuclear localization. (a) qRT-PCR and luciferase reporter assay (8XGTII-lux) to measure YAP/TAZ transcriptional activity. MDA-MB-231 cells were transfected with control siRNA (siCTL) or siRNA against HMG-CoA Reductase (siHMGCR). 72h after transfection cells were collected and analyzed for mRNA expression (left) or luciferase activity (right). Data were normalized to siCTL. Error bars represent mean ± s.d., from n=3 biological replicates. **(b)** Representative images of YAP/TAZ in MDA-MB-231 cells after treatment with inhibitors: Zoledronic Acid (ZA) (50μM), FTI-277 (1μM), YM-53601 (1μM), GGTI-298 (1μM) for 24h. Experiment repeated four times. Data are derived from three independent experiments where at least 300 cells were scored. Scale bars, 15 μm. **(c)** Luciferase reporter assay (8XGTII-lux) to measure YAP/TAZ transcriptional activity. MDA-MB-231 cells were treated with DMSO (NT) or Geranylgeranyl transferase inhibitor (GGTI-298) 1μM for 24h. Data were normalized to NT. Error bars represent mean ± s.d., from n=4 biological replicates. **(d)** Immunofluorescence images shown in Fig. 14d, here presented with their nuclear staining (Hoechst) and zoom. Scale bars, 15 μm. **(e)** Cells were treated with DMSO (NT) or Cerivastatin (CER) 1μM alone or with farnesyl phyrophosphate (FPP) or Squalene (SQ) for 24h before fixation. Experiment repeated four times. Data are derived from n= 4 independent experiments where at least 300 cells were scored. Error bars represent mean ± s.d.;. **(f)** MDA-MB-231 cells were transfected with luciferase 8XGTII-lux reporter. After 24h cells were treated with DMSO (NT) or Zoledronic Acid (ZA) alone or with GGPP for 24h. Data were normalized to NT. Error bars represent mean ± s.d., from n=4 biological replicates. **(g)** Western blot of MDA-MB-231 cells after treatment with DMSO (NT) or Zoledronic Acid (ZA) for 24h. Representative blots are shown. Experiment repeated three times. **(h)** qRT-PCR analysis in MDA-MB-231 transfected with indicated siRNAs. Error bars represent mean ± s.d., from n=3 biological replicates. **(i)** Parental (CTL), siRNA-resistant WT-YAP and 5SA-YAP-overexpressing MDA-MB-231 cells were transfected with a combination of YAP/TAZ siRNA (siYAP/TAZ). The day after, cells were treated with Cerivastatin for 24h and analyzed by immunofluorescence. Representative images are shown. Experiment repeated four times. Data are derived from three independent experiments where at least 300 cells were scored. Scale bars, 15 μm. *P< 0.05, **P< 0.01; Student's t-test is used throughout.

FIGURE 22
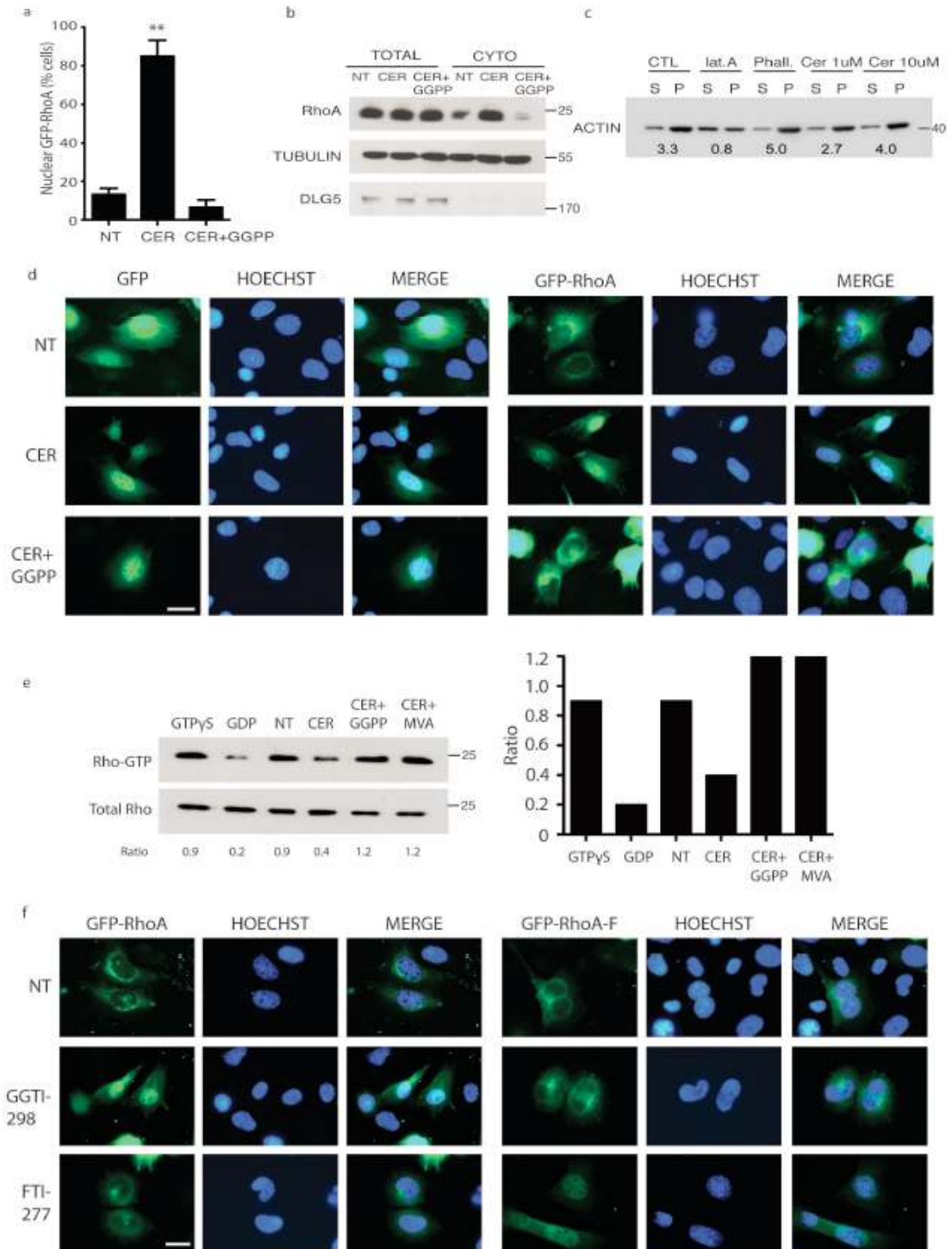
Figure 22. Statins inhibit Rho-GTPases localization and activity by reducing the levels of GGPP. (a) Quantification of H1299 cells with nuclear GFP-RhoA after treatment with DMSO (NT) or Cerivastatin (CER) 1μM alone or with geranylgeranyl pyrophosphate (GGPP) 20μM for 24h. Data are derived from n=3 independent experiments where at least 300 cells were scored. Error bars represent mean ± s.d.. **(b)** Cytoplasmic fraction of H1299 cells after treatment with DMSO (NT) or Cerivastatin (CER) 1μM alone or with geranylgeranyl pyrophosphate (GGPP) 20μM for 24h was analyzed by western blot. Representative blots are shown. Experiment repeated three times. **(c)** G-actin/F-actin assay on MCF10A cells. Cells were treated over day with the indicated drugs, lysed and centrifuged in F-actin stabilization buffer to quantify the relative amount of filamentous actin (F-actin) content in the pellet (P) versus free globular actin (G-actin) content in the supernatant (S). LatrunculinA served as positive control for F-actin dissociation. Phalloidin for F-actin stabilization. Representative blots are shown. Experiment repeated three times. **(d)** Immunofluorescence images shown in Fig. 15a, here presented with their nuclear staining (Hoechst). Scale bars, 15 μm. **(e)** Quantification of GTP-bound RhoA together with total cell lysates was assessed by western blot after Rhotekin pull-down assay. Cells were treated with DMSO (NT) or with Cerivatsatin (CER) 1μM alone or with geranylgeranyl pyrophosphate 20μM (GGPP+CER) or mevalonic acid (MVA+CER) 0.5mM for 24h. Ratio was calculated by densitometric analysis of western blot. Representative blots are shown. Experiment repeated three times. **(f)** Immunofluorescence images shown in Fig. 15c, here presented with their nuclear staining (Hoechst). Subcellular localization images of transiently transfected GFP-RhoA and GFP-RhoA-F in H1299 cells after treatment with FTI-277 1μM for 24h were added. Scale bars, 15 μm. *P< 0.05, **P< 0.01; Student's t-test is used throughout.
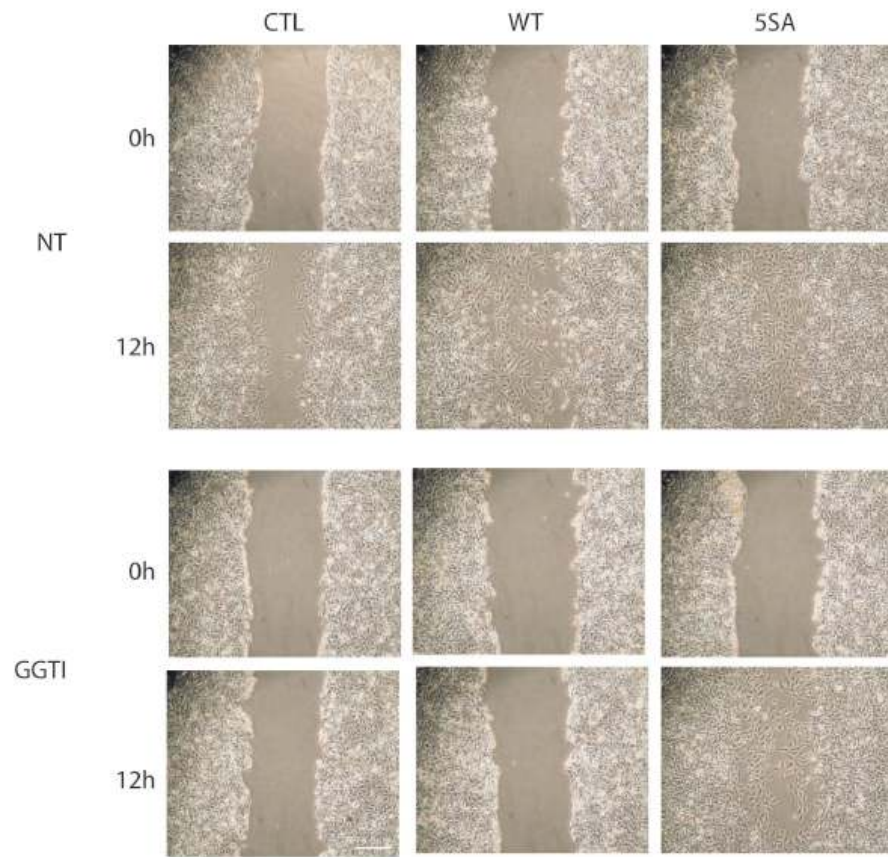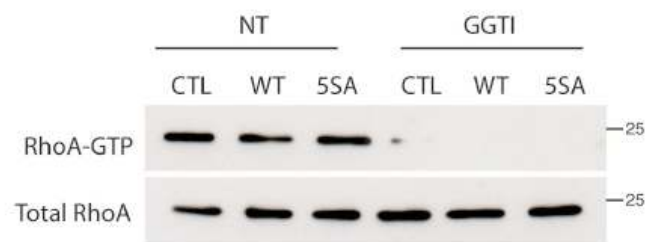
FIGURE 23

Figure 23. Statins and GGTI inhibit YAP/TAZ through Rho-GTPases and show tumor-suppressor activities. (a) Quantification of cells with nuclear GFP-RhoA-F in MDA-MB-231 cells stably expressing the GFP-RhoA-F construct after treatment with DMSO (NT) or with Cerivastatin (CER) 1μM. Data are derived from n=3 independent experiments where at least 300 cells were scored. Error bars represent mean ± s.d.. **(b)** Quantification of cells with nuclear YAP/TAZ in MDA-MB-231 cells stably expressing the GFP-RhoA-F construct after treatment with DMSO (NT) or with Cerivastatin (CER) 1μM. Data are derived from n=4 independent experiments where at least 300 cells were scored. Error bars represent mean ± s.d.. **(c)** qRT-PCR analysis in MDA-MB-231 stably expressing the GFP-RhoA-F construct. Cells were treated with DMSO (NT) or Cerivastatin (CER) 1μM alone or with mevalonic acid 0.5 mM for 48h. Error bars represent mean ± s.d., from n=3 biological replicates. **(d)** Percentage of H1299 cells with nuclear YAP/TAZ. Cells stably expressing the indicated constructs were treated with DMSO (NT) or GGTI-298 (1μM) for 24h. Data are derived from n=3 independent experiments where at least 300 cells were scored. Error bars represent mean ± s.d.. **(e)** Luciferase reporter assay (8XGTII-lux). Cells were treated as in d. Data are normalized to NT. Error bars represent mean ± s.d., from n=3 biological replicates. **(f)** Viability assay (ATPlite) of control and YAP-5SA stably expressing MDA-MB-231 cells after treatment with increasing amount of Cerivastatin (0, 0.1, 1, 10 μM and 10μM with mevalonic acid 0.5 mM) for 48h. Data are normalized to NT. Error bars represent mean ± s.d., from n=3 biological replicates. **(g)** Viability assay (WST-1) of control and YAP-5SA stably expressing MCF10A MII cells after treatment with increasing amount of Cerivastatin (0, 0.1, 1, 10 μM and 10μM with mevalonic acid 0.5 mM) for 48h. Data are normalized to NT. Error bars represent mean ± s.d., from n=3 biological replicates. **(h)** Control and YAP-5SA stably expressing MCF10A MII cells were treated with increasing amount of Cerivastatin (0, 0.1, 1, 10 μM) for 48h. Cleaved PARP was detected by western blot. Representative blots are shown. Experiment repeated three times. **(i)** Clonogenic assay on MDA-MB-231 cells. Cells were transfected with the indicated siRNA. After 1 day cells were seeded in 10-cm petri dishes. Growing colonies were fixed after one week and stained with crystal violet. Experiment repeated two times. Scale bar, 2cm. **(j)** To evaluate the intra-tumoral effect of zoledronic acid on the mevalonate pathway, total RNA was extracted from tumors from control (saline) or zoledronic acid (ZA) treated mice and the mRNA levels of the mevalonate pathway target gene LDLR were determined by qRT-PCR. n=5 mice. *P< 0.05, **P< 0.01; Student's t-test is used throughout.
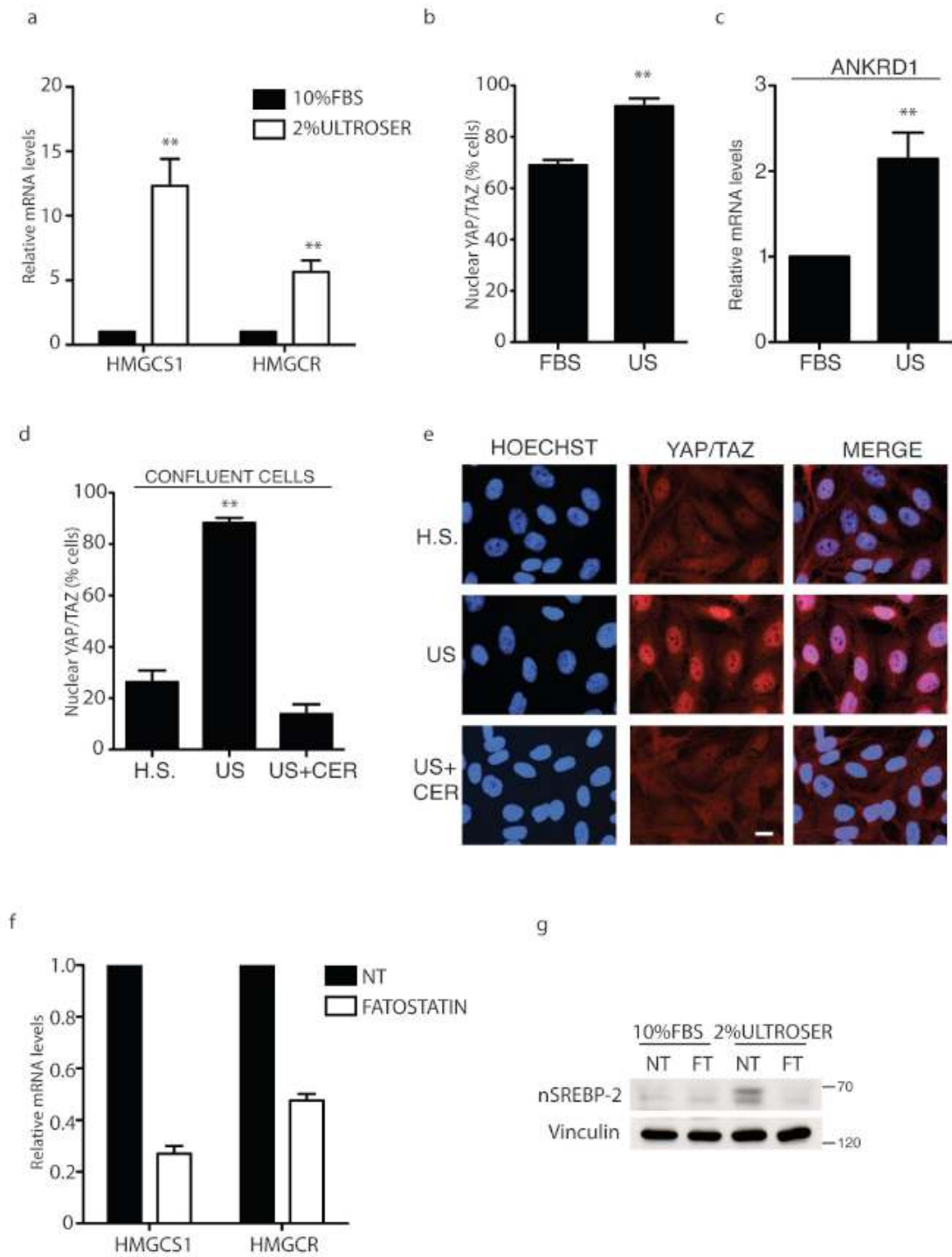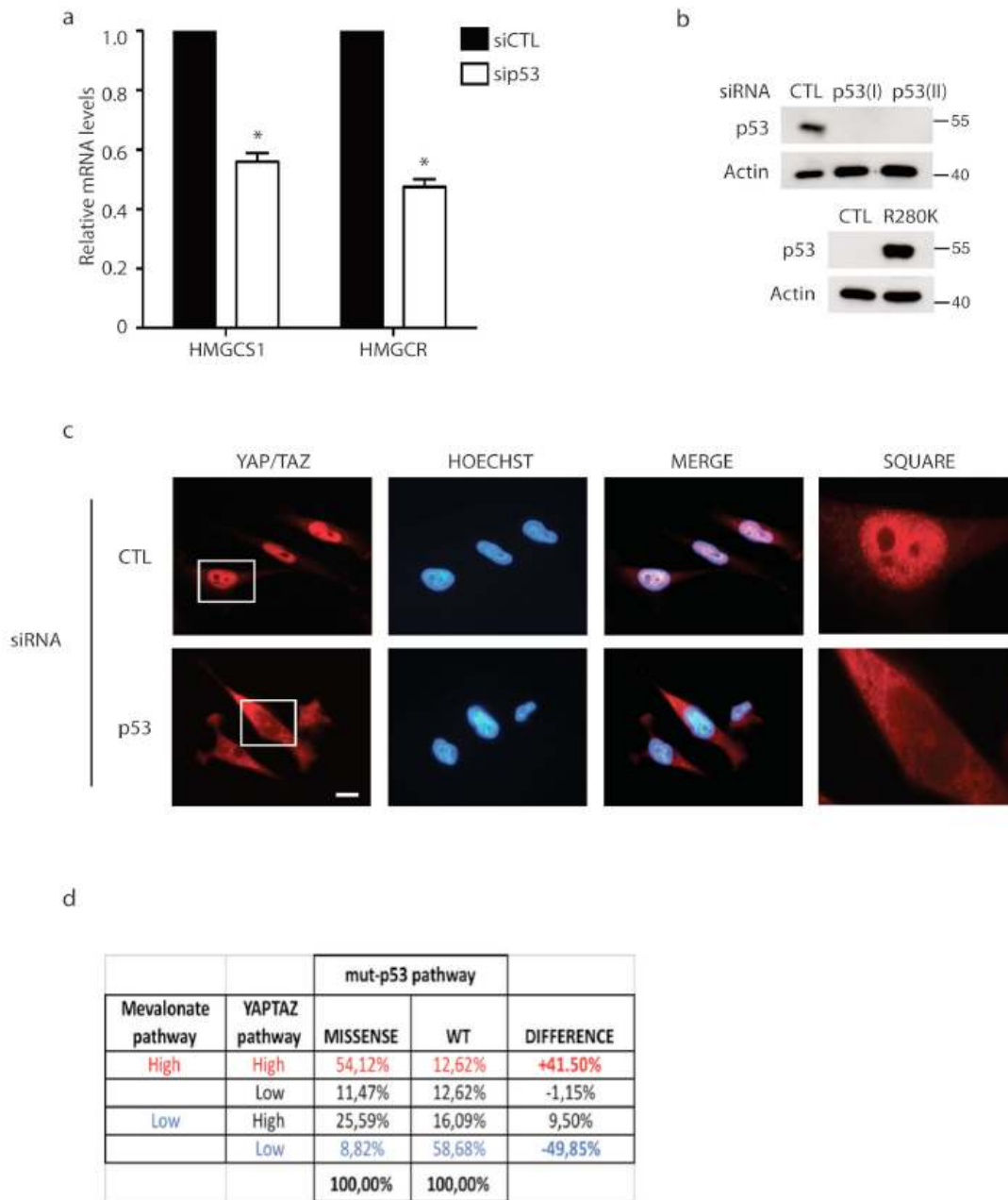
FIGURE 24

a

b

Figure 24. GGTI inhibits cell migration by reducing YAP activity. (a) MCF10A MII cells expressing vector (CTL), YAP wild type (WT), and YAP-5SA (5SA) were analyzed for migration by a wound-healing assay after treatment with DMSO (NT) or GGTI-298 1μM for 12h. Experiment repeated three times. Scale bar, 200μm. **(b)** Quantification of GTP-bound RhoA together with total cell lysates was assessed by western blot after Rhotekin pull-down assay. Cells were treated with DMSO (NT) or with GGTI-298 1μM for 12h. Experiment repeated three times.

FIGURE 25

Figure 25. Activation of the mevalonate pathway increases YAP/TAZ activity. (a) qRT-PCR analysis in MDA-MB-231 to measure SREBPs transcriptional activity. MDA-MB-231 cells were plated in medium with 10%FBS or 2%ULTROSER (US) for 48h. SREBPs target genes (HMGCS1 and HMGCR) expression was analyzed by qRT-PCR. Error bars represent mean ± s.d., from n=3 biological replicates. **(b)** Nuclear YAP/TAZ localization in MDA-MB-231 cells placed in medium with 10% FBS or 2% ULTROSER (US) for 24h. Data are derived from n=3 independent experiments where at least 300 cells were scored. Error bars represent mean ± s.d.. **(c)** qRT-PCR in MDA-MB-231 cells placed in medium with 10% FBS or 2% ULTROSER (US) for 24h. Error bars represent mean ± s.d., from n=4 biological replicates. **(d)** Nuclear YAP/TAZ localization in confluent MCF10A MII cells placed in medium with 5% Horse Serum (H.S.) or 2% ULTROSER (US) and treated with Cerivastatin (CER) 1μM for 24h. Data are derived from n=4 independent experiments where at least 300 cells were scored. Error bars represent mean ± s.d.. **(e)** Representative images relative to d. Scale bars, 15 μm. **(f)** qRT-PCR analysis in MDA-MB-231 to measure SREBPs transcriptional activity. MDA-MB-231 cells were placed in medium with 2% ULTROSER and treated with DMSO (NT) or SREBPs inhibitor Fatostatin 40μM for 48h. SREBPs target genes (HMGCS1 and HMGCR) expression was analyzed by qRT-PCR. Error bars represent mean ± s.d., from n=3 biological replicates. **(g)** Cleaved SREBP-2 (nSREBP-2) levels were detected after 48h treatment with DMSO (NT) or SREBPs inhibitor Fatostatin (FT) 40μM in cells cultured with 10%FBS or 2%ULTROSER (US). Representative blots are shown. Experiment repeated three times. *P< 0.05, **P< 0.01; Student's t-test is used throughout.

FIGURE 26

Figure 26. Mutant-p53 activates YAP/TAZ through the mevalonate pathway. (a) qRT-PCR analysis in MDA-MB-231 to measure SREBPs transcriptional activity after mutant p53 silencing. SREBPs target genes (HMGCS1 and HMGCR) expression was analyzed by qRT-PCR. Error bars represent mean ± s.d., from n=3 biological replicates. **(b)** p53 levels relative to Fig. 18e (upper panel) and 6i (bottom panel). Representative blots are shown. Experiment repeated three times. **(c)** Immunofluorescence images shown in Fig. 18f, here presented with their nuclear staining (Hoechst) and zoom. Scale bars, 15 μm. **(d)** Contingency table frequencies of samples classified as having high or low levels of Mevalonate Pathway signature, of YAP/TAZ signature and of mutant p53 "ten genes" signature. The association among high/low levels of Mevalonate signature, YAP/TAZ, and ten genes resulted statistically significant (Pearson's Chi-squared Test, $p<10^{-16}$). n= 657 tumor samples. All error bars are s.d. (*P< 0.05, **P< 0.01; Student's t-test is used throughout).

FULL SCANS
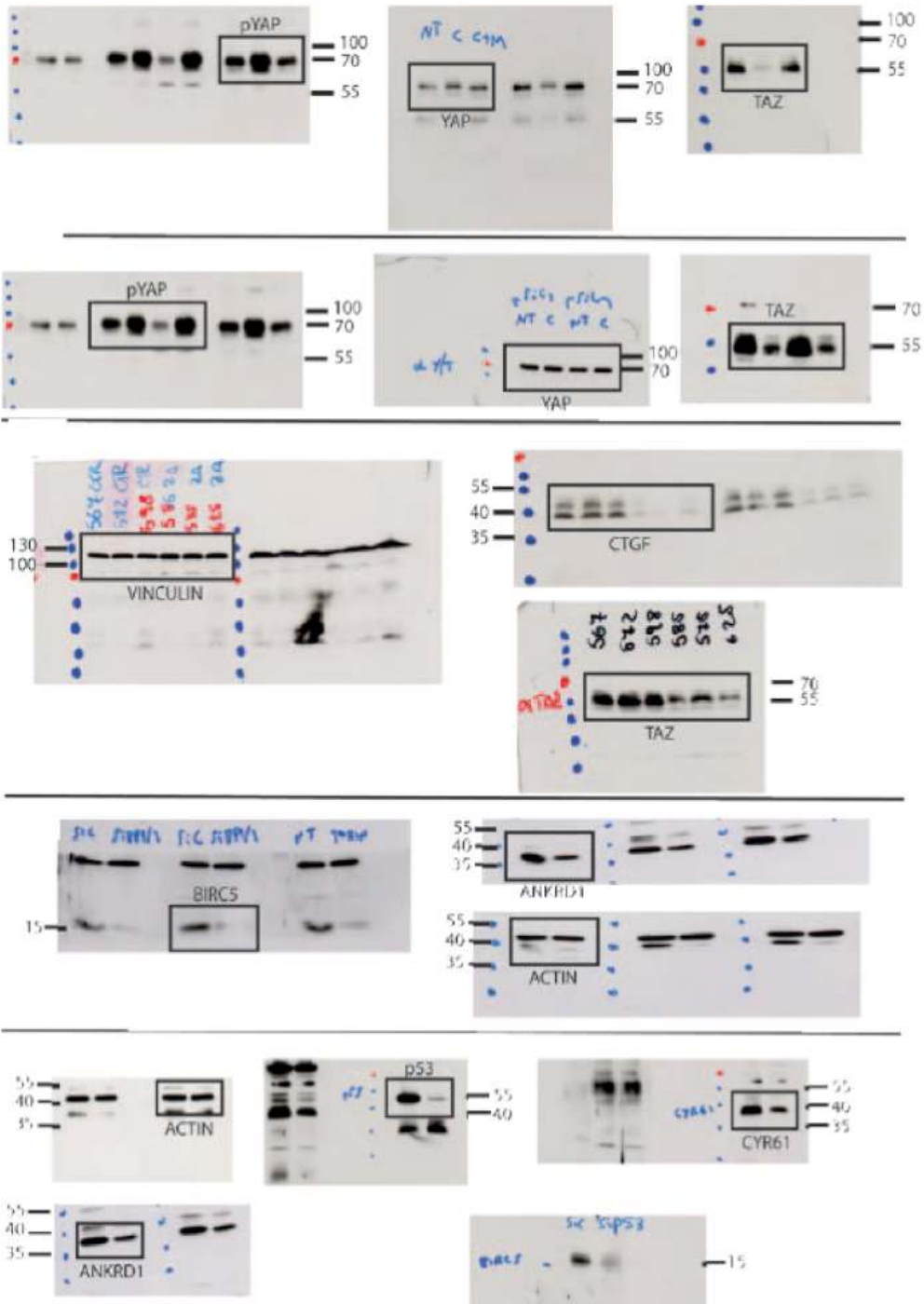
TABLES

TABLE 1

Ten gene signature	Symbol	Description	EntrezID
NCAPH	NCAPH	Non-SMC condensin I complex, subunit H	23397
CPSF6	CPSF6	Cleavage and polyadenylation specific factor 6, 68kDa	11052
DEPDC1	DEPDC1	DEP domain containing 1	55635
C21orf45	C21orf45	Chromosome 21 open reading frame 45	54069
CENPA	CENPA	Centromere protein A	1058
WDR67	WDR67	WD repeat domain 67	93594
BUB1	BUB1	Budding uninhibited by benzimidazoles 1 homolog (yeast)	699
FAM64A	FAM64A	Family with sequence similarity 64, member A	54478
CCNE2	CCNE2	Cyclin E2	9134
EPB41L4B	EPB41L4B	Erythrocyte membrane protein band 4.1 like 4B	54566

YAP/TAZ signature	Symbol	Description	EntrezID
KRT34	KRT34	Keratin 34	3885
STXBP6	STXBP6	Syntaxin binding protein 6 (amisyn)	29091
OLR1	OLR1	Oxidized low density lipoprotein (lectin-like) receptor 1	4973
THBS1	THBS1	Thrombospondin 1	7057
INHBA	INHBA	Inhibin, beta A	3624
CTGF	CTGF	Connective tissue growth factor	1490
SERTAD4	SERTAD4	SERTA domain containing 4	56256
ANKRD1	ANKRD1	Ankyrin repeat domain 1 (cardiac muscle)	27063
HSD3B1	HSD3B1	Hydroxy-delta-5-steroid dehydrogenase, 3 beta- and steroid delta-isomerase 1	3283
ORC1L	ORC1L	Data not found	4998
CENPM	CENPM	Centromere protein M	79019
WDR69	WDR69	WD repeat domain 69	164781
ITGB2	ITGB2	Integrin, beta 2 (complement component 3 receptor 3 and 4 subunit)	3689
IGFBP3	IGFBP3	In multiple clusters	3486
TGM2	TGM2	Transglutaminase 2 (C polypeptide, protein-glutamine-gamma-glutamyltransferase)	7052
ADAMTS1	ADAMTS1	ADAM metallopeptidase with thrombospondin type 1 motif, 1	9510
BDNF	BDNF	Brain-derived neurotrophic factor	627
TMEM171	TMEM171	Transmembrane protein 171	134285
SERPINE2	SERPINE2	In multiple clusters	5270
PTGS2	PTGS2	Prostaglandin-endoperoxide synthase 2 (prostaglandin G/H synthase and cyclooxygenase)	5743
CCDC18	CCDC18	Coiled-coil domain containing 18	343099
PLCB4	PLCB4	Phospholipase C, beta 4	5332
DEPDC1B	DEPDC1B	DEP domain containing 1B	55789
ZBED2	ZBED2	Zinc finger, BED-type containing 2	79413
MATN3	MATN3	Matrilin 3	4148
CCNA2	CCNA2	Cyclin A2	890
TBXA2R	TBXA2R	Thromboxane A2 receptor	6915
SERPINE1	SERPINE1	Serpin peptidase inhibitor, clade E (nexin, plasminogen activator inhibitor type 1), member 1	5054
SLIT2	SLIT2	Slit homolog 2 (Drosophila)	9353
BCAR4	BCAR4	Data not found	NC_000016.9
ZWINT	ZWINT	ZW10 interactor	11130
RAD51	RAD51	RAD51 homolog (RecA homolog, E. coli) (S. cerevisiae)	5888
DIAPH3	DIAPH3	Diaphanous homolog 3 (Drosophila)	81624
MCM10	MCM10	Minichromosome maintenance complex component 10	55388
NAV3	NAV3	Neuron navigator 3	89795
C18orf24	SKA1	Data not found	220134
SHCBP1	SHCBP1	SHC SH2-domain binding protein 1	79801
RAD51AP1	RAD51AP1	RAD51 associated protein 1	10635
DDAH1	DDAH1	Dimethylarginine dimethylaminohydrolase 1	23576
RIMS2	RIMS2	Regulating synaptic membrane exocytosis 2	9699
RRM2	RRM2	Ribonucleotide reductase M2	6241
CDC6	CDC6	Cell division cycle 6 homolog (S. cerevisiae)	990
PRR16	PRR16	Proline rich 16	51334
DAB2	DAB2	Disabled homolog 2, mitogen-responsive phosphoprotein (Drosophila)	1601
PLK4	PLK4	Polo-like kinase 4	10733
ASF1B	ASF1B	ASF1 anti-silencing function 1 homolog B (S. cerevisiae)	55723
KIF14	KIF14	Kinesin family member 14	9928
FMN2	FMN2	Formin 2	56776
CDC25C	CDC25C	Cell division cycle 25 homolog C (S. pombe)	995
GINS2	GINS2	GINS complex subunit 2 (Psf2 homolog)	51659

Mevalonathe signature	Symbol	Description	EntrezID
ACAT2	ACAT2	Acetyl-CoA acetyltransferase 2	39
HMGCS1	HMGCS1	3-hydroxy-3-methylglutaryl-CoA synthase 1 (soluble)	3157
HMGCR	HMGCR	3-hydroxy-3-methylglutaryl-CoA reductase	3156
IDI1	IDI1	Isopentenyl-diphosphate delta isomerase 1	3422
FDPS	FDPS	Farnesyl diphosphate synthase	2224
SQLE	SQLE	Squalene epoxidase	6713
LSS	LSS	Lanosterol synthase (2,3-oxidosqualene-lanosterol cyclase)	4047
NSDHL	NSDHL	NAD(P) dependent steroid dehydrogenase-like	50814
DHCR7	DHCR7	7-dehydrocholesterol reductase	1717

Table 1. Mutant-p53, YAP/TAZ and the Mevalonate pathway gene signatures. The table contains the gene signatures used in Fig. 18j and Fig. 26d as obtained from published data.

TABLE 2

PRIMER NAME	PRIMER SEQUENCE
GFP F	CATCATGGATCCATGGTGAGCAAGGGC
RhoA-CLVL R	GAGGAGCTCGAGTCACAAGACAAGGCACCC
RhoA-CVLS R	GGAATTCGAATTCTCACGAAAGGACGCAACCAGATTTTTTCTTCCCACGTC

GENE	PRIMER NAME	PRIMER SEQUENCE
H3	H3 F	GTGAAGAAACCTCATCGTTACAGGCCTGGT
	H3 R	CTGCAAAGCACCAATAGCTGCACTCTGGAA
Ctgf	CTGF F	AGGAGTGGGTGTGTGACGA
	CTGF R	CCAGGCAGTTGGCTCTAATC
Birc5	BIRC5 F	AGCATTCGTCCGGTTGCGCT
	BIRC5 R	TCGATGGCACGGCGCACTTT
Ankrd1	ANKRD1 F	CACTTCTAGCCCACCCTGTGA
	ANKRD1 R	CCACAGGTTCCGTAATGATTT
Cyr61	CYR61 F	AGCCTCGCATCCTATACAACC
	CYR61 R	TTCTTTCACAA GGCGGCACTC
Srebp1	SREBP1 F	GACATCGAAGGTGAAGTCGGCG
	SREBP1 R	CCCTGCCCCACTCCCAGCATA
Srebp2	SREBP2 F	TGCCCTTCAAGTACCAACCC
	SREBP2 R	GGTTGTCCGCCTTTCTCCTT
Hmgcs1	HMGCS1 F	GGGCAGGGCATTATTAGGCTAT
	HMGCS1 R	TTAGGTTGTCAGCCTCTATGTTGAA
Hmgcr	HMGCR F	GGACCCCTTTGCTTAGATGAAA
	HMGCR R	CCACCAAGACCTATTGCTCTG
Ldlr	LDLR F	AAGCCATTCACTTCCCCAATC
	LDLR R	GCCTCACCGTGCATGTTTTA
rp49	rp49 F	ATCGGTTACGGATCGAACAA
	rp49 R	GACAATCTCCTTGCGCTTCT
diap1	diap1 F	GAAAAAGAGAAAAGCCGTCAAGT
	diap1 R	TGTTTGCCTGACTCTTAATTTCTTC
Expanded	Expanded F	GATGCTGGACACCGAACTC
	Expanded R	CTTGCTCGGGATCTGC

GENE	siRNA NAME	siRNA SEQUENCE
TP53	siTP53(I)	GACUCCAGUGGUAAUCUUAC
TP53	siTP53(II)	GGUGAACCUUAGUACCUAA
Srebp1	siSrebp1	CCACUCCAUUGAAGAUGUA
Srebp2	siSrebp2	GCCCUCUAUUGGAUGAUGC

Table 2. Primers and siRNAs sequences. The table contains sequences of primers and siRNAs.

ACKNOWLEDGEMENTS

APPENDIX

During my PhD I have been involved in the following publications:

- <u>Sorrentino, G.</u>, Mioni, M., Giorgi, C., Ruggeri, N., Pinton, P., Moll, U., Mantovani, F., and Del Sal, G. (2013). **The prolyl-isomerase Pin1 activates the mitochondrial death program of p53**. Cell Death Differ *20*, 198-208.

ABSTRACT: In response to intense stress, the p53 tumor suppressor rapidly mounts a direct mitochondrial death program that precedes transcription-mediated apoptosis. By eliminating severely damaged cells, this pathway contributes to tumor suppression as well as to cancer cell killing induced by both genotoxic drugs and non-genotoxic p53-reactivating molecules. Here we have explored the role played in this pathway by the prolyl-isomerase Pin1, a crucial transducer of p53's phosphorylation into conformational changes unleashing its pro-apoptotic activity. We show that Pin1 promotes stress-induced localization of p53 to mitochondria both *in vitro* and *in vivo*. In particular, we demonstrate that upon stress-induced phosphorylation of p53 on Ser46 by HIPK2, Pin1 stimulates its mitochondrial trafficking signal, i.e. monoubiquitination. This pathway is induced also by the p53-activating molecule RITA, and we demonstrate the strong requirement of Pin1 for the induction of mitochondrial apoptosis by this compound. These findings have significant implications for treatment of p53-expressing tumors and for prospective use of p53-activating compounds in clinics.

- Rustighi, A., Zannini, A., Tiberi, L., Sommaggio, R., Piazza, S., <u>Sorrentino, G.</u>, Nuzzo, S., Tuscano, A., Eterno, V., Benvenuti, F.*, et al.* (2014). **Prolyl-isomerase Pin1 controls normal and cancer stem cells of the breast**. EMBO Mol Med *6*, 99-119.

ABSTRACT: Mammary epithelial stem cells are fundamental to maintain tissue integrity. Cancer stem cells (CSCs) are implicated in both treatment resistance and disease relapse, and the molecular bases of their malignant properties are still poorly understood. Here we show that both normal stem cells and CSCs of the breast are controlled by the prolyl-isomerase Pin1. Mechanistically, following interaction with Pin1, Notch1 and Notch4, key regulators of cell fate, escape from proteasomal degradation by their major ubiquitin-ligase Fbxw7α. Functionally, we show that Fbxw7α acts as an essential negative regulator of breast CSCs' expansion by restraining Notch activity, but the establishment of a Notch/Pin1 active circuitry opposes this effect, thus promoting breast CSCs self-renewal, tumor growth and metastasis in vivo. In human breast cancers, despite Fbxw7α expression, high levels of Pin1 sustain Notch signaling, which correlates with poor prognosis. Suppression of Pin1 holds promise in reverting aggressive phenotypes, through CSC exhaustion as well as recovered drug sensitivity carrying relevant implications for therapy of breast cancers.

- <u>Sorrentino, G.</u>, Ruggeri, N., Specchia, V., Cordenonsi, M., Mano, M., Dupont, S., Manfrin, A., Ingallina, E., Sommeggio, R., Piazza, S., Rosato, A., Piccolo, S., Del Sal, G. (2014). **Metabolic control of YAP and TAZ by the mevalonate pathway**. Nature Cell Biology, doi:10.1038/ncb2936